ANNALES DU BATIMENT ET DES TRAVAUX PUBLICS

ISSN : 1270-9840

SÉRIE BIMESTRIELLE **N° 1/2011**

(anciennement : Annales de l'I.T.B.T.P., Revue créée en 1948)

FÉVRIER 2011

ABONNEMENT : http://www.eska.fr
Editions ESKA
12, rue du Quatre-Septembre - 75002 PARIS
Tél. : 01 42 86 55 65 - Fax : 01 42 60 45 35

FABRICATION : AGPA EDITIONS
4, rue Camélinat - 42000 Saint-Etienne
Tél. : 04 77 43 26 70 - Fax : 04 77 41 85 04
E-mail : agpaedit@wanadoo.fr

PUBLICITÉ - À la rédaction

IMPRESSION

summary
sommaire

éditorial

French innovations in the field of construction industry
Innovations françaises dans le secteur de la construction

ANNALES DU BATIMENT ET DES TRAVAUX PUBLICS

Photos de couverture : les auteurs
Crédits photos : les auteurs

ANNALES DU BATIMENT ET DES TRAVAUX PUBLICS

BULLETIN D'ABONNEMENT

À retourner aux Éditions ESKA
12, rue du Quatre-Septembre, 75002 PARIS
Tél. 01 42 86 55 65 – Fax 01 42 60 45 35

Nom .....
Raison sociale.....
Adresse .....
Code postal ..... Ville ..... Pays .....

Je m'abonne pour **l'année 2011** (6 numéros/an) à la revue « ***Annales du BTP*** » :

☐ Tarif FRANCE individuel (TTC) : **230** € ☐ Tarif ETRANGER individuel (HT) : **277** €
☐ Tarif FRANCE institution (TTC) : **287** € ☐ Tarif ETRANGER institution (HT) : **331** €

À partir du 2e abonnement :

☐ Tarif FRANCE individuel (TTC) : **184** € ☐ Tarif ETRANGER individuel (HT) : **221** €
☐ Tarif FRANCE institution (TTC) : **231** € ☐ Tarif ETRANGER institution (HT) : **265** €
Surtaxe aérienne 2,90 € par volume (2,90 x 6) soit 17,40 €

Je joins : ☐ Un chèque bancaire à l'ordre des Editions ESKA
☐ Un virement bancaire aux Editions ESKA -
BNP Paris - Champs Elysées - 30004-00804 - Compte 000101399.56

** 1/2011*

LISTE DES ANNONCEURS

éditorial

Dear readers,

The journal Annales du Bâtiment et des Travaux publics, *presenting innovations in this important sector of the economy, is destined for a readership of engineers, scientists and advisors.*

The reader will find rubrics on building materials, structure calculations, construction methods, maintenance and repair of buildings, the physics and study of energy in buildings, sustainable construction and development …

In recent years the journal has proposed articles in English, but this is the first time that a whole issue has been drawn up in English with, for some articles, a bilingual presentation or an extended abstract in French.

The Annales are taking advantage of CONEXPO 2011 which is to be held in Las Vegas from 22 to 26 March to ensure that particularly remarkable French innovations become better known especially in the field of building materials.

We hope this initiative will be appreciated by the traditional French-speaking readers of the journal and by the new English readers that we will reach at CONEXPO. Wishing you all an excellent read in this particularly rich issue.

Prof. François BUYLE-BODIN
Editor-in-chief

Chères lectrices, chers lecteurs,

Les *Annales du Bâtiment et des Travaux publics* sont une revue présentant les innovations de cet important secteur économique, destinée à un lectorat d'ingénieurs, de scientifiques et de prescripteurs,

Le lecteur y trouve des rubriques sur les matériaux de construction, le calcul des structures, les méthodes de construction, la maintenance et la réparation des ouvrages, la physique et l'énergétique du bâtiment, la construction et l'aménagement durables…

Ces dernières années, la revue avait proposé des articles en langue anglaise, mais c'est la première fois qu'un numéro dans son ensemble est rédigé en anglais, avec pour certains articles une présentation bilingue ou un résumé étendu en langue française.

Les Annales profitent en effet de l'édition 2011 de CONEXPO, qui se tiendra à Las Vegas du 22 au 26 mars pour faire connaître des innovations françaises particulièrement remarquables essentiellement dans le domaine des matériaux de construction.

En espérant que cette initiative sera appréciée par les lecteurs traditionnels francophones de la revue et par les nouveaux lecteurs de langue anglaise que nous atteindrons à CONEXPO, je vous souhaite une excellente lecture de ce numéro particulièrement riche.

Prof. François BUYLE-BODIN
Rédacteur en chef

abstracts — résumés

STUDY OF THE PERFORMANCE OF FRP REINFORCING BARS SUBJECTED TO EXTREME CONDITIONS OF APPLICATION

MATHIEU ROBERT, PATRICE COUSIN, BRAHIM BENMOKRANE

Fibre-reinforced polymer (FRP) materials have emerged as a practical alternative material for producing reinforcing bars for concrete structures. This is due to their relatively low cost-to-performance ratio and noncorrosive nature compared to traditional steel reinforcing bars. In addition, FRP materials exhibit properties, such as high tensile strength, that make them suitable for use as structural reinforcement. However, their durability in an alkaline environment is still of concern and factors that can affect the long-term behaviour of GFRP materials have to be investigated. Moisture, high pH of surrounding environment, extreme temperature and the presence of micro cracks can affect the long-term properties of FRP reinforcing bars. This paper summarizes the long-term durability study of glass fibre-reinforced polymer (GFRP) reinforcing bars subjected to different conditionings simulating the real environment of application. In particular, the behaviour of GFRP bars subjected moisture, high pH of moist concrete, extreme temperatures, and to tensile prestress was investigated showing the great durability of GFRP reinforcing bars.

KEYWORDS: *FRP, composites materials, reinforcement, concrete, high temperature, absorption, mechanical properties, rate of reaction, prediction model.*

PERFORMANCE DES ARMATURES COMPOSITES DE PRF SOUMISES À DES ENVIRONNEMENTS D'APPLICATION EXTRÊMES

Les matériaux polymères renforcés de fibres (PRF) sont de plus en plus utilisés dans les ouvrages du génie civil à cause de leurs nombreux avantages par rapport à l'acier d'armature. Toutefois, certaines conditions d'application peuvent potentiellement affecter leur durabilité, rendant cruciales les études exhaustives de leur comportement à long terme pour permettre leur plein développement. Les solutions aqueuses, l'alcalinité du milieu environnant, la température d'application et l'état des barres sont tous des paramètres pouvant compromettre les propriétés à long terme des barres d'armature en polymère renforcé de fibres de verre (PRFV), de carbone (PRFC) ou d'aramide (PRFA). Le présent article synthèse présente l'étude de la durabilité à long terme de barres de PRFV soumis à des vieillissements accélérés en laboratoire simulant la réalité. Le comportement de barres de PRFV face à l'humidité, à l'alcalinité du béton humide, aux températures extrêmes et aux chargements en traction ont été investigué, montrant la bonne durabilité des composites de PFRV pour des applications en génie civil.

MOTS-CLÉS : PRF, composites, durabilité, armature, béton, température, absorption, propriétés mécaniques, taux de réaction, modèle de prédiction.

POTENTIAL POUZZOLANICITY OF GLASS CULLET FINES AND AGGREGATES

RACHIDA IDIR, MARTIN CYR, AREZKI TAGNIT-HAMOU

Mixed glasses of different colors are economically difficult to reuse for the fabrication of new glass products but their use in cement-based materials is a promising way to recycle this material. This paper deals with the pouzzolanique activity of mixed glass cullet, by evaluating the pouzzolanique behavior of a large range of glass particle sizes, from less than 40 µm (540 m^2/kg) up to 2.5 mm (2.2 m^2/kg). Five different classes of glass are assessed separately, in terms of compressive strength tests on mortars, consumption of lime (TG), morphology (SEM) and composition of hydrates (EDX and X-ray fluorescence).

The results show that the pouzzolanique activity increases with glass fineness and that, compared to a reference material without glass, equivalent or superior compressive strength can be obtained when using up to 40% of glass of 540 m^2/kg fineness. Transition fineness around 30 m2/kg (140 µm) is highlighted, for which the pouzzolanique activity becomes substantial. However, a slight but significant pouzzolanique activity is detected for coarse particles (>1 mm), as confirmed by the consumption of Ca(OH)2, the formation of C-S-H-like hydrates and an increase of 10% (5 MPa) in the compressive strength compared to an inert admixture.

KEYWORDS: *recycled glass; glass powder; glass aggregate; pouzzolane; pouzzolanique reaction; alkali-silica reaction*

PROPRIÉTÉS POUZZOLANIQUES DES FINES ET DES GRANULATS DE VERRE DE RECYCLAGE

Le recyclage du verre mixte contenant plusieurs couleurs pour la fabrication de nouveaux verres n'est actuellement pas économiquement viable. Ceci explique la recherche d'autres débouchés que le stockage ou l'enfouissement en décharges. L'une des applications envisageables est sa valorisation dans la fabrication des ciments et des bétons. Néanmoins, il est nécessaire de gérer les deux principaux comportements que peut avoir ce verre lorsqu'il est mis en contact avec une matrice cimentaire, à savoir :

– un comportement néfaste associé à la réaction alcali-silice, si le verre est utilisé sous la forme de grosses particules ;

– un comportement bénéfique associé à la réaction pouzzolanique, si le verre est utilisé sous la forme de fines particules.

Cet article traite de l'utilisation du verre mixte en remplacement de ciment qui présente une alternative aux voies de recyclage déjà existantes. Il évalue le comportement pouzzolanique du verre de recyclage d'une large gamme de tailles de particules de verre, de la classe la plus fine (< 41µm) jusqu'aux particules les plus grossières de taille 2.5-5mm. Cinq différentes classes de verre ont été évaluées séparément, en termes de tests de résistance à la compression sur mortiers, de consommation de chaux (ATG), de morphologie (MEB) et de composition des hydrates (EDS et fluorescence X).

Les résultats montrent que :

– Le verre de recyclage présente une activité pouzzolanique qui augmente avec la finesse de ses particules.

– Par rapport au témoin sans verre, des résistances équivalentes ou même supérieures peuvent être obtenus en utilisant jusqu'à 40% du verre d'une finesse 540 m²/kg

– Des indices d'activité pouzzollanique supérieurs à 90% peuvent être obtenus après:

• 7 jours de cure pour 10% de verre, quelle que soit la finesse du verre;

• 90 jours de cure pour 20% de verre, uniquement lorsque la surface spécifique est supérieure à 200 m²/kg.

– Une finesse de transition d'environ 30 m^2/kg (140 µm) est mise en évidence, pour laquelle l'activité pouzzollanique devient importante.

– Une légère mais significative activité pouzzollanique est détectée pour les grosses particules (> 140 µm), confirmée par une consommation de $Ca(OH)_2$, la formation de C-S-H et un accroissement de 10% (5MPa) de la résistance à la compression comparé un à ajout inerte.

– Toutefois, la possible alcali-réactivité de ces particules devrait être prise en compte, car la RAS a été détectée pour les particules dont la surface spécifique est inférieure à 4,5 m^2/kg.

– La composition des néoformations dépend de la cinétique de la réaction et de la disponibilité du calcium et des alcalins en un endroit donné et à un âge donné. Le déficit des alcalins par rapport au calcium conduit à des hydrates de faible (N+K)/S (fort C/S) ayant une composition proche de C-S-H, tandis que l'inverse pourrait favoriser des rapports (N+K)/S élevé, typique des gels de RAS.

MOTS-CLÉS : verre de recyclage; poudre de verre; granulats de verre; pouzzolane; réaction pouzzollanique; réaction alcali-silice.

BASIC OXYGEN FURNACE SLAG (BOF SLAG): CHARACTERIZATION AND EVOLUTIVITY

ESSIA BELHADJ, CÉCILE DILIBERTO, ANDRÉ LECOMTE

Basic oxygen furnace slag (BOF slag) are by-products of the conversion of pig iron to steel. According to the high quantities produced, they are a valuable mineral resource for the construction, in form of aggregates or additions in certain hydraulic binders. However, they have chemical properties that directly control their stability or any hydraulic potential (free lime, etc...). A good knowledge of physico-chemical properties of BOF slag is a necessary preliminary step to their valorization. This work proposes a comprehensive methodology for the characterization of steel slag by complementary analytical techniques (XRF, XRD, TGA ...). Its application to a variety of BOF slag shows that they essentially contain C_2S, C_2F, $Ca(OH)_2$, $Fe_{1-x}O$, CaO. $CaCO_3$, SiO_2 and MgO are also detected in few quantities. But this composition may change by hydration and carbonation, these two reactions are related to storage temperature and humidity.

KEYWORDS: *BOF Slag, chemical composition, valorisation, building material, free lime*

LAITIERS D'ACIÉRIE DE CONVERSION : CARACTÉRISATION ET ÉVOLUTIVITÉ

Les laitiers de convertisseurs à oxygène ou BOF slag (Basic Oxygen furnace) sont des co-produits de l'industrie sidérurgique. Suivant la nuance d'acier produite, 100 à 200Kg de BOF slag sont générés par tonne d'acier [MAH, 08]. En 2005, 1,2 millions de tonnes ont été produites en France. Le principe de la conversion de la fonte en acier est de réduire la teneur en carbone par soufflage d'oxygène. Au cours de ce procédé, de la chaux est introduite dans le convertisseur pour fixer les éléments indésirables contenus dans la fonte et pour protéger les briques réfractaires du four. A la fin de la conversion, les BOF slag sont séparés de l'acier par gravimétrie.

Les laitiers d'aciérie sont peu exploités ; l'agriculture en consomme une faible partie en amendement agricole pour neutraliser l'acidité du sol. Mais la plus importante utilisation des BOF slag concerne le domaine des techniques routières, comme granulats, puisqu'ils possèdent une bonne résistance mécanique et leur coût est peu élevé [MOT, 01]. Malheureusement cette utilisation a été restreinte durant les dernières années à cause de l'expansion volumique des BOF slags due à l'hydratation de l'oxyde de calcium contenu dans ces matériaux [CAI, 00].

Grâce à leur composition chimique proche de celle des ciments Portland, la valorisation des BOF slag dans les liants hydrauliques est envisageable. Cette valorisation aura un impact environnemental en préservant les ressources naturelles et en limitant l'émission de CO_2 due à la clinkérisation. Cependant, ces matériaux ont des propriétés hydrauliques faibles en raison de la différence minéralogique par rapport au ciment Portland, notamment l'absence de silicate tricalcique et la forte teneur en oxyde de fer [Mur, 97]. En effet, la wüstite ($Fe_{1-x}O$) qui est une des phases principales des BOF slag ne réagit pas au contact de l'eau. D'autre part leur utilisation peut être limitée en raison de leur forte évolutivité. En effet, l'oxyde de calcium contenu dans ces matériaux réagit facilement avec l'humidité de l'air pour donner de la chaux éteinte $Ca(OH)_2$, qui elle-même se carbonate au contact du CO_2 ambiant en formant de la calcite $CaCO_3$. De ce fait, la teneur en CaO diminue au cours du temps ce qui peut ralentir la réactivité de ces matériaux.

La valorisation des BOF slag demande au préalable une caractérisation physico-chimique approfondie, afin d'avoir une bonne connaissance de leur composition chimique et de trouver le meilleur moyen de les valoriser. La plupart des travaux de recherche publiés sur ce sujet portent sur la caractérisation qualitative des BOF slag et sur la quantification de leur teneur en chaux, suite au problème de gonflement. Cependant, la quantification et l'identification des propriétés des autres phases (C_2S, C_2F, etc.) sont aussi un atout pour l'utilisation des BOF slag que ce soit sous forme d'agrégats ou d'un constituant à part entière du ciment.

Ce travail concerne la caractérisation chimique et physique de différents laitiers d'aciérie (fraîches et vieilles productions). Différentes méthodes d'analyse qualitatives et quantitatives de ces matériaux ont été développées. Les compositions massique et minéralogique ont été déterminées par fluorescence X et diffraction des rayons X. L'arrangement des phases au sein des grains a été observé à la microsonde de castaing couplée avec des analyses EDS afin d'identifier les compositions élémentaires de chaque phase ainsi que les impuretés qu'elles peuvent renfermer. La teneur en chaux libre est déterminée par un dosage acido-basique complété par des analyses thermogravimétriques afin de différencier les teneurs respectives en $Ca(OH)_2$ et en CaO. La teneur en $CaCO_3$ a été déterminée également par cette technique. Des dosages chimiques et des extractions sélectives ont permis de compléter la quantification des phases minérales. Les propriétés physiques ont été étudiées sur une poudre de granulométrie 0/0,125 mm. La surface spécifique a été déterminée par le test Blaine selon la norme EN 196-6. La masse volumique absolue a été mesurée par pesée hydrostatique dans un liquide non réactif. L'évolutivité de ces matériaux a été suivie par dosages des phases CaO, $Ca(OH)_2$ et $CaCO_3$ sur des BOF slag de teneurs initiales en chaux variables et de conditions de conservation différentes.

MOTS-CLÉS : Laitiers de conversion, matériaux de construction, valorisation, chaux libre, carbonatation

USE OF SHAPE MEMORY ALLOY WIRES FOR THE CREATION OF PRESTRESS STATES IN CONCRETE BEAMS

HANH TRAN, ALEKSANDRA DEBSKA, XAVIER BALANDRAUD, JEAN-FRANÇOIS DESTREBECQ

The study deals with the use of shape memory alloys (SMAs) to create prestress states in concrete prismatic beams. Nickel-titanium SMA wires with suitable transformation temperatures are used to this purpose. The wires are first stretched in a martensitic state at ambient temperature. Then they are placed onto the surface of the beams. A thermal cycle is applied to transform the martensite to austenite, in order to activate the shape memory effect in the wires. The strain evolution in the concrete beams is measured with strain gauges. A prestress effect is clearly observed in the beams during the procedure until cooling down to ambient temperature. The influence of the initial stretch of the wires and the transformation temperatures is discussed.

KEYWORDS: *shape-memory alloy, nickel-titanium, concrete, prestress.*

UTILISATION DE FILS EN ALLIAGE À MÉMOIRE DE FORME POUR LA CRÉATION DE PRÉCONTRAINTES DANS LES POUTRELLES EN BÉTON

L'étude traite de l'utilisation de fils d'alliages à mémoire de forme (AMF) pour créer des états de précontraintes dans des poutrelles en béton. Le principe consiste à étirer des fils AMF à l'état martensitique à température ambiante avant de les fixer solidement sur les poutrelles. L'effet mémoire est ensuite activé par élévation de la température de manière à provoquer le retour des fils à l'état austénitique. Cette transformation en déformation gênée provoque l'apparition d'une force de traction dans les fils qui agit comme une force de précontrainte. Cette force est évaluée pour chaque poutrelle testée à partir de la courbure induite, déduite de mesures par jauges extensométriques. Les essais réalisés ont permis de décrire le processus de développement de la force de précontrainte durant la phase d'activation de l'effet mémoire. L'intensité de la force obtenue dépend du nombre de fils et de la pré déformation donnée aux fils à l'état martensitique. Il est mis en évidence que la force finale de précontrainte après retour à température ambiante est bornée par la valeur atteinte pour une valeur particulière de la prédéformation. L'examen de la relation entre la prédéformation et la courbure induite à température ambiante par l'effet de précontrainte indique que l'effet qui limite la force de précontrainte dans les fils résulte d'une production partielle de martensite lors du refroidissement, mais que cet effet n'est pas affecté par le nombre des fils fixés à la poutrelle. Ces résultats montrent que le choix des températures de transformation est un point clé pour assurer la permanence de la précontrainte et éviter les pertes en cas de baisse de température. En conclusion, la présente étude démontre la possibilité d'induire des états de précontrainte dans des poutrelles en béton à l'aide de fils en AMF. Si le coût élevé des alliages Nickel-Titane peut sembler a priori un obstacle à leur utilisation pour la création de précontraintes dans des composants en béton, l'activation de l'effet mémoire par simple élévation de température constitue un avantage par rapport aux procédés classiques de précontrainte. Il existe par ailleurs des AMF à base fer avec des performances moindres que celles des Nickel-Titane, mais de coût mieux adapté à des applications industrielles. Un champ possible d'application pourrait être l'utilisation d'AMF comme méthode alternative de précontrainte pour l'amélioration du comportement ou le renforcement de structures existantes.

MOTS-CLÉS : alliage à mémoire de forme, Ni-Ti, béton, précontrainte

CONCRETE RENOVATION EFFECTIVE DEEP HYDRO IMPREGNATIONS - FIELD EXPERIMENTS

MICHEL DONADIO

Deeply penetrating hydrophobic impregnations can help to increase the design life of a civil engineering structure, by providing an effective chloride barrier. Although its efficiency is somewhat reduced if cracking occurs after the treatment, a considerable reduction in chloride penetration is still achieved. They are also efficient for ASR litigation. Results from field experiments show the positive return on investment when using these types of deeply penetrating hydrophobic impregnation. However, lower active content formulations have a tendency for the active ingredient to remain at the surface and quickly lose efficiency when subjected to weathering. Therefore the right type of product must be selected for each project (e.g. for civil engineering structures subjected freeze and thaw cycles, product satisfaying the class II penetration depth of EN 1504-2 shall be selected).

RÉNOVATION DES BÉTONS EFFICACITÉ DES IMPRÉGNATIONS HYDROFUGES À HAUT POUVOIR DE PÉNÉTRATION RÉSULTATS SUR SITE

Les imprégnations hydrophobes à haut pouvoir de pénétration peuvent contribuer à augmenter la durée de service d'une structure de génie civil en fournissant une barrière efficace à la pénétration des chlorures et autres agents agressifs solubles dans l'eau. Des résultats sur site montrent l'efficacité de ce type d'imprégnation hydrophobe en particulier pour lutter contre les problèmes de corrosion et d'alcali réaction. Toutefois, les produits ayant un faible taux de matière active ont tendance à rester en surface du béton et à perdre rapidement leur efficacité quant ils sont soumis aux intempéries.

De ce fait, le type de produit le plus approprié doit être sélectionné en fonction des particularités de chaque projet; des essais préliminaires devant être réalisés pour déterminer la consommation requise pour obtenir une pénétration donnée. Par exemple, pour un pont en béton armé soumis aux cycles gel dégel et sels de déverglaçage, le produit sélectionné doit satisfaire les essais de gel/dégel et être de classe II (pénétration >10 mm) suivant la norme NF EN 1504-2.

MINERAL FOAMS WITH IMPROVED PERFORMANCES

C. BAUX, C. LANOS, A. PHELIPOT-MARDELÉ

Mineral foam materials represent an alternative to fibrous lightweight products that are to be reconsidered. Following a reminder of the conditions of foam formation in fluid environments we review different foam production systems and provide details concerning gypsum foams. Several types of gypsum foams are achieved by modifying formulation parameters and production conditions. Thermal and mechanical performances of these gypsum foams are then assessed and compared to the ones obtained for cellular and hemp concrete. Physical properties of these foams are analyzed (including pore size, membrane thickness and bubbles connectivity). Relevant results allow the identification of several optimal conditions necessary to mineral foam formation applicable to other mineral binder types.

KEYWORDS: *gypsum foam, density, mechanical strength, thermal conductivity.*

MOUSSES MINÉRALES À PERFORMANCES OPTIMISÉES

Les techniques d'isolation de bâtiments anciens par l'extérieur par des systèmes autoporteurs ou la constitution de parois monocouches thermiquement performantes imposent le développement de matériaux présentant un bon compromis entre performances mécaniques et performances thermiques. L'évolution du contexte réglementaire visant à réduire l'utilisation de certains composés fibreux minéraux (fibre de roche, laine de verre) et composés polymères (résines polyester, polyuréthane) doit également être prise en compte lors de la conception d'un système novateur.

Outre les éco-matériaux tels que les bétons de chanvre, de roseau, de lin, de bois le développement de mousses minérales constitue une alternative qu'il convient de reconsidérer.

L'occlusion d'une bulle gazeuse dans une matrice minérale repose sur un équilibre entre la fluidité du mélange lors de sa réalisation, la tension de surface, l'état de pression, la masse volumique. Les principes physiques conduisant à la formation de telles structures sont rappelés.

Dans un deuxième temps différents systèmes de production de mousses minérales sont passés en revue. Dans de tels systèmes, le caractère alvéolaire des mélanges minéraux est obtenu à l'état fluide en induisant la production d'un gaz, en obtenant la stabilisation par un tensio-actif, en modifiant l'occlusion d'air…

Trois modes de production de mousses alvéolaires sont ensuite comparés. Ils sont appliqués au cas du gypse. La connectivité des bulles, les conditions de cristallisation et d'orientation de la matrice minérale sont étudiées.

Des mousses de gypse de masses volumiques variables (entre 250 et 1500 kg/m^3) sont ensuite produites en utilisant différents agents porogènes et tensio-actifs et en modifiant leur formulation (ratio eau/liant, adjuvant/liant). Les performances mécaniques et thermiques de ces mousses minérales sont évaluées et comparées à celles obtenues sur des matériaux alvéolaires plus complexes à produire (béton cellulaire, béton mousse) ou à celles d'éco-matériaux. Les performances obtenues s'avèrent très pertinentes montrant tout l'intérêt du développement de tels matériaux avec un mode de production compatible avec une formulation limitant l'eau de gâchage et aboutissant à une matrice à performances mécaniques optimisées.

MOTS-CLÉS : mousse de gypse, densité, résistance mécanique, conductivité thermique.

BIOPOLYMERS: A NEW WAY FOR THE PROTECTION OF CONCRETE STEEL REINFORCEMENTS

FEUGEAS FRANÇOISE, ROUX SÉBASTIEN, BUR NICOLAS, TRIBOLLET BERNARD

*The aim of this study is to evaluate an admixture whose active component is an eco-respectful biopolymer having steel corrosion inhibiting properties. Many means of concrete steel reinforcements protection against corrosion are on the market, but few of them are eco-friendly. This study has an environmental stake for the sustainable development of concrete structures improving their aging resistance and using eco-friendly products. Bacteria (*Lactobacillus reuteri*) allow the production of a biopolymer called EPS 180 whose presence as admixture in concrete will improve their eco-friendly quality regarding: (i) their production using eco-respectful products like biopolymers and Ground Granulated Blast Furnace Slag (GGBS for CEM V). Actually, corrosion of rebars is a frequent pathology of civil engineering works against which the means are generally not satisfying the environmental criteria. The biopolymers, produced by bacteria of milk, are harmful for human beings and a little quantity of biopolymers is used for the tested admixture. The samples were manufactured using 2 cement bases including a CEM V that is more eco-friendly than traditional CEM I because containing industrial byproducts. Capillary imbibition tests and water total porosity showed the low influence of the admixture on the pore structure of mortars. After immersion in natural seawater of cement pastes reinforced with steel C15 rebars, electrochemical measurements showed that the biopolymer does not affect the free corrosion potential of reinforcement nor the composition of passive layer but inhibits the reaction cathodic reduction of oxygen.*

UTILISATION DE SUBSTANCES EXTRACELLULAIRES POLYMÉRIQUES COMME INHIBITEURS DE CORROSION DES ARMATURES EN BÉTON

L'objectif de cette étude est d'évaluer un adjuvant dont le principe actif est un biopolymère écorespectueux aux propriétés inhibitrices de corrosion des aciers. Différents moyens de lutte contre la corrosion des armatures des bétons armés sont disponibles sur le marché mais bon nombre d'entre eux ne peuvent pas être considérés comme écorespectueux. L'enjeu de cette étude est le développement durable des ouvrages en béton armé par l'amélioration de leur résistance au vieillissement et par l'utilisation de produits éco-respectueux. Des bactéries (*Lactobacillus reuteri*) sont utilisées pour la fabrication d'un biopolymère appelé EPS 180 dont l'utilisation comme adjuvant dans les bétons va permettre de les rendre plus éco-respectueux dans la mesure ou : (i) leurs armatures sont protégées de la corrosion, (ii) ils sont fabriqués avec des produits éco-respectueux comme les biopolymères et les laitiers de haut fourneaux (CEM V). La corrosion des armatures est en effet une pathologie fréquente des ouvrages de génie civil pour laquelle les moyens de lutte ne sont généralement pas satisfaisants sur le plan environnemental. Les biopolymères, fabriqués à partir de substances extrapolymériques issues de bactéries du lait, sont sans danger pour l'homme et une très petite quantité de ces produits permet d'obtenir l'adjuvant testé. Des échantillons ont été réalisés à partir de deux nuances cimentaires, le traditionnel CEM I et un CEM V, plus écorespectueux car contenant des sous-produits industriels. Des essais d'imbibitions capillaires et de porosité totale à l'eau ont montré la faible influence de l'adjuvant aux biopolymères sur la structure poreuse des mortiers. Après immersion en eau de mer naturelle de pâtes de ciment renforcées d'armature en acier C15, des mesures électrochimiques ont montré que ce biopolymère n'influence pas le potentiel libre de corrosion des armatures ni la composition de leur couche passive mais inhibe de la réaction cathodique de réduction de l'oxygène.

RELIABILITY ANALYSIS OF STAINLESS STEEL COVER PLATE JOINTS

J. AVERSENG, A. BOUCHAÏR, A. CHATEAUNEUF

Stainless steel becomes more and more important in construction, particularly due to its highly ductility and strain hardening capacity. However, an experimental study on cover-plate joints conducted at the LaMI revealed some limits of actual design rules (EN1993-1-4), especially when considering complex failure modes, such as bearing, that involve large deformations. In this study, a non-linear finite element model reproducing the complex behaviour of cover plate joints is used to distinguish the major parameters influencing the behaviour of these joints. A meta-model based on the quadratic response surface method is built from a large set of results and exploited through a reliability approach allowing to quantify the impacts of the different parameters. The objectives are to assess and enrich the available

calculation methods for stainless steel joints in the objective of reliability level of Eurocodes.

KEYWORDS: *stainless steel, joint, bearing, finite elements, reliability.*

ANALYSE FIABILISTE D'ASSEMBLAGES COUVRE-JOINT EN ACIER INOXYDABLE

Les aciers inoxydables sont amenés à jouer un rôle de plus en plus important dans le domaine de la construction. Ils présentent en effet de nombreux points forts, parmi lesquels une grande ductilité et un grand potentiel d'écrouissage permettant une dissipation significative d'énergie sous chargements cycliques, sous chocs, ainsi qu'une redistribution importante d'efforts avant rupture. Ce type d'acier présente, comme autres avantages, une excellente résistance à la corrosion et une meilleure résistance au feu par rapport à l'acier au carbone utilisé en structures. Toutes ces caractéristiques en font un matériau particulièrement intéressant pour des applications en zones d'assemblage, qui peuvent bénéficier de sa grande capacité de déformation et de résistance sous des niveaux élevés de contraintes. Des études récentes sur le comportement mécanique d'éléments de structure en acier ont permis d'apporter des éléments de comparaison avec les exigences de l'EN 1993-1-4 qui constitue une extension des règles établies pour les structures en acier au carbone afin de prendre en compte les particularités apportées par l'acier inoxydable. Une étude a été menée au LaMI sur des assemblages boulonnés, en acier inoxydable, de type couvre-joint qui sont les plus courants. Les résultats issus de cette étude ont permis d'évaluer la validité des expressions analytiques de calcul de la capacité résistante de ces assemblages en considérant les modes de ruine complexes associés à la déformation en pression diamétrale. En effet, une vérification de résistance sous sollicitations ELU peut ne pas suffire à limiter les déformations sous sollicitations ELS. Cette approche est en effet implicitement admise pour l'acier au carbone dont le faible rapport entre les limites ultime et élastique est généralement compris entre 1,1 et 1,5. Or, ce rapport peut dépasser 2 pour les aciers inoxydables austénitiques alors que le rapport des sollicitations entre ELU et ELS est compris entre 1,35 et 1,5. Cette étude expérimentale est complétée par un modèle éléments finis non linéaire, développé sous Cast3m, en vu de représenter de façon réaliste le comportement de ces assemblages. Ce modèle prend en compte la zone de contact entre la partie filetée du boulon et les trous des plats assemblés. La géométrie de l'assemblage a été choisie en vu de favoriser un mode de ruine de type pression diamétrale. La loi force-déplacement, qui illustre le comportement global de l'assemblage, intègre les différentes sources de déformation présentes (sections brute et nette, pression diamétrale et cisaillement du boulon). Les résultats obtenus sont validés par comparaison avec les données expérimentales sur trois assemblages de différentes dimensions. Cette étude numérique a permis de distinguer les paramètres les plus influents sur le comportement des assemblages étudiés qui sont la loi constitutive du matériau, l'épaisseur et la longueur du plat, la pince longitudinale et la largeur de l'assemblage. Cependant, cette approche déterministe ne permet pas de tenir compte de la variabilité des caractéristiques géométriques et matérielles de ces assemblages. Ainsi, une approche fiabiliste est proposée pour évaluer les dispositions de l'Eurocode 3, en vu de donner aux formules de vérification des assemblages en acier inoxydable le même niveau de fiabilité que pour l'acier au carbone. Cette étude contribuerait à enrichir les méthodes de calcul disponibles pour l'acier inoxydable qui présentent un certain conservatisme au niveau des applications structure à cause du manque de données et de retour d'expérience dans le domaine. La méthodologie adoptée pour l'étude fiabiliste s'appuie sur une mise à jour et un paramétrage du modèle éléments finis pour générer des résultats intégrant les variabilités paramétriques. La mise en place du plan d'expérience des résultats numériques permet de construire une base de données de lois de comportement de l'assemblage, en fonction des paramètres géométriques et matériels les plus influents. De cette base, un méta modèle basé sur les techniques de Surfaces de Réponses Quadratiques (SRQ) est construit avec une erreur de calage maintenue inférieure à 5%. Sur le plan déterministe, cette SRQ est comparée aux formules analytiques proposées dans l'Eurocode 3, montrant leur conservatisme dans le cas de l'acier inoxydable. L'analyse fiabiliste est menée sur la SRQ afin d'éviter des temps de calcul excessifs. Cette analyse est basée sur la prise en compte des incertitudes liées aux dimensions géométriques (tolérances de fabrication), aux paramètres de la loi de comportement de l'acier inoxydable et aux charges appliquées à l'assemblage. Deux critères de défaillance ont été considérés : capacité résistante de l'assemblage et déformation excessive sous pression diamétrale du plat assemblé. Pour l'objectif de fiabilité prescrit par les Eurocodes, les règles de dimensionnement sont confrontées aux résultats de l'analyse fiabiliste, en vue de la validation de l'approche de dimensionnement des assemblages en acier inoxydable. Le niveau de conservatisme de l'EC3 est estimé, pour ces assemblages, à travers la comparaison des coefficients partiels de sécurité. La définition de la résistance en pression diamétrale est discutée à partir des résultats fiabilistes considérant le ratio élevé entre la limite ultime et la limite élastique.

MOTS-CLÉS : acier inoxydable, assemblage, pression diamétrale, élément finis, fiabilité.

STUDY OF THE PERFORMANCE OF FRP REINFORCING BARS SUBJECTED TO EXTREME CONDITIONS OF APPLICATION

PERFORMANCE DES ARMATURES COMPOSITES DE PRF SOUMISES À DES ENVIRONNEMENTS D'APPLICATION EXTRÊMES

Mathieu ROBERT[1], Patrice COUSIN[2], Brahim BENMOKRANE[3]

[1]Post-Doctoral Fellow, Department of Civil Engineering., University of Sherbrooke, Sherbrooke, Quebec, Canada, J1K 2R1, Phone: (819) 821-8000 ext. 62967, Fax: (819) 821-7974, E-mail: Mathieu.Robert2@USherbrooke.ca

[2]Research Associate, Department of Civil Engineering, University of Sherbrooke, Sherbrooke, Quebec, Canada J1K 2R1, Phone: (819) 821-8000 ext. 62967, Fax: (819) 821-7974, E-mail: Patrice.Cousin@USherbrooke.ca

[3]NSERC Research Chair Professor in Innovative FRP Composite Materials for Infrastructures, Department of Civil Engineering, University of Sherbrooke, Sherbrooke, Quebec, Canada, J1K 2R1, Phone: (819) 821-7758, Fax: (819) 821-7974, E-mail: Brahim.Benmokrane@USherbrooke.ca

1. INTRODUCTION

Many steel reinforced concrete infrastructures exposed to harsh environments present durability issues and are likely not to reach the lifetime expected or have already attained the service limit. Steel corrosion induced by chlorides and/or carbonation are the main causes of deterioration of steel reinforced concrete structures. The amplitude of the phenomenon and economic factors have pushed research engineers, industries and public institutions to develop new technologies to better protect reinforcing steel or providing non corrosive materials in replacement of steel [1]. In anticipation of offering an alternative material, research works have been conducted to develop and use fibre reinforced polymer (FRP) composites in civil engineering applications.

A composite material may be defined as a material constituted of at least two dissimilar materials providing complementary properties, which offers a better general performance than each of its components [2]. FRP composite materials are composed of reinforcing fibres embedded and protected by a polymeric resin matrix. The main fibres used for civil engineering applications are glass, carbon and aramid fibres. Glass fibre being the main fibre used because of its good properties, high strength/cost ratio, good usability and excellent availability. Mechanical properties of glass fibre reinforced polymer reinforcements depend on the characteristics, orientation and shape of fibre, fibre/matrix volumetric ratio, the bonding at the interface between fibres and matrix and on the manufacturing processing. The function of the resin matrix is to keep the fibres in place, transfer and distribute stresses through fibres, bring a lateral support against buckling under compression and protect fibres from abrasion and surrounding environment. Because of their high chemical resistance, vinylester-based resin is generally used for civil engineering applications [3]. This article deals with the FRP reinforcing bars for concrete structures (figure 1). Several concrete structures using FRP as structural internal reinforcement have been built in North America and worldwide. Also, several design codes and guides dealing with composite material as reinforcement for concrete structures have been developed [4-7]. Also, codes and guides on specification, construction, and certification of FRP reinforcing bars for concrete structures has been issued [8-10].

De nos jours, bon nombre de structures en béton armé ayant été exposées à des environnements agressifs éprouvent des problèmes de durabilité et risquent de ne pas atteindre leur durée de vie utile anticipée ou excèdent déjà cette dernière. La corrosion de l'acier d'armature due aux chlorures et /ou à la carbonatation est la principale cause de détérioration des structures en béton armé. L'ampleur du phénomène et les considérations économiques ont initié le développement de nouvelles technologies permettant de protéger l'armature d'acier contre la corrosion ou de simplement la remplacer par des matériaux moins sensibles à la corrosion [1]. C'est dans cette optique que des recherches ont été orientées vers le développement et l'utilisation des polymères renforcés de fibres (PRF) pour leur utilisation en génie civil.

Par définition, un matériau composite est constitué de l'assemblage d'au moins deux matériaux de nature différente mais complémentaire, créant ainsi un matériau dont les performances générales sont supérieures à celles de chacun de ces composants pris séparément [2]. Les matériaux composites de PRF sont constitués d'un renfort (fibres) protégé et supporté par une résine polymère appelée matrice. Les principales fibres ayant fait l'objet d'études pour leur utilisation en génie civil au cours des dernières années sont les fibres de verre, de carbone et d'aramide. La fibre de verre domine dans la majorité des applications. Sa vaste gamme de propriétés, son rapport résistance/coût élevé, sa disponibilité et sa facilité de mise en œuvre en font la plus importante fibre au niveau industriel. Les propriétés mécaniques des armatures de polymères renforcés de fibres de verre (PRFV) dépendent principalement des caractéristiques des fibres, de leur orientation, de leur forme, de leur rapport volumétrique par rapport à la matrice, de la qualité de l'interface entre les fibres et la résine ainsi que du procédé de fabrication. Le rôle de la matrice est de maintenir les fibres en place, de transmettre et de distribuer les sollicitations mécaniques extérieures au renfort, de fournir un support latéral agissant contre le voilement des fibres sous compression et de les protéger contre l'abrasion mécanique et les conditions environnementales. Les résines de type vinylester sont habituellement utilisées pour les applications du génie civil vu leur bonne résistance chimique [3]. Les applications des composites de PRF en génie civil portent essentiellement sur les armatures de renforcement interne du béton dont il sera question dans le présent article (figure 1). Plusieurs ouvrages utilisant des composites de PRF comme renforcement interne du béton ont déjà été construits en Amérique du Nord et ailleurs dans le monde, et plusieurs codes et guides de calcul traitant de l'armature en matériaux composites pour les structures de béton ont été développés [4-7]. Aussi, des codes et guides de spécifications des propriétés pour l'homologation des produits de composites de PRF pour leur utilisation en génie civil ont été développés [8-10].

Figure 1: GFRP reinforcing bars

One of the biggest challenges for the acceptance of FRP in civil engineering applications concerns their durability and more specifically their capacity to maintain their structural performance in severe and changing environmental conditions of service [11]. The durability of FRP reinforcing rods is related to the three different phases of the material: fibre, resin and interface (figure 2), which may be affected by deteriorations and degradations caused by exposure to various environments and could potentially lead to a reduction of long term durability and performance.

Face au développement sans précédent de nouveaux produits performants, l'industrie de la construction a dû modifier son approche conservatrice, ce qui a permis aux nouvelles technologies liées à l'utilisation des composites de PRF de susciter une attention toute particulière de la part des ingénieurs de réalisation de travaux publics et des gestionnaires de systèmes d'infrastructure. La résistance à l'application à grande échelle des matériaux composites de PRF est fondée en partie sur le manque d'informations sur le comportement à long terme de ces matériaux dans les conditions de service les plus critiques. Un des grands défis actuels à relever quant à l'acceptation des composites de PRF en génie civil concerne la durabilité de ces matériaux et plus spécifiquement leur capacité à maintenir

leur performance structurale dans des conditions environnementales sévères et changeantes [11]. La durabilité des barres d'armature en PRF est en fait liée aux trois composantes fondamentales de tout matériau composite, soit les fibres, la résine, et l'interface entre les fibres et la résine (figure 2). En effet, ces trois composantes peuvent montrées des lacunes ou des traces de dégradation suite à l'exposition à divers environnements pouvant mener à une perte de durabilité et de performances à long terme.

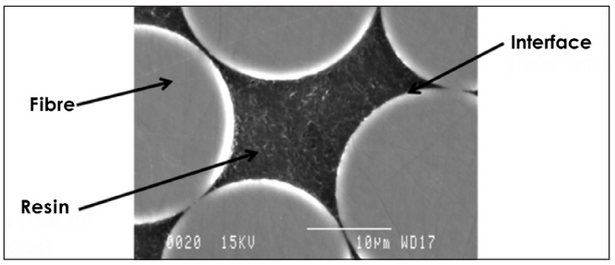

Figure 2: Typical microstructure of GFRP bar

The polymeric component of FRP materials protects fibres against the chemical attack of corrosive ions, especially hydroxyl ions, present in the pore water of the surrounding concrete. The degradation process of GFRP reinforcing bars may be caused by the deterioration of one (or more) of its phase: fibre, resin matrix or interface. The degradation mechanisms are more complex compared to those occurring in a monophasic material, such as steel.
Mechanical properties of GFRP bars are controlled by the fibre component [12]. Once the fibres are not deteriorated, the material will keep most of its mechanical strength and will be able to support the loads. If the protective resin degrades, the fibres located in the outer part of the bar will rupture and the bar resistance will start to decrease. According to Uomoto's work [13], the interface between the glass fibre and resin controls the chemical resistance of GFRP against alkaline corrosion. The increase of the bonding degree at the interface may highly improve the chemical resistance of these materials. Many studies dealing with the resistance of GFRP to alkalis have shown that the alkaline environment of concrete is among the most critical environments for glass fibre [14]. Actually, the main issue is the potential degradation caused by the concrete pore solution, the pH of which may reach 13.5. In alkaline environments, glass fibre may degrade according to several mechanisms, such as corrosion, hydrolysis and leaching. Several studies on the corrosion mechanisms of GFRP reinforcing bars and environmental effects have been published [15-20]. Yilmaz and Glasser [15] describe fibre glass attack by the dissolution of silica (SiO_2) by alkaline ionic species (hydroxyl groups) according to equation (1). In this equation, the first by-product, SiOH, forms a gel on the glass fibre surface, whereas the second one, SiO^-, is dissolved.

Au niveau de la résistance chimique des matériaux composites de PRF, la résine protège les fibres contre l'attaque des ions nocifs provenant de l'environnement et spécialement les ions OH^- de la solution interstitielle du béton. Le processus de dégradation des PRFs est une conséquence de la dégradation de un ou de plusieurs de ses constituants ainsi que de l'interface entre ceux-ci. Une détérioration des fibres, de la résine et de l'interphase entre fibres et résine gouvernent la durabilité des armatures de PRFV compliquant le mécanisme de dégradation des armatures de PRF comparativement à celui de l'acier d'armature.
Comme les propriétés mécaniques des barres de PRFV sont contrôlées par les fibres [12], si celles-ci ne sont pas détériorées, les armatures de PRFV peuvent dans la plupart des cas supporter la charge mécanique. Si la résine protégeant les fibres est attaquée et dégradée, les fibres se brisent de la surface vers le centre de la barre réduisant la résistance. Selon Uomoto [13], l'interface entre les fibres de verre et la résine contrôle la résistance des barres de PRFV contre les alcalis et son amélioration est efficace pour augmenter la résistance aux alcalis des armatures de PRFV jusqu'à un degré élevé. Beaucoup d'études réalisées sur la résistance des barres de PRFV aux alcalis [14] ont montré que le milieu alcalin du béton constitue l'un des environnements les plus critiques pour les fibres de verre. A l'heure actuelle, le principal souci est la dégradation potentielle causée par la solution interstitielle du béton dans laquelle le pH peut atteindre 13,5. Dans un environnement alcalin, les filaments de fibres de verre sont susceptibles de se dégrader suite à une combinaison de mécanismes allant de la corrosion, à l'hydrolyse et à la lixiviation. Plusieurs études ont été publiées sur les mécanismes de dégradation des armatures de PRFV et sur les effets environnementaux [15-20]. Yilmaz et Glasser [15] expliquent l'attaque des fibres de verre par le processus de dissolution de la silice (SiO_2) par des ions alcalins (ions hydroxydes) selon l'équation (1). Dans l'équation (1), le sous-produit SiOH forme un gel sur la surface des fibres de verre tandis que le deuxième sous- produit SiO^- se retrouve en solution.

$$\left[-\overset{|}{Si}-O-\overset{|}{Si}\right]+OH^- \rightarrow 2-\overset{|}{Si}-OH(solid)+\overset{|}{Si}-O^-(solution) \quad (1)$$

This dissolution can cause a weight loss and a diameter decrease of the glass fibre, reducing the mechanical properties of the bar. Another mechanism of degradation, resulting from the reaction of silica with the alkaline environment, is the formation of calcium silicate expressed in the equation (2) [18].

Cette dissolution cause la perte de poids et de diamètre de la fibre entraînant par le fait même une perte de la résistance et du module élastique. Un autre mécanisme de dégradation résultant de la réaction de la silice avec le milieu alcalin est la formation de silicate de calcium exprimé dans l'équation (2) [18].

$$Ca(OH)_2 + SiO_2 \rightarrow CaSiO_3 + H_2O \quad (2)$$

Different studies have shown that alkaline environments are more critical than water at the beginning of the degradation but become almost similar later [21]. The mecha-

nisms of fibre degradation by water were discussed by Mercier and Maréchal [22]. They have reported that immersion of glass fibres in water can lead to their dissolution through the diffusion of hydroxide ions outside the glass fibres, called lixiviation. This lixiviation is exacerbated by the amount of alkalis present inside the glass fibres and the temperature of the wet environment. After lixiviation, the formation of large amounts of hydroxides leads to an increase of the pH of the solution. Then, these hydroxide ions attack the fibre surface, leading to the formation of cracks and micro cracks, which decrease the resistance and can result in a premature fracture of glass fibres [23-24].

The diffusion of moisture and alkalis from the concrete into the polymer matrix can lead to changes in the mechanical, thermo mechanical and physico-chemical properties of GFRP reinforcing bars. The main effect of the absorption is the possible degradation of the polymer resin through hydrolysis or plasticizing effects. The chemical resistance of thermoset resins is largely governed by the chemical nature of the polymer chain. Weak adhesion of the polyester resin can result in serious deterioration when hydroxyl ions penetrate into the structure. The matrix could be damaged through cracking and micro cracking due to volume expansion during moisture absorption, whereas its stiffness could be reduced by plasticization. A subsequent mechanism of degradation by breaking of polymer chains triggered by hydrolysis and leaching out of low molecular weight material from the bulk resin could further damage the matrix. Meanwhile, the matrix formed by vinylester, which contents much less ester units as compared to polyester, is also hardly deteriorated by hydroxyl ions compared to a polyester matrix [19, 24, 25].

The interface (or interphase) is a heterogeneous region of some micrometers in thickness between the matrix and fibres. This interface plays a critical role as it insures the load transfer between the fibres and matrix [24, 26]. The application of a coupling agent (silane) at the surface of the fibres improves the bonding at the interface and protects the fibre surface against environmental attacks. However, this chemical bond is not stable in presence of humidity and alkalis and it is particularly subjected to long-term degradation [24, 26]. When moisture and alkali ions diffuse through the composite, this bonding is gradually reduced, leading to the deterioration of the interface. The resistance of this interface is directly related to the amount of coupling agent which cannot be extracted from the fibre surface.

A high level of sustained load combined with chemical attacks, increases the degradation of the interface. Different types of damage may be observed: (1) osmotic cracking of the matrix, (2) differential swelling and (3) delamination of the fibres.

The extensive research performed on FRP reinforcements led to the publication of codes and design guides on the use of the FRP reinforcing bars and prestressing tendons as reinforcement for new or existing concrete structures. Design codes and guides in North-America and Japan [4-7] provide strength reduction factors or material factors to account for the effects of environmental conditions, creep under sustained loads, and fatigue under repeated loads. The use of an environmental reduction factor (C_E) was a simple solution to overcome the difficulties caused by the absence of data on the long-term durability of FRP's. Several codes require an environmental reduction coefficient of approximately 0.7. This factor mitigates the use of new generation of FRP products, which are less vulnerable to environmental attacks than the previous products. These environmental reduction coefficients are considered to be very conservative and are being criticized by many experts and engineers, because they are based on the behaviour of the early generations of FRP products that were of lower quality and on limited long-term behaviour data.

This paper presents an overview of several aspects affecting the long-term durability of GFRP reinforcing bars subjected to laboratory accelerated aging simulating the genuine environment of application. The durability of GFRP bars submitted to various environmental conditions such as wet concrete, extreme temperatures and micro cracks-inducing pre-loading will be evaluated though the residual mechanical properties.

La plupart des études ont montré que l'environnement alcalin est plus critique que l'eau au début de la dégradation mais qu'après un certain temps leurs effets sont presque similaire [21]. Les mécanismes de dégradation des fibres par l'eau ont été discutés par Mercier et Maréchal [22], rapportant des phénomènes de dissolution des fibres dans l'eau et la diffusion des ions hydroxyde hors de la structure de verre, appelé lixiviation. Celle-ci est accentuée par la quantité d'alcalis présente dans la structure de verre et la température de l'environnement humide. Suite à la lixiviation il y a une formation d'excès d'hydroxydes ce qui augmente par conséquent le pH de la solution. Ces ions attaquent ensuite la surface des fibres générant ainsi des fissures qui dégradent la résistance et peut résulter en une fracture prématurée ou une rupture des fibres de verre [23-24].

L'humidité et les alcalis du béton diffusent à l'intérieur des polymères organiques à différents degrés amenant des changements dans les caractéristiques mécaniques, thermomécaniques et physico-chimiques de ces derniers. Le principal effet de l'absorption se manifeste sur la résine elle-même à travers l'hydrolyse ou la plastification. La durabilité chimique des résines thermodurcissables est gouvernée en grande partie par la nature chimique de la chaîne de polymère. La structure des résines polyester et vinylester consiste en de longues chaînes moléculaires formées par la polymérisation de composés organiques non saturés. Celles-ci sont elles- mêmes réticulées pour former un réseau dense et rigide. La grande résistance chimique des résines vinylester préserve leur résistance et assure leur durabilité. Cette performance chimique de la résine vinylester dans un environnement alcalin a été confirmée par plusieurs études [19, 24, 25].

L'interface est une région hétérogène entre la matrice et les fibres et elle mesure quelques micromètres d'épaisseur. Cette interface joue un rôle critique dans une armature de composite dans le transfert de charge entre fibres et la matrice [24, 26]. L'usage d'un agent de couplage (silane)

sur la surface des fibres de verre améliore la résistance de l'interface fibre/matrice et protège la surface des fibres contre les attaques environnementales. Cependant la liaison chimique entre l'agent de couplage silane et la surface des fibres de verre n'est pas stable face à l'humidité et aux alcalis et est particulièrement susceptible à une dégradation à long terme [24, 26]. Lorsque l'humidité et les alcalis diffusent dans le composite, cette liaison est détruite progressivement et cause des dommages à l'interface. La résistance de l'interface du composite est directement liée à la quantité d'agent de couplage ne pouvant pas être extraite de la surface des fibres.

Combinée à l'attaque chimique, un chargement mécanique soutenu élevé accentue la dégradation de l'interface fibres/matrice. Différents dommages peuvent être subis par la région de l'interface : (1) fissuration osmotique de la matrice, (2) gonflement différentiel de l'interface et (3) décollement.

Les progrès réalisés par les différentes recherches ont permis d'élaborer des codes et manuels de calcul sur l'utilisation des produits de PRF dans le renforcement et la réhabilitation des structures de génie civil (nouvelles structures et structures existantes). Les codes et guides de calcul nord-américains et japonais [4-7] fournissent des facteurs de réduction de résistance en tenant compte des efforts soutenus, de la fatigue et des conditions environnementales. Les guides canadiens semblent être moins conservateurs quant aux valeurs de contraintes admissibles prises en compte dans le calcul mais elles restreignent l'utilisation de certains types de PRF dans certaines conditions [27]. Le développement d'un coefficient de réduction environnementale (C_E) permettait de surmonter rapidement les difficultés causées par l'absence de données sur la durabilité à long terme des PRF et de permettre aux ingénieurs de calcul d'utiliser plus rapidement ce nouveau matériau. Plusieurs codes et guides de conception utilisent couramment des coefficients de réduction environnementale conservateurs d'environ 0,7. Cette réduction majeure ne permet pas aux nouvelles générations de barres de PRFV de bénéficier pleinement de la grande résistance qu'elles possèdent. Ces coefficients de réduction environnementale conservateurs sont remis en question par plusieurs chercheurs et ingénieurs. En effet les valeurs de ces coefficients sont basées sur des matériaux de première génération de moindre qualité et sur un nombre limité de données sur le comportement à long terme des barres de PRFV recueillis par la réalisation de vieillissements accélérés en laboratoire ne reflétant pas toujours adéquatement les conditions réelles d'application.

Dans cet article synthèse, un survol de plusieurs aspects de la durabilité à long terme de composites de PRFV soumis à des vieillissements accélérés en laboratoire simulant l'environnement d'application sera effectué. Il sera question d'évaluer la durabilité des barres de PRFV en termes de réduction des propriétés mécaniques lorsque soumises à différentes conditions environnementales telles que le béton humide, les températures extrêmes d'application et suite à des pré-chargements initiant la création de fissuration dans la microstructure des barres.

2. EXPERIMENTAL PROGRAM

2.1. Material

Experimental results presented in this paper were obtained during research work conducted in the laboratory of durability of FRP composite materials of the department of civil engineering of the University of Sherbrooke, Sherbrooke, Canada. Sand-coated glass FRP reinforcing bars manufactured by a Canadian company (Pultrall inc., Thetford Mines, Quebec, Canada) are used in this study (Figure 1). The bars are made of continuous E-glass fibres embedded in vinylester matrix using a pultrusion process. The GFRP bars used have a nominal diameter of 12 mm.

Les résultats expérimentaux présentés dans cet article ont été obtenus à partir de travaux de recherche réalisés dans le laboratoire de durabilité des matériaux composites de PRF du département de génie civil de l'Université de Sherbrooke, Sherbrooke, Québec, Canada. Des barres de PRFV de 12 mm de diamètre à recouvrement de sable fabriquées par Pultrall Inc., Thetford Mines, Québec, ont été utilisées (figure 1). Les barres ont été fabriquées à partir de fibres de verre continues de type E imprégnées avec une résine vinylester par un procédé de pultrusion.

2.2. Test Plan

2.2.1. Aging in Moist Concrete

Accelerated aging of GFRP reinforcing bars embedded in concrete, used in this study, were designed to simulate an aggressive alkaline environment of saturated concrete. The embedded samples were immersed in tap water. The technique currently used is believed to be representative of the real life situation. Indeed, the pH of the solution surrounding the bars is a result of the absorption of water by the concrete, thus allowing the liberation of the alkaline ions of the concrete directly in the bars environment. The aging was performed by immersing the mortar-wrapped GFRP bars in a wood container specially manufactured for the study. Figure 3 shows the containers that were tightly closed with a polyethylene film on their inner surfaces. A polyethylene sheet was also placed on top of the wood containers to avoid excessive evaporation of water during the conditioning. Bars were spaced from each other and from the bottom of the container to allow the free circulation of the solution between and around the GFRP bars. Furthermore, the water level was kept constant throughout the study to avoid a pH increase which could be due to a water level decrease and a significant increase of the concentration of the alkaline ions in the solution. The temperatures of immersion were chosen to accelerate the degradation effect of aging; however, they were not too high to produce any thermal degradation mechanisms. The specimens were completely immersed at three different temperatures (23, 40 and 50ºC) and were removed from the water after four different periods of time (60, 120, 180 and 240 days). After each period, usually six GFRP bars were removed from the water, tested under tension to compare their tensile strength retention values to those of the refer-

ence specimens. Microstructural and physical analyses were also performed after immersion.

Des conditionnements par immersion en eau d'aqueduc ont été subis par certaines des barres d'armature utilisées dans cette étude pour simuler le milieu alcalin agressif du béton d'enrobage. Ces barres étaient préalablement enrobées d'un mortier consistant en trois parties de sable, une partie de ciment Type 10 (Type I, ASTM) et un rapport eau/ciment de 0,40, menant à un pH de 12,15 mesuré par extraction de la solution interstitielle après les conditionnements. Cette technique de vieillissement représente une bonne simulation de la réalité. Le pH de la solution en contact avec les barres d'armature est le résultat de l'absorption d'eau par le mortier, permettant ainsi la libération des ions alcalins du béton dans l'environnement immédiat des barres. Ces vieillissements ont été réalisés par l'immersion complète des barres enrobées dans des bacs de vieillissement spécialement fabriqués à cet effet. Un film de polyéthylène a aussi été placé par-dessus les bacs pour éviter une évaporation excessive de l'eau pendant les conditionnements. Les barres ont été espacées les unes des autres ainsi que du fond du bac pour permettre la libre circulation de la solution autour de ces dernières. La figure 3 montre les barres positionnées dans leur bac d'immersion. De plus, le niveau d'eau a été gardé constant tout au long de l'étude pour éviter une augmentation du pH de la solution de vieillissement qui aurait pu être causée à une augmentation de la concentration des ions alcalins dans la solution. La dégradation a été accélérée par l'utilisation de la température, tout en choisissant cette dernière afin d'éviter l'introduction de mécanismes de dégradation thermique. En plus des propriétés physiques et microstructurale des barres, la rétention des propriétés en traction des barres ont été mesurés après différents temps d'immersion (60, 120, 180 et 240 jours).

Figure 3: Wood container built for aging of the cement mortar-wrapped GFRP bar specimens

2.2.2. Extreme Temperatures

Properties of GFRP bars submitted to extreme temperatures were measured. All GFRP bar specimens were tested under extreme temperature conditions using a MTS environmental chamber cooled by liquid nitrogen (Figure 2). Sub-zero temperatures equal to -100º, -80º, -60º, -40º, -20º and also 0ºC were chosen to simulate the effect of Nordic climate on GFRP bars. The temperatures below -60 ºC were used to amplify the effects of temperature on mechanical and microstructural behaviour of the FRP materials. Elevated temperatures equal to 50º, 100º, 150º, 200º, 250º and 325ºC were chosen to simulate short-term environmental conditions in the case of fire. All the tests were conducted using a steady-state temperature (heat then load) regime. To be sure that the temperature at the core of the GFRP bars reached the desired temperature, an extra GFRP bar was kept in the same conditions and its core temperature was monitored using a thermocouple that was inserted in the core of this bar. When the desired temperature was reached (from the thermocouple reading), it was kept constant and the GFRP specimens were tested at that temperature.

Les propriétés des barres soumises à des températures extrêmes d'applications ont été mesurées. Pour ce faire, tous les échantillons testés ont subis des conditionnements en chambre environnementale sous des températures contrôlées. Une chambre environnementale MTS refroidie à l'azote liquide et directement installée sur la presse d'essai a été utilisée (figure 4). Des températures sous le point de congélation égales à -100º, -80º, -60º, -40º, -20º et 0ºC ont été utilisées pour simuler les effets d'un climat nordique canadien sur le comportement des barres d'armature. Des températures élevées égales à 50º, 100º, 150º, 200º, 250º et 325ºC ont été choisies pour simuler les conditions à court terme dans le cas d'un incendie. Pour s'assurer que les

Figure 4: Test setup for tensile tests at controlled temperature

échantillons testés atteignent bien la température désirée, tous les échantillons ont été placés dans la chambre environnementale au moins deux heures avant les essais mécaniques et un thermocouple a été fixé sur un échantillon de référence pour mesurer la température au centre de ce dernier. Les propriétés physiques et microstructurale, ainsi que les propriétés en traction ont été mesurées suite à ces vieillissements à températures contrôlées.

2.2.3. Pre-Loading of GFRP Bars Samples

The effect of cracking and microcracking on the long-term behaviour of GFRP bars was evaluated. GFRP bars were preloaded at 80 percent of their theoretical ultimate tensile strength (854 MPa) (UTS) to initiate cracks and microcracks in polymer and glass fibres. All bars were preloaded under tension according to ASTM D 7205 standard. The test was carried out using a MTS 810 testing machine and load was increased until required load was reached. For each tensile preloading, the specimen was mounted on the press with the steel pipe anchors gripped by wedges of the upper and the lower jaws of the machine. The rate of loading ranged between 250 and 500 MPa/min and the maximum load was maintained for 10 minutes, and then was reduced at the rate of 250 to 500 MPa/min. The study of the long-term behaviour of pre-loaded GFRP bars was performed by using accelerated aging in moist moist concrete, as described above.

L'effet de la fissuration sur les comportements à long terme des barres de PRFV a été mesuré. Pour ce faire, des barres ont été préalablement chargées jusqu'à 80% de leur charge ultime théorique en traction (854 MPa) pour ainsi initier des fissures et des microfissures dans le polymère ou les fibres de verre. Toutes les barres ont été pré-chargées sous tension en suivant la norme ASTM D 7205. Les chargements ont été réalisés en utilisant une presse hydraulique MTS 810 et en augmentant la charge jusqu'au niveau désiré, soit 80% de la charge ultime en traction. Le montage expérimental utilisé est le même que celui présenté à la figure 4. Pour chaque pré-chargement en traction réalisé, l'échantillon était installé sur la presse avec des ancrages d'acier à ses extrémités et fixé aux mâchoires supérieure et inférieure de la machine. Le taux de chargement se situait entre 250 et 500 MPa/min et le niveau de chargement a été maintenu pendant 10 minutes avant que la charge soit enlevée à un taux de déchargement allant de 250 à 500 MPa/min. L'étude du comportement à long terme des barres fissurées par pré-chargement a été réalisée par des vieillissements en solution après enrobage dans un mortier, comme décrit précédemment.

2.3. Mechanical Characterization

Tensile tests were performed on bars aged in solution, bars subjected to controlled temperatures and bars pre-loaded at 80 percent of their UTS. The measured tensile strengths of the bars before and after exposure were considered as a measure of the durability performance of the specimens. All bars were tested under tension according to the ACI 440.3R-04 B2. Each specimen was instrumented with a Linear Variable Differential Transformer (LVDT) to capture the elongation during testing. The test was carried out using a Baldwin testing machine and the load was increased until failure. For each tensile test, the specimen was mounted on the press with the steel pipe anchors gripped by the wedges of the upper and the lower jaw of the machine. Just before the test, the concrete cover was carefully removed from the middle third of the specimens with a hammer to avoid any damage to the bar. The rate of loading ranged between 250 and 500 MPa/min. The applied load and bar elongation were recorded during the test using a data acquisition system monitored by a computer. Due to the brittle nature of GFRP, no yielding occurs and the stress-strain behaviour was linear.

Des essais de traction ont été réalisés sur les barres conditionnées en solution, vieillies à températures contrôlées et pré-chargées en traction en vue de mesurer la rétention des propriétés en traction après vieillissements. Tous les essais de traction réalisés sur les barres de PRFV conditionnées l'ont été selon la norme ASTM D 7205. Chaque échantillon était instrumenté avec un extensomètre permettant d'enregistrer l'élongation pendant l'essai. Les essais ont été réalisés à l'aide d'une presse hydraulique MTS 810 en augmentant la charge jusqu'à la rupture de l'échantillon. Tout comme pour les pré-chargements, les échantillons étaient installés sur la presse avec des ancrages d'acier à leurs extrémités et fixés aux mâchoires supérieure et inférieure de la machine. Dans le cas des échantillons testés suite à des vieillissements avec enrobage de mortier, ce dernier a été soigneusement enlevé de l'échantillon juste avant l'essai en utilisant un marteau. Le taux de chargement se situait entre 250 et 500 MPa/min. La charge appliquée et l'élongation de l'échantillon ont été enregistrées pendant les essais en utilisant un système d'acquisition de données relié à un ordinateur. Aucune déformation plastique n'est survenue lors des essais et les courbes de contraintes déformations étaient dans tous les cas linéaires, exprimant le caractère fragile des barres de PRFV.

2.4. Physical Characterization

2.4.1. Density Measurements after Pre-Loading

The density of the reference and preloaded composite samples without mortar cover was determined by displacement in water according to ASTM D792 (Test Method A) using a Mettler AG204 DeltaRange® microbalance. The specimens (3 per sample) were weighed in air (P_S). Then, each specimen was placed in a cylinder, which was filled with water. After having weighted the cylinder containing the sample and water (P_{S+W}), the specimen was removed and the cylinder was filled with water up to the same level. The cylinder containing only water was then weighed (P_W). If considering the density of water as equal to 1.00, the density of the sample, ρ, was obtained using the equation Eq. 3.

La densité des échantillons de référence et des échantillons pré-chargés à 80% de leur charge ultime en traction a été

déterminée par mesure de déplacement d'eau selon la norme ASTM D792 (méthode A), en utilisant une balance Mettler AG204 DeltaRange®. Les échantillons (3 par type d'échantillons) ont tout d'abord été pesés dans l'air (P_{ech}) avant d'être placé dans un cylindre gradué subséquemment rempli d'eau. Après avoir pesé le cylindre contenant l'échantillon et l'eau, ($P_{ech+eau}$), l'échantillon était enlevé du cylindre et ce dernier était rempli d'eau jusqu'au même niveau puis pesé (P_{eau}). En considérant que la densité de l'eau est égale à 1, la densité de l'échantillon, ρ, a été obtenu en utilisant l'équation (3).

$$\rho = Ps / Ps + Pw + Ps + w \quad (3)$$

A drop of density was considered as a confirmation of the increase of void content and as a measurement of the damage caused to the GFRP bars by preloading.

Une chute de la densité après le pré-chargement est considérée comme une confirmation de l'augmentation du taux de vide dans l'échantillon testé et une mesure du dommage causé par le pré chargement.

2.4.2. Scanning Electron Microscopy (SEM)

SEM observations and image analysis were performed to evaluate the microstructure of aged specimens and the integrity of the GFRP material after exposure to extreme temperatures. All specimens were first cut, polished and coated with a thin layer of gold–palladium by a vapor-deposit process for observing in the SEM. Microstructural observations were thereafter performed on a JEOL JSM-840A SEM. These observations were conducted to determine the potential degradation of the polymer matrix, possible glass fibers and interface.

Des observations en MEB et l'analyse d'image ont été réalisés pour évaluer les changements de microstructure des échantillons conditionnés et l'intégrité des matériaux de PRF ayant subis des vieillissements à températures extrêmes. Tous les échantillons ayant été observés en MEB ont tout d'abord été coupés, puis polis et revêtus d'une couche d'or-palladium par un procédé d'électrodéposition. Les observations microstructurales ont été réalisées à l'aide d'un microscope JEOL JSM-840A. Ces observations sont réalisées pour déterminer la dégradation potentielle de la matrice, des fibres ou de l'interface entre les fibres et la matrice.

2.4.3. Differential Scanning Calorimetry (DSC)

DSC was used to obtain information on the thermal behavior and characteristics of polymeric materials and composites such as glass transition temperature (Tg), melting point, curing process, crystallinity, thermal stability, and relaxation. In the study, specimens weighting 12 to 15 milligrams were cut from different GFRP samples (non-conditioned and conditioned) and placed in aluminum pans and were analyzed using a TA Instruments DSC Q10 calorimeter. Specimens were heated from 25°C to 195°C at a rate of 5ºC/min. Glass transition temperature was determined for both the specimens in accordance with ASTM E 1356 standard. If decrease in T_g was observed for conditioned samples, it was an indication of plasticizing effect or chemical degradation. Aged sample maintaining a lower T_g than for the reference showed an irreversible chemical degradation.

La DSC est utilisée pour obtenir des informations sur le comportement thermique des matériaux polymères et des composites, comme la température de transition vitreuse (Tg), le point de fusion, le processus de cure, la cristallinité, la stabilité thermique et la relaxation. Dans la présente étude, des échantillons coupés de barres de référence (non-conditionnées et conditionnées) ont été placés dans des cupules d'aluminium et analysés à l'aide d'un calorimètre TA Intruments DSC Q10. Les échantillons ont été chauffés de 25° à 195°C à un taux de 5ºC/min. La Tg a été déterminée selon la norme ASTM E 1356 pour tous les échantillons testés. Une chute de Tg observée chez un échantillon ayant subi un conditionnement, est l'indication d'une dégradation chimique ou d'une plastification de la matrice. La DSC permet donc de confirmer les effets des vieillissements en laboratoires sur la structure du matériau polymère testé.

2.4.4. Dynamical Mechanical Analysis (DMA)

DMA was used to determine changes in the mechanical properties of FRP composite materials either under isothermal conditions or as a function of temperature. Glass transition temperature, stiffness, and damping properties could also be measured by this technique. Dynamic mechanical testing provided a method to determine elastic and loss moduli of materials and could be used to evaluate and compare composite parameters, such as adhesion and interface properties, some of the processing treatments, curing, and stress state. In the present study, some GFRP bar specimens were tested by DMA under flexure to measure the effect of temperature on the flexural modulus of elasticity for temperatures ranging from -100º to 350ºC. The tests were carried out according to ASTM D 5023 standard and using a TA Instruments DMA Q800 testing machine equipped with a three point bending device. The span between the supports was kept equal to 50 mm. The rate of loading is chosen to allow a deflection of 10 microns.

La DMA est utilisée pour déterminer les changements de propriétés mécaniques des PRF sous des conditions isothermes ou en fonction de la température. La température de transition vitreuse et la rigidité des matériaux peuvent aussi être mesurées par cette technique. La DMA permet donc la détermination des modules élastique et de perte du matériau testé et peut être utilisée pour évaluer et comparer certains paramètres reliés au composite, tels que l'adhésion et les propriétés d'interface, le paramètres de moulage, la cure du polymère et l'état de contrainte. Dans la présente étude, des échantillons de barres de PRFV ont été testés en flexion pour mesurer l'effet de la température sur le module élastique en flexion pour une gamme de températures allant de -100º à 350ºC. Les essais ont été réalisés selon la norme ASTM D 5053 en utilisant une machine d'analyse TA Instruments DMA Q800 équipée d'un montage de flexion en trois points. L'espacement entre les appuis a été fixé à 50 mm et le taux de chargement a été choisi pour permettre une déflection constante de 10 microns.

2.4.5. Thermo gravimetric Analysis (TGA)

TGA determined the changes in weight of FRP composites as a function of temperature. The TGA could be used to calculate glass fibre and moisture contents and to study the thermal stability of matrix. In the study, the thermal stability of specimens was investigated by using TGA, and the weight loss traces were recorded as function of temperature in the range of 20–800 °C according to ASTM E 1868 standard. The mass variations recorded could give indications concerning the different phenomena of degradation occurring in the matrix and also explain the loss of mechanical properties observed at very high temperatures. Thermo gravimetric analysis was carried out by using TA Instrument Q500 TGA equipment under air with a heating rate of 20°C min^{-1}.

La TGA détermine les changements de masse des composites de PRF en fonction de la température. La TGA peut être utilisée pour calculer le taux de fibres et d'humidité des échantillons testés, ainsi que pour étudier la stabilité thermique du polymère utilisé comme matrice. Dans la présente étude, la stabilité thermique des échantillons a été étudiée selon la norme ASTM E1868 en utilisant la TGA. Les pertes de masse ont été enregistrées en fonction de la température entre 20º et 800ºC permettant de déterminer l'effet des températures extrêmes d'application sur les barres d'armature en PRFV testées. Les analyses thermogravimétriques ont été réalisées à l'aide d'un analyseur de type TA Instrument TGA Q500 dans un atmosphère d'air en utilisant un taux de chauffe de 20ºC/min.

3. EXPERIMENTAL RESULTS

3.1. Effect of Immersion

3.1.1. Tensile Strength Retention

Table 1 shows the experimental results obtained during the tensile tests concerning the ultimate strength of aged bars tested after immersion. Figure 5 shows the retention of the ultimate strength of aged bars according to the duration of immersion of embedded bars at various temperatures. As shown in Table 1, the tensile strength for unconditioned bar was equal to 788 ± 54 MPa. Note that the tensile strength of bars was reduced to 665 ± 62 MPa after 240 days exposure to water at 50°C.

Figure 5 shows a slight decrease of the ultimate tensile strength with immersion duration. The recorded results show that the longer the time of immersion, the larger the loss of resistance. Furthermore, it is clear that the temperature of immersion affects the loss of resistance. It can be seen that for duration of immersion of 8 months, the loss of resistance is equal to 16, 10 and 9 % at 50º, 40º and 23ºC, respectively. This phenomenon is due to the increasing of the diffusion rate of the solution and to the acceleration of the chemicals reaction of degradation with the temperature of immersion, leading to a larger absorption rate of the solution for the same time of immersion and accelerated reaction of degradation. The absorption of solution can lead to a degradation of the fibres and fibre/matrix interface, leading to a loss of the ultimate tensile.

Le tableau 1 montre les résultats expérimentaux obtenus pendant les essais de traction des échantillons enrobés de mortier et conditionnés par immersion en solution à différentes températures et temps d'immersion. La figure 5 montre la rétention de la résistance ultime en traction en fonction de la durée d'immersion et de la température de conditionnement des barres enrobées. Comme présenté au tableau 1, la résistance en traction des barres de référence non conditionnées est égale à 788 ± 54 MPa. Cette résistance chute à 665 ± 62 MPa après une immersion de 240 jours dans l'eau à 50ºC.

La figure 5 montre pour sa part une légère diminution de la résistance en traction avec l'augmentation du temps d'immersion. Les résultats enregistrés montrent que plus le temps d'immersion est grand, plus la perte de résistance est grande. De plus, il apparaît clair que la température de vieillissement affecte la perte de résistance en traction. La figure 5 montre que pour une immersion de 8 mois, la perte de résistance est égale à 16, 10 et 9% à 50º, 40º et 23ºC, respectivement. Ce phénomène est dû à l'accroissement du

Time of immersion (days)	Temperature (ºC)	Mean Tensile Strength (MPa)	COV (%)
0	23	788	6,9
60	23	753	8,2
	40	755	3,7
	50	767	3,8
120	23	702	2,0
	40	666	7,8
	50	720	3,2
180	23	717	2,6
	40	708	4,8
	50	711	2,5
240	23	714	3,5
	40	708	7,1
	50	665	9,3

Table 1: Experimental tensile strength of reference specimens and specimens aged in moist concrete

taux de diffusion de la solution dans l'échantillon et à l'accélération de la réaction chimique de dégradation à mesure que la température d'immersion augmente. Ces phénomènes mènent donc à un plus grand taux d'absorption à saturation et à une dégradation plus rapide des propriétés du matériau testé. De façon générale, l'absorption de solution peut mener à la dégradation des fibres et de l'interface entre les fibres et la matrice, menant à une perte de résistance ultime en traction.

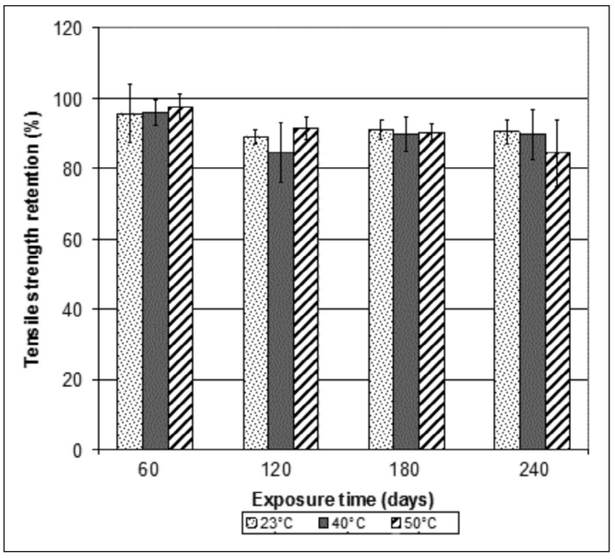

Figure 5: Tensile strength retention of conditioned GFRP bars aged in moist concrete at 23°, 40°, and 50°C

Figure 6 shows the change in the elastic modulus of aged bars with time of immersion at various temperatures. Indeed, it can be seen from the measured results that after 240 days, the loss of elastic modulus is negligible and all aged bars are not affected by the higher temperature or the exposure to moist concrete. This result shows that elastic modulus of bars is not affected by aging in concrete environment.

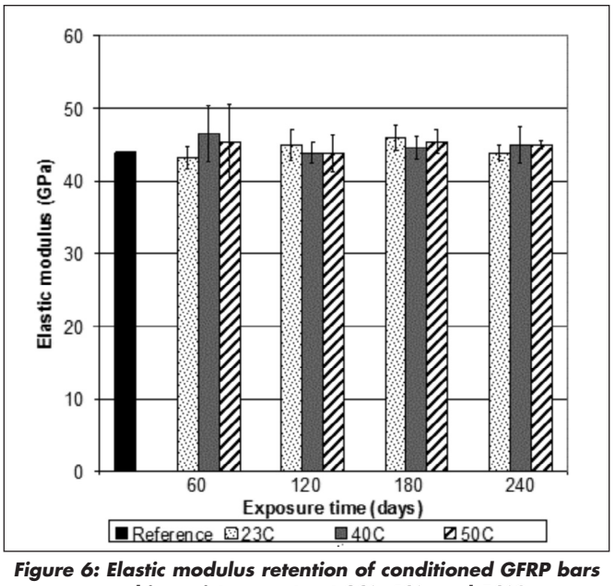

Figure 6: Elastic modulus retention of conditioned GFRP bars aged in moist concrete at 23°, 40°, and 50°C

La figure 6 montre les changements de module élastique des barres conditionnées en fonction du temps d'immersion à différentes températures. Il peut être observé à la figure 6 que même après 240 jours d'immersion, la perte de rigidité du composite est négligeable et qu'aucune des barres n'est affectée par les températures élevées ou le mortier humide. Ces résultats montrent clairement que la rigidité des composites n'est pas affectée par les vieillissements en mortier humide simulant les vraies conditions d'application.

3.1.2. Change in Density

Table 2 shows the measured density for reference sample and samples preloaded at 80 percent of the UTS. As expected, higher the load level, lower the density. In fact, a loss of 15 percent of the density was measured after preloading of the GFRP bar specimen at 80 percent of the UTS. This result could be explained due to the creation of cracks and microcracks by preloading of GFRP bars. Matrix cracking and debonding at fibre/matrix interface cause an increase of void content of the GFRP bar and decrease in the measured density. This result was in accordance with microstructural observations performed by SEM (Figure 8).

Le tableau 2 montre la densité mesurée pour les échantillons de référence et pré-chargés à 80% de leur charge ultime en traction. Comme envisagé, l'application d'un niveau de chargement élevé (80% de la charge ultime en traction) mène à une diminution de la densité de l'échantillon. En effet, une diminution d'environ 15 % de la densité à été observée. Ce résultat peut être expliqué par la création de fissures et de microfissures durant l'étape de pré-chargement des barres de PRFV. La fissuration de la matrice polymère et le délaminage à l'interface entre les fibres et la résine peuvent causer une augmentation du taux de vide de la barre de PRFV et en diminuer la densité. La fissuration et la microfissuration de la barre ont été confirmées en microscopie électronique à balayage (figure 8).

Condition	Measured Density	COV (%)
Reference	2,12	2,1
Pre-loaded at 80% of the UTS	1,81	1,8

Table 2: Experimental density measured before and after pre-loading of GFRP bars

3.1.3. Effect on Tensile Properties of Pre-Loaded Bars

Table 3 shows the experimental results obtained during the tensile tests concerning the ultimate strength and the modulus of elasticity of reference and pre-loaded (80% UTS) bars tested after 60, 120, 180 and 240 days of immersion in water at different temperatures.

Le tableau 3 montre les résultats expérimentaux (résistance ultime en traction et module d'élasticité) obtenus durant les essais de traction de barres pré-chargées à 80% de leur charge ultime en traction (854 MPa) puis immergées dans l'eau pendant 60, 120, 180 ou 240 jours à différentes températures.

Time of immersion (days)	Temperature (°C)	Mean Tensile Strength (MPa)	COV (%)	Mean Modulus of Elasticity (GPa)	COV (%)
0	23	854	2	43	2
60	23	846	5	44	3
	40	847	6	43	3
	50	838	4	43	4
120	23	849	2	42	5
	40	832	8	43	4
	50	837	3	44	2
180	23	836	3	42	4
	40	823	5	43	6
	50	808	3	41	4
240	23	810	4	43	3
	40	784	7	42	2
	50	768	9	43	2

Table 3: Experimental tensile strength of reference specimens and pre-loaded specimens aged in moist concrete

Results presented in Table 3 show slight decrease (6 to 11%) of the ultimate tensile strength after 240 days of immersion of pre-loaded bars embedded in mortar. This decrease was similar to the loss of tensile strength measured on same bar subjected to same conditionings but without preloading. This phenomenon was due to the increasing of diffusion rate of the solution into the sample due to the presence of cracks and microcracks and to the acceleration of chemical reactions of degradation with the temperature of immersion, leading to a larger absorption rate of the solution for the same time of immersion. The higher absorption of solution could lead to a higher degradation of the fibres and fibre/matrix interface, leading to a loss of the ultimate tensile.
Concerning the stiffness of embedded pre-loaded GFRP bars after aging in the water, it was seen from the measured results presented in Table 3 that after 240 days, the loss of elastic modulus was negligible and all aged bars were not affected by the higher temperature or the exposure to moist mortar. This result showed that elastic modulus of bars was not affected by aging in concrete environment and was in accordance with the results found by testing similar bars subjected to same aging but without pre-loading.

Les résultats présentés au tableau 3 montrent une légère chute (6 à 11%) de la charge ultime en traction après 240 jours d'immersion à 50°C de barres pré-chargées et enrobées de mortier. Cette chute est similaire à la perte enregistrée pour le même type de barres conditionnées sans avoir été pré-chargées et fissurées (voir tableau 1). La diminution de résistance en traction peut être expliquée par l'augmentation du taux de diffusion de la solution dans l'échantillon avec l'augmentation de la température d'immersion, menant à un taux d'absorption plus élevé pour un même temps d'immersion et à l'accélération des réactions chimiques de dégradation. L'absorption de solution, d'autant plus facilitée par la présence de fissures dans la microstructure des barres pré-chargées en traction, peut mener à une dégradation de l'interface entre les fibres et la résine, expliquant la perte de résistance en traction avec les vieillissements en béton humide.
En ce qui a trait à la rigidité des échantillons pré-chargés puis vieillis en béton humide pendant 240 jours, il peut être vu au tableau 3 que le perte de module élastique est négligeable et que les barres vieillies ne sont pas affectées par les températures élevées ou l'exposition au béton humide. Ces résultats expérimentaux sont similaires à ceux trouvés pour les mêmes barres mais conditionnées sans pré-chargement en traction, montrant que la présence de fissuration n'affecte pas le module élastique des barres conditionnées en béton humide.

3.1.4. Effect on Failure Mode

The tensile test of unconditioned specimens, specimens aged in moist concrete at 50°C during 240 days and pre-loaded specimens aged in moist concrete at 50°C during 240 days showed an approximately linear behaviour up to failure. Specimens failed through the rupture of fibres. The failure was accompanied by the delamination of fibres and resin, as shown in Figure 7. From this observation, it could be concluded that the aging in moist concrete or the presence of pre-existing cracks and microcracks due to the pre-loading of bars, have no significant effects on the failure mode occurring during tensile tests.

La figure 7 montre que le mode de rupture des échantillons de référence, des échantillons conditionnés en béton humide à 50°C pendant 240 jours et des échantillons pré-chargés à 80% de la charge ultime en traction puis vieillis en béton humide à 50°C pendant 240 jours, est le même. À partir de cette observation, il peut être conclu que le pré-chargement des barres de PRFV, et la présence de fissures et de microfissures dans la microstructure des barres, n'ont pas d'effets significatifs sur les propriétés à long-terme des échantillons testés.

3.1.5. Microstructural Effect of Pre-Loading

The micrographs of Figure 8 show the longitudinal bar surface of reference and GFRP bar pre-loaded at 80 percent of the UTS. In particular, the fibres and the interface between the fibres and the resin should be observed. Observations of these interfaces and of the microstructure in general demonstrated that the pre-loading affected the microstructure of GFRP bar. The only visible damage occurred at the fibre level since the elongation at the rupture was lower for the fibres compared to the polymer matrix. No damage occurred at the matrix and fibre/matrix interface, even at very high stress level (up to 80 percent of the UTS). These observations were in accordance density measurements in the way that the increase of microcracking at high stress levels leads to a decrease of density.

Les micrographies présentées à la figure 8 montrent la coupe longitudinale d'une barre de référence non-conditionnée et d'une barre pré-chargée à 80% de sa charge ultime en traction. Les fibres et l'interface entre les fibres et la résine doivent être observées. L'observation de ces interfaces et de la microstructure en général démontre que le pré-chargement affecte la microstructure de la barre de PRFV puisque des fibres semblent avoir été fissurées par l'application de la charge. Il peut aussi être observé qu'aucun dommage significatif n'est visible au niveau de la résine ou de l'interface entre les fibres et la résine, même après l'application d'une grande charge (80% de la charge ultime de traction). Les seuls dommages visibles sont au niveau des fibres puisque la déformation des fibres est limitée comparativement à celle de la matrice polymérique.

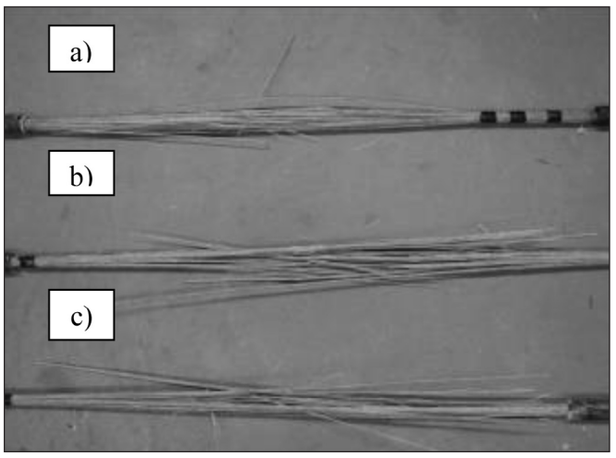

Figure 7: Typical failure mode for GFRP bars: a) reference, b) bar aged in moist concrete at 50°C during 240 days c) bar pre-loaded at 80% of the UTS and aged in moist concrete at 50°C during 240 days.

3.1.6. Microstructural Effect of Aging in Moist Concrete

The visual and microstructural observations of reference and pre-loaded bars showed no significant damage after 240 days of immersion in the tap water at the highest temperature (50ºC). The micrographs of Figure 9 show the fibres/matrix interface for reference and pre-loaded bars aged in moist concrete at 50ºC during 240 days. Observation of these interfaces and of the microstructure, in general, demonstrate that the conditionings of mortar-wrapped bars in water do not affect the microstructural properties of the GFRP bars, even if the bars show pre-existing cracks or microcracks. The micrographs of external surfaces of unconditioned specimen, specimen aged in moist concrete at 50ºC during 240 days and specimen pre-loaded at 80 percent of the UTS and aged in moist concrete at 50ºC during 240 days are shown in Figure 10. The comparison of these micrographs shows that there was no significant damage occurring to mortar-wrapped GFRP bar surface, even at high temperature (50ºC) and when bar presents pre-existing cracks and microcracks.

Les observations visuelles et microstructurale des barres enrobées de mortier et immergées 240 jours dans l'eau à 50ºC ne montrent aucun dommage significatif autant pour les barres de référence que pour les barres pré-chargées.

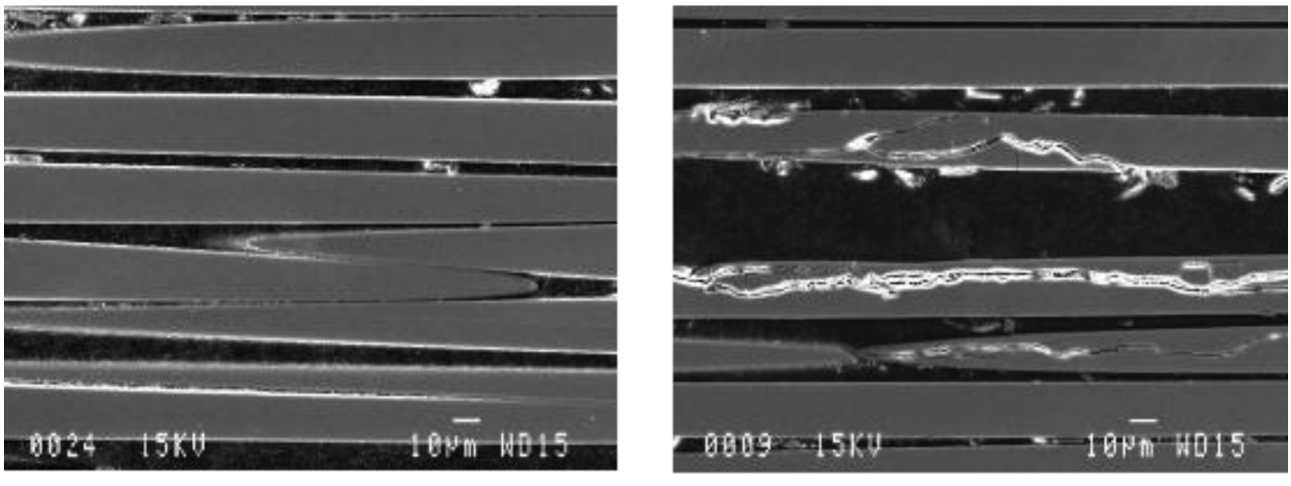

Figure 8: Micrograph of longitudinal GFRP bar surface pre-loaded under tensile load: a) Reference GFRP bar at low magnification, and b) GFRP bar loaded at 80% of the UTS at high magnification

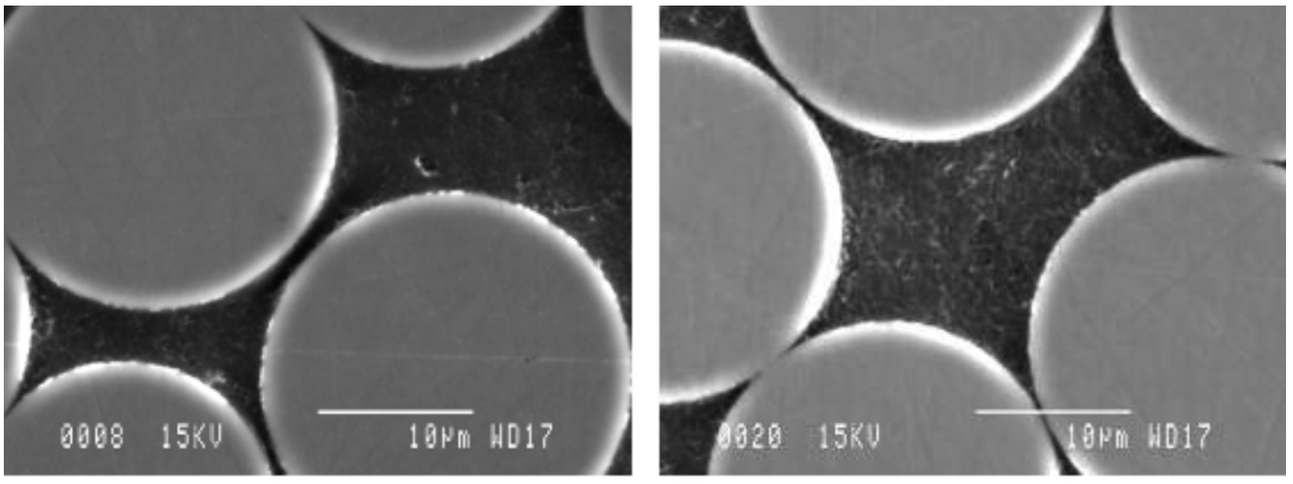

Figure 9: Micrographs of fibre/matrix interface (X3000) of: a) unconditioned GFRP bar specimen, b) Conditioned GFRP bar specimen aged in moist concrete at 50°C for 240 days.

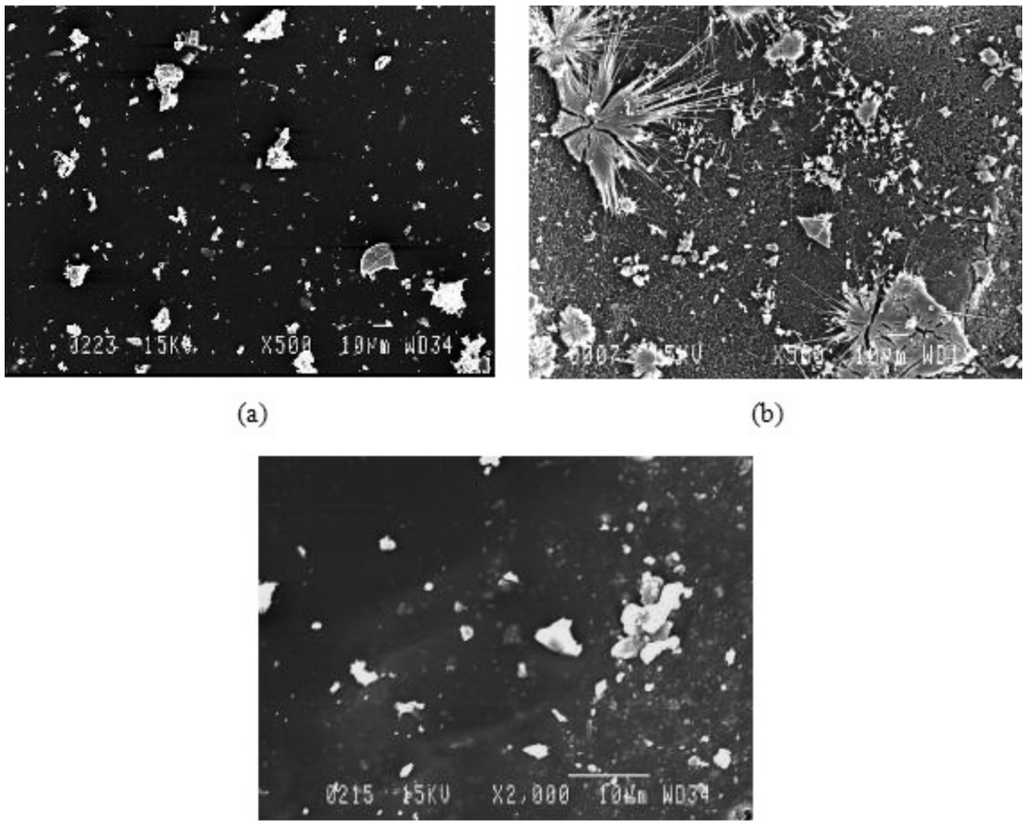

Figure 10: Micrographs of external surfaces for : a) reference, b) bar aged in moist concrete at 50°C during 240 days, c) bar pre-loaded at 80% of the UTS and aged in moist concrete at 50°C during 240 days.

La figure 9 montre les micrographies des interfaces fibres/résine pour les mêmes échantillons. L'observation de ces interfaces et de la microstructure en général démontre que les conditionnements dans l'eau de barres enrobées de mortier n'affectent pas leur microstructure même si ces dernières sont fissurées. Les micrographies de la figure 10 montrent les surfaces externes d'une barre de référence non-conditionnée, d'une barres non pré-chargée immergée 240 jours dans l'eau à 50°C et d'une barre pré-chargée à 80% de sa charge ultime en traction puis immer-

gée dans l'eau à 50°C pendant 240 jours. L'observation de ces micrographies montre clairement qu'aucune dégradation matricielle significative ne survient chez les barres enrobées de béton puis immergées à haute température (50°C) même si ces dernières présentent des fissures initiées par pré-chargement

3.1.7. Effect on Polymer Matrix

Table 4 presents the glass transition temperature (T_g) values found by DSC for unconditioned specimen, specimen aged in moist concrete at 50°C during 240 days and specimen pre-loaded at 80 percent of the UTS and aged in moist concrete at 50°C during 240 days. Note that for the unconditioned and aged samples, the T_g corresponding to the second heating run is higher than that of the first scan. This shift indicates that the samples were not fully cured and that a post-curing phenomenon occurred during the second heating run. However, it can be seen from the results presented in Table 4 that no significant changes of the T_g value occur after aging in water at 50°C for 240 days, even for pre-loaded bars. This result shows that no major effect on the thermal properties of the resin, which could occur after conditioning of mortar-wrapped FRP bars, was detected by DSC.

Le tableau 4 montrent les valeurs expérimentales de la température de transition vitreuse (T_g) pour l'échantillon de référence non-conditionné, la barre immergée 240 jours dans l'eau à 50°C et la barre pré-chargée à 80% de sa charge ultime en traction puis immergée dans l'eau à 50°C pendant 240 jours recueillis par calorimétrique différentielle à balayage. Il est à noter que pour un même échantillon, la T_g recueillie lors de la deuxième chauffe du matériau est plus élevée que celle recueillies lors de la première. Cette augmentation indique que la matrice polymère de l'échantillon en question n'est pas complètement polymérisée et qu'un phénomène de postcure est survenu lors de la deuxième chauffe, expliquant l'augmentation de la Tg. Il est possible de voir à partir des résultats présentés au tableau 4 qu'aucun changement significatif de la Tg n'est survenu suite aux vieillissements par immersion à haute température de barres enrobées de béton, fissurées ou non. Ces résultats montrent que les immersions n'affectent pas les propriétés thermiques de la résine polymère servant de matrice pour les barres de PRFV.

3.2. Effect of Extreme Temperatures

3.2.1. Effect of Extreme Temperatures on Mechanical Properties

Figure 11 shows the relation between the tensile, shear and flexural strength of GFRP bars and the test temperature respectively. Figure 12 presents the relationship between the flexural modulus of elasticity (Storage Modulus (SM)) and temperature in the range of -100° to 350°C. The SM (flexural modulus) was used to measure the effect of temperature on the stiffness of the FRP material. The drop of SM (flexural modulus) beginning around 120°C corresponded to the glass transition of the polymer and the lower plateau to the viscoelastic state.

La figure 11 montre la dépendance de la résistance en traction des barres de PRFV avec la température d'essai. Pour sa part, la figure 12 présente la relation entre le module élastique en flexion (Storage Modulus (SM)) et la température d'essai sur une échelle allant de -100° à 350°C. Le module élastique en flexion est utilisé pour mesurer l'effet de la température sur la rigidité des barres de PRFV testées. La chute du module en flexion débutant vers 120°C correspond à la température de transition vitreuse du polymère et le plateau inférieur correspond à l'état viscoélastique de ce polymère. Les écart-types sur les mesures sont présentées directement sur la figure 11.

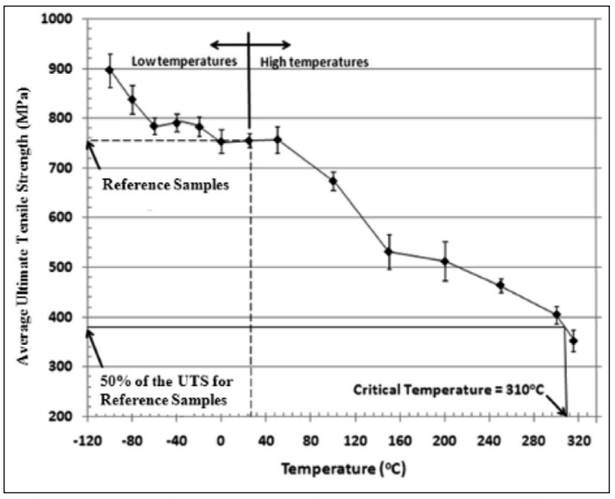

Figure 11: Tensile strength of GFRP bars tested at different temperatures

Condition	Temperature (°C)	Time of immersion (days)	T_g 1st run (°C)	T_g 2nd run (°C)
Reference			105	134
Embedded in moist concrete	50	240	104	129

Table 4: Glass transition Temperature measured by DSC

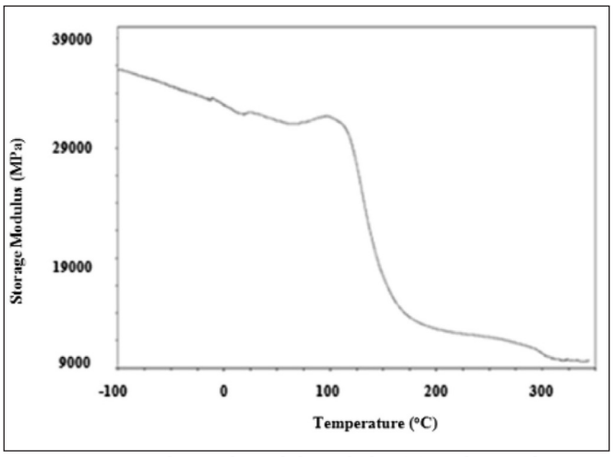

Figure 12: Flexural modulus of elasticity of GFRP bar specimen found by DMA between -100° and 350°C

Three different zones were identified in Figure 11: 1) the reference plateau between -40° and 50°C; 2) the zone where the stiffness increasing at temperatures lower than -50°C; and 3) the mechanical strength decreasing zone for temperatures near and above the glass transition temperature (T_g) of the polymer. The mechanical strengths between -40° and 50°C were stable. In this range of temperatures, the molecular chain mobility of the polymer did not change since the temperature was below T_g. This result showed that for standard environmental conditions of Nordic countries as Canada and north of USA (temperature ranging from -40 to 50 °C), the mechanical properties of GFRP bars were not changed. For temperatures lower than -50°C, the molecular chains mobility of the polymer decreased, leading to an increase of the mechanical stresses needed to rupture the material. Below T_g (around 120°C), the matrix was in a glassy state. When increasing the temperature and reaching the decomposition region, the breaking of molecular bonds started and the ductility of the material increased, leading to a decrease of mechanical strengths and stiffness of the material. At very high temperatures (greater than 300°C), strong degradation of the polymer occurred (combustion, oxidation…) and load transfer provided by the matrix was severely reduced.
If the critical temperature for FRP internal reinforcements is found from a tensile strength loss of 50 percents, such as for steel reinforcements, the results presented in Figure 11 can be used to determine the critical temperature for tested GFRP bars. Based on the experimental results, the critical temperature is equal to 310°C which is similar to the critical temperature found by Bisby and Kodur [28] for similar GFRP bars, and lower than the critical temperature of steel reinforcement, which is close to 500°C.

Trois différentes zones peuvent être identifiées sur la figure 11: 1) le plateau de référence entre -40 et 50°C , 2) la zone de températures sous -50°C, marquée par une augmentation de la rigidité, et 3) la zone de chute des propriétés mécaniques à des températures au-dessus de la température de transition vitreuse (T_g) du polymère. Il est donc clair que les propriétés mécaniques sont stables entre -40° et 50°C. Dans cet intervalle de température, la mobilité des chaines moléculaires du polymère ne change pas puisque la température est sous la T_g de ce dernier, expliquant la stabilité des résultats. Ce résultats montre que pour les conditions environnementales standard des pays nordiques comme le Canada et le nord des États-Unis, marqués par des températures allant de -40° à 50°C, les propriétés mécaniques ne sont pas significativement affectées. À des températures sous -50°C, la mobilité des chaines moléculaires du polymère décroît, menant à une augmentation des contraintes nécessaires à la rupture du matériau. Sous Tg (autour de 120°C), les polymères se trouvent dans un état plutôt vitreux. Lorsque la température est augmentée et que la région de décomposition est atteinte, les liens moléculaires commencent à se briser entraînant une augmentation de la ductilité du polymère et à une chute de la résistance mécanique et de la rigidité du matériau. À température très élevée (plus de 300°C), une dégradation sévère du polymère survient (combustion, oxydation…) et le transfert de charge assuré jusque là par la matrice polymère est sévèrement réduit.
Si la température critique d'utilisation des renforcements internes en PRF est calculée à partir d'une réduction de 50% de la résistance en traction, comme c'est le cas pour l'acier d'armature, les résultats présentés à la figure 11 peuvent être utilisés pour déterminer cette température critique pour les barres d'armature en PRFV testées. La température critique mesurée est donc égale à 310°C approximativement, laquelle est semblable à la température critique trouvée par Bisby et Kodur [28] pour des barres de PRFV, comparativement à 500°C pour l'acier standard.

Figure 13 shows the failure mode for unconditionned and specimens exposed to temperature of 150°C during 2 hours. The tensile test of unconditioned specimens showed approximately a linear behavior up to the failure at any temperature. Specimens failing through the rupture of fibres were accompanied by delamination of the fibres and matrix. A similar, but less dramatic failure was observed for specimens tested at high temperatures. It this case, it was noted that the delamination of fibres and matrix was more important than for unconditioned specimens. It was noted that the ultimate elongation slightly decreased at low temperatures but no significant change was noted at high temperatures. The increase of the tensile strength and flexural modulus and the decrease of ultimate elongation were constant in the temperature range. No ductile-brittle transition occurred in the GFRP materials at low temperature, contrary to steel which could present a ductile-brittle transition between -20° and -30°C [29].

La figure 13 montre le mode de rupture pour un échantillon de référence non-conditionné et pour un échantillon conditionné pendant deux heures et testés à 150°C. Les essais de traction des différents échantillons montrent un comportement plutôt linéaire jusqu'à la rupture. La rupture était dirigée par la rupture des fibres et était accompagnée d'un délaminage des fibres de la résine. Une rupture similaire mais moins dramatique a été observée pour les échan-

tillons testés à hautes températures. Dans ce cas, il a été noté que le délaminage des fibres et de la matrice était plus important que pour les échantillons de référence. Il a aussi été noté qu'une légère baisse de l'élongation à la rupture survenait à basse température, mais aucun changement signification n'a été noté à haute température. L'augmentation de la résistance en traction et du module élastique en flexion, ainsi que la diminution de l'élongation à la rupture sont toutes deux constantes dans l'intervalle de températures testées. Aucune transition ductile-fragile n'est survenue à basse température pour les barres de PRFV, contrairement à l'acier pouvant présenter une telle transition vers -20º ou -30ºC [29].

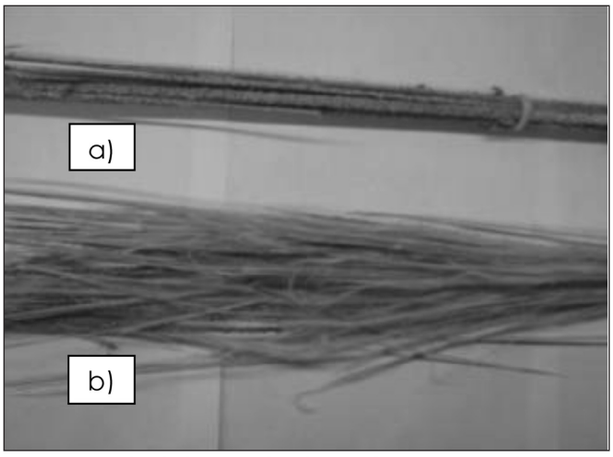

Figure 13: The failure mode of GFRP bars : a) tested at room temperature, and b) tested at 150°C.

3.2.2. Effect on Polymer Matrix

Figure 14 shows the mass variation of specimens as a function of temperature measured by TGA. It was seen that major weight loss occurred between 300 and 450ºC. This important drop, up to 18%, was due to the thermal degradation of the polymer. At these temperatures, thermal degradation occurred and the molecular chains of the polymer broke, leading to the formation of microcracks both at the fibre/matrix interface and in the matrix phase (Figure 15). The weight losses measured by TGA showed a major degradation of the resin from 300ºC to 450ºC. Below this range of temperatures of degradation, the properties were recovered when the GFRP specimens were heated to the desired temperature and then tested at the ambient temperature. At this point, the experimental results suggest that irreversible loss of mechanical properties occurred above 300ºC.

La figure 14 montre la perte de masse des échantillons de PRFV mesurée par TGA en fonction de la température. Il peut être vu qu'une perte de masse majeure survient entre 300º et 450ºC. Cette importante chute de près de 18%, est due à la dégradation thermique du polymère. À ces températures, une dégradation thermique survient et les chaînes moléculaires du polymère se brisent, menant à la formation de microfissures dans la matrice et à l'interface entre les fibres et la résine (figure 15).

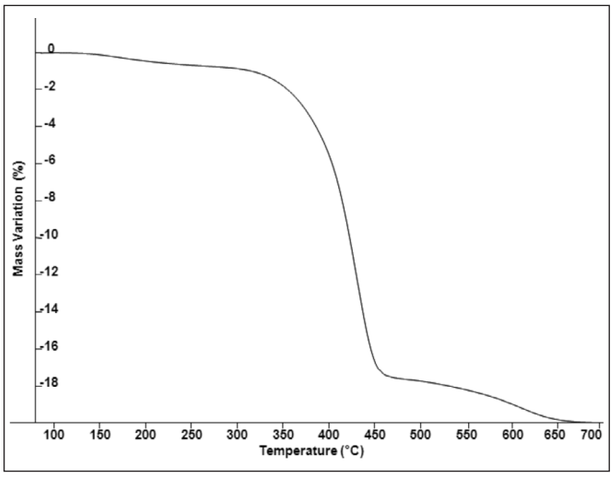

Figure 14: Mass variation of GFRP bar specimen when heated between 20° and 800°C.

Table 5 shows T_g measured by DSC for reference and specimen heated at 350ºC for 2 hours. Noted that, for reference samples, an exothermic peak corresponding to post-curing occurred after T_g. The T_g of the reference specimen was equal to 113ºC, whereas the specimens heated at 350ºC for 2 hours was equal to 67ºC. This showed that the matrix weakened when heated at elevated temperatures, which explained the causes of the observed large decrease of mechanical properties.

Le tableau 5 présente les T_g obtenus par DSC pour un échantillon de référence et un échantillon chauffé pendant 2 heures à 350ºC. Il est à noter qu'un pic exothermique correspondant à une postcure du polymère est survenu après la T_g dans le cas de l'échantillon de référence. La T_g de l'échantillon de référence est égale à 113ºC, tandis que celle de l'échantillon chauffé à 350ºC pendant 2 heures est de 67ºC. Ce résultat montre clairement une dégradation de la matrice lorsque cette dernière est chauffée à des températures élevées (350ºC). Cette dégradation, menant à un affaiblissement de la matrice polymère, peut expliquer la chute significative des propriétés mécaniques.

Condition	Temperature (ºC)	Duration (hours)	T_g 1st run (ºC)	T_g 2nd run (ºC)
Reference	20	2	113	135
High Temperature	350	2	68.5	67

Table 5: Glass transition Temperature measured by DSC

3.2.3. Microstructural Effect of Extreme Temperatures

The polymer matrix degradation was confirmed by microstructural analysis. The micrographs presented in Figure 15 show the polymer, the fibre and the interface between the fibres and matrix for reference specimen and specimen conditioned at 350ºC for two hours. The comparison of these micrographs showed that significant dam-

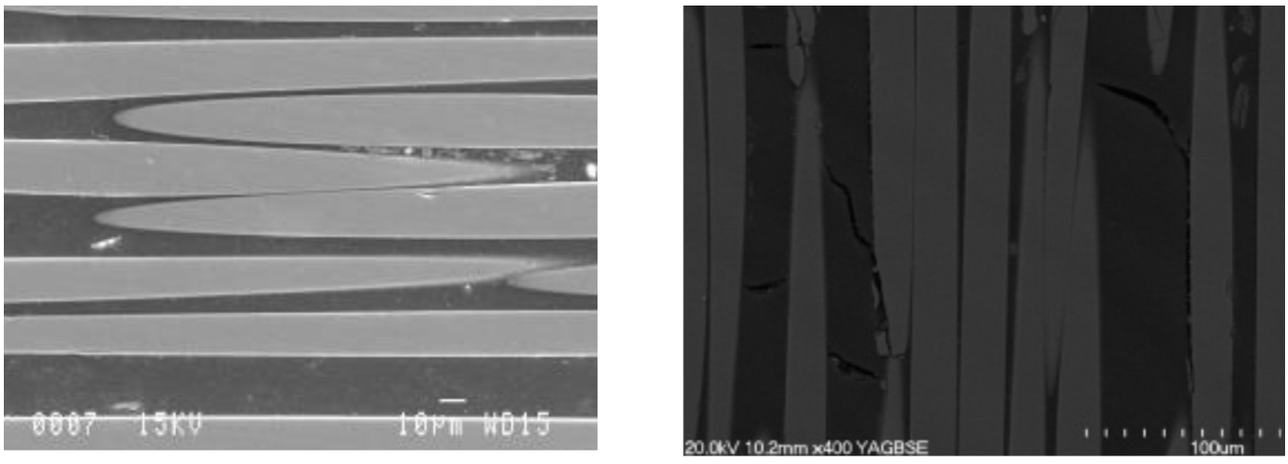

(a) (b)

Figure 15: Micrographs of longitudinal fibre/ matrix interface of: a) unconditioned GFRP bar specimen, b) Conditioned GFRP bar specimen aged in air at 350°C for 2 hours.

age occurred for GFRP bar conditioned at 350ºC (Figure 15b) as compared to reference sample (Figure 15a). The presence of microcracks in specimen tested at 350ºC confirmed the degradation of the polymeric matrix and explained the loss of mechanical properties.

La dégradation de la matrice polymère est confirmée par l'analyse microstructurale. Les micrographies présentées à la figure 15 montrent le polymère, les fibres et l'interface entre les fibres et la résine pour un échantillon de référence et un échantillon conditionné à 350ºC pendant 2 heures. La comparaison de ces micrographies montre que des dommages significatifs sont survenus pour les barres de PRFV conditionnées à 350ºC (figure 15b) comparativement à l'échantillon de référence (figure 15a). La présence de microfissures dans l'échantillon conditionné à 350ºC confirme la dégradation de la matrice polymérique et explique la perte de propriétés mécaniques.

4. CONCLUSIONS

Based on the results of this study the following conclusions may be drawn:

1. The aging of mortar-wrapped GFRP bars in tap water is significantly less pronounced than traditional aging in simulated pore solution. The loss in the tensile strength and the microstructural/physical effects were significantly reduced.
2. Even at high temperature (50ºC), where the environment is the more aggressive, the change in tensile strength is minor. For example, increasing the temperature of the solution from 40 to 50ºC during 240 days results in a decrease of the tensile strength retention by 10 to 16% of the original tensile strength.
3. No significant microstructural changes were observed after 240 days immersion of GFRP bars embedded in concrete in tap water at 50ºC. The interfaces between the bars and concrete and between the resin and the fibres don't seem to be affect by the moisture absorption and high temperatures.
4. The polymer matrix is not affected by moisture absorption and high temperatures: no changes of the glass transition temperature occur as observed by differential scanning calorimetry.
5. High stress level (more than 60% of the UTS) leads to fibre cracking, resulting in an increase of moisture uptake at saturation and a decrease of GFRP density related to the higher void content.
6. After 240 days water immersion of pre-loaded bar embedded in mortar, the retention rate of tensile strength are 95, 96 and 98% at 50, 40, and 23ºC, respectively.
7. No significant microstructural changes were observed after 240 days immersion of GFRP bars embedded in mortar in tap water at 50ºC after a pre-loading of 80% of the UTS. The interface between the resin and the fibres did not seem to be affected by the moisture absorption and high temperatures.
8. DSC analysis did not show any non-reversible degradation of the polymer chemical structure due to the aging of pre-loaded bars in moist concrete at 50ºC during 240 days. No changes of the glass transition temperature occur as observed by differential scanning calorimetry.
9. Mechanical properties (tensile, shear and flexural strengths) and flexural elastic modulus of GFRP bars increased when the temperature decreased. This phenomenon was due to the increase of stiffness of the amorphous polymer matrix due to low temperatures.
10. At severe temperatures experienced in Northern regions such as Canada (temperature ranging from -40º to 50ºC), the tensile strength and flexural modulus of elasticity appeared to be stable, which showed that the mechanical behavior of GFRP bars was not affected by temperature in this range of temperature.

La présente étude permet de tirer les conclusions suivantes :

1. *Le vieillissement par immersion dans l'eau de barres de PRFV enrobées de béton est moins sévère et reflète mieux la réalité que les vieillissements traditionnels en solution alcaline. La perte de résistance en traction et les effets microstructuraux et physiques sont significativement réduits.*
2. *Même à haute température (50°C), lorsque l'environnement est le plus agressif, les changements de résistance en traction sont mineurs. Par exemple, augmenter la température de vieillissement de 40° à 50°C mène à une diminution du taux de rétention de la résistance en traction initiale de 6%.*
3. *Aucun changement microstructural n'a été observé sur les barres enrobées de béton et immergées dans l'eau à 50°C pendant 240 jours. Les interfaces entre les barres et le béton et entre la résine et les fibres ne semblent pas avoir été affectées par l'absorption d'humidité et par les températures élevées.*
4. *La matrice polymérique n'est pas affectée par l'absorption d'humidité et les températures élevées. Les mesures en calorimétrie différentielle à balayage n'ont montrées qu'aucun changement de la température de transition vitreuse ne survenait.*
5. *Le pré-chargement en traction des échantillons de PRFV à des niveaux de chargement élevés (plus de 60% de la charge ultime en traction) mènent à la fissuration des fibres. Cette initiation de fissures crée une augmentation de l'absorption d'humidité à saturation et une diminution de la densité du composite de PRFV. Ces effets physiques sont liés à l'augmentation du taux de porosités des échantillons pré-chargés vu la fissuration des fibres.*
6. *Après 240 jours d'immersion dans l'eau de barres de PRFV pré-chargées à 80% de leur charge ultime en traction et enrobées de béton, les taux de rétention de leur résistance en traction initiale sont de 95, 92 et 90% à 23°, 40° et 50°C, respectivement.*
7. *Aucun dommage microstructural n'a été observé sur les échantillons pré-chargés à 80% de leur charge ultime en traction, enrobés de béton et conditionnés dans l'eau à 50°C pendant 240 jours. L'interface entre les fibres et la résine ne semble pas avoir été affectée par l'absorption d'humidité et les températures élevées.*
8. *La matrice polymère des échantillons pré-chargés à 80% de leur charge ultime en traction, enrobés de béton et conditionnés dans l'eau à 50°C pendant 240 jours n'est pas affectée par l'absorption d'humidité et les températures élevées. Les mesures en calorimétrie différentielle à balayage n'ont montrées qu'aucun changement de la température de transition vitreuse ne survenait*
9. *Les propriétés mécaniques résiduelles (résistances en traction et module élastique en flexion des barres de PRFV) augmentent avec la baisse de la température. Ce phénomène est dû à l'augmentation de la rigidité de la matrice polymère amorphe à basses températures.*
10. *À des températures généralement observées dans les régions nordiques comme le Canada (températures allant de -40° à 50°C), la résistance résiduelle à la traction et le module élastique en flexion semble demeurer stable, montrant que le comportement mécanique des barres de PRFV n'est pas affecté par la température dans cette gamme de températures.*

5. ACKNOWLEDGMENTS

This research was supported by the National Science and Engineering Research Council (NSERC) of Canada, the Fonds Québécois de la Recherche sur la Nature et les Technologies (FQRNT) and the Canadian Network of Centres of Excellence on Intelligent Sensing for Innovative Structures (ISIS Canada). The authors also want to thank the FRP bar manufacturer (Pultrall inc.) and The Ministry of Transportation of the province of Québec for their technical support.

Ces travaux de recherche ont été supportés par le Conseil de recherches en sciences naturelles et en génie du Canada (CRSNG), le Fonds Québécois de la Recherche sur la Nature et les Technologies (FQRNT) et le Réseau de Centres d'excellence du Canada sur les innovations en structures avec systèmes de détection intégrés (ISIS Canada). Les auteurs tiennent également à remercier la compagnie Pultrall inc. et le Ministère des transports du Québec pour leur implication.

6. REFERENCES

[1] Nkurunziza, G., Benmokane, B., Debaiky, A. S., Masmoudi, R. (2005). Effect of sustained load and environment on long-term tensile properties of glass FRP reinforcing bars. *ACI Structural Journal*, vol. 102, n°4, p. 615-621.

[2] Berthelot, J.-M (1992) Matériaux composites: comportement mécanique et analyse des structures, Masson, Paris, 620 p.

[3] Robert, M., Cousin, P., Benmokrane, B. (2009). Influence de la température sur le comportement des composites pour le genie civil. *Les Annales du Bâtiment et des Travaux Publics*, vol. 6, p. 21-27.

[4] American Concrete Institute (2006). Guide for the Design and Construction of Concrete Reinforced with FRP Bars. *American Concrete Institute*, Farmington Hills, Michigan, 2006, 44p (code ACI 440.1R-06).

[5] Canadian Standards Association (2002). Design and Construction of Building Components with Fibre Reinforced Polymer. *Canadian Standards Association*, Rexdale, Ontario, Canada, 177 p (code CAN/CSA-S806-02).

[6] Canadian Standards Association (2006). Canadian Highway Bridge Design Code. *Canadian Standards Association*, Rexdale, Ontario, Canada, 757 p (code CAN/CSA-S6-06).

[7] Japanese Society of Civil Engineering (1997). Recommendations for Design and Construction of Concrete Structures using Continuous Fiber Reinforced Materials. *Japanese Society of Civil Engineers*, 120 p (code JSCE 1997).

[8] Canadian Standards Association (2010). Specification for fibre-reinforced polymers. *Canadian Standards Association*, Rexdale, Ontario, Canada, 44 p (code CAN/CSA-S807-10).

[9] American Concrete Institute (2008). Specification for Construction with Fiber-Reinforced Polymer Reinforcing Bars. *American Concrete Institute*, Farmington Hills, Michigan, 2008, 5p (code ACI 440.5-08).

[10] Intelligent sensing for innovative structures. (2006). *Specifications for Product Certification of Fibre Reinforced Polymers (FRPs) as Internal Reinforcement in Concrete Structures*. The Canadian Network of Centres of Excellence, ISIS Canada, University of Manitoba, Winnipeg, Manitoba, Canada, 27 p.

[11] Benmokrane, B., El-Salakawy, E. (1997). *In* the Proceedings of the Third International Conference on Durability and Field Applications Of Fibre Reinforced Polymer (FRP) Composites for Construction, CDCC, 569 p.

[12] Benmokrane B, Wang P, Ton-That T, Rahman H, Robert J. (2002). Durability of glass fibre reinforced polymer reinforcing bars in concrete environment. *Journal of Composite for Construction*, vol. 6, nº2, p.143–153.

[13] Uomoto, T. (2004). Development of new GFRP with high alkali resistivity. *In* the Proceedings of the 4th International Conference on Advanced Composite Materials in Bridges and Structures, ACMBS-IV, Calgary, Alberta.

[14] Vijay, P. V., Gangarao, H.V.S., et Kalluri, R.(1998) Hygrothermal Response of GFRP Bars under Different Conditioning Sschemes, *In* the Proceedings of the 1st International Conference on Durability of fiber Reinforced Polymer for Construction (CDCC'98), Sherbrooke, Canada, p.243-252.

[15] Yilmaz, V.T. et Glasser, F. P. (1991). Reaction of Alkali-resistant Glass Fibres with Cement, Part I, Review, Assessment, and Microscopy. *Glass Technology*, vol.32, nº3, p.91-98.

[16] Tannous, F.E. (1997). *Durability of AR Non-Metallic Reinforcement Bars and Prestressing Tendons.* Thèse de doctorat, Université d'Arizona, Tucson, Arizona, 287 p.

[17] Porter, M. L., and Barnes, B., A. (1998). Accelerated aging degradation of glass fiber composites. *In* Proceedings of the 2nd International Conference on Composites in Infrastructure, vol. II, ICCI, Tucson, Arizona, p. 446-459.

[18] Swit, G. (2000). *Durability of Stressed E-glass Fibre in Alkaline Medium*. In Recent Developments in Durability Analysis of Composite Systems, Cardon, Fukuda, Reifsneider and Verchery Editions, Balkema, Rotterdam, pp. 473-476

[19] Valter, T. et Ralejs, T. (2001). Durability and Service Life Prediction of GFRP for Concrete Reinforcement. *In* the Proceedings of FRPRCS-5 fibre-reinforced plastics for reinforced concrete structures, University of Cambridge, vol.1, p.505-514

[20] Sen, R., Mullins, G., et Salem, T. (2002) Durability of E-Glass/Vinylester Reinforcement in Alkaline Solution, ACI Structural Journal, vol. 99, nº3, p. 369-375.

[21] Chu, W., Karbhari, V.M. (2005). Effect of Water Sorption on Performance of Pultruded E-Glass/Vinylester Composites, *Journal of Materials in Civil Engineering*, vol. 17, nº1, p. 63-71.

[22] Mercier, J.-P., et Maréchal, E.(1993) Chimie des polymères, Synthèse, réactions, dégradations. *Presses Polytechniques et Universitaires Romandes*, Université Pierre et Marie Curie, Paris VI, 448 p.

[23] Bank L. C., Gentry T. R., Barkatt A., Prian L., Wang F. and Mangla S. R. (1998). Accelerated aging of pultruded glass/vinyl ester rods,*In* the Proceedings of the Second International Conference on Fiber Composites in Infrastructure ICCI, vol. 2, p. 423-437.

[24] Benmokrane B, Ton-That, T., Robert, J.F., and Mukhopadhyaya, P. (1999). *Durability studies of composite GFRP C-bar reinforcing rods.* Technical Progress Report No.8 submitted to Marshall Industries Composites, inc., Department of Civil Engineering, Faculty of Engineering, University of Sherbrooke, Sherbrooke, Quebec, Canada, 105 p.

[25] Dejke, V. (2001) *Durability of FRP reinforcement in concrete-Literature Review and Experiments,* Thèse de doctorat, Chalmers University of Technology, Goteborg, Sweden, January 2001,212 p.

[26] Thomason, J.L. (1995). The Interface Region in Glass Fibre-reinforced Epoxy Resin Composites: 3. Characterization of Fibre Surface Coatings and the interphase. *Composites*, vol. 26, nº7, p.487-498.

[27] Byars, E. A., Waldron, P., Dejke, V, and Demis, S. (2001). Durability of FRP in Concrete – Current Specifications and a New Approach. *FRP Composites in Civil Engineering*, vol. 2, p. 1497-1507.

[28] Bisby, L.A., Kodur, V.K.R. (2007). Evaluating the fire endurance of concrete slabs reinforced with FRP bars: Considerations for a holistic approach. *Composites : Part B*, vol.38, p.547-558.

[29] Panigrahi, B.K. (2006). Microstructures and properties of low-alloy fire resistant steel. *Bulletin of Material Science*, vol.29, nº1, p.59-66.

POTENTIAL POZZOLANICITY OF GLASS CULLET FINES AND AGGREGATES

Rachida IDIR[a,b,c], Martin CYR[a], Arezki TAGNIT-HAMOU[b]

[a]Université de Toulouse; UPS, INSA; LMDC (Laboratoire Matériaux et Durabilité des Constructions); 135, avenue de Rangueil; F-31 077 TOULOUSE cedex 4, France.

[b]Département de génie civil, Université de Sherbrooke, Laboratoire Matériaux Cimentaires Alternatifs, 2500 boul. Université, Sherbrooke (Québec), J1K 2R1, Canada

[c]Laboratoire Eco-Matériaux, Centre d'Etudes Techniques de l'Equipement, Direction Régionale et Interdépartementale de l'Équipement et de l'Aménagement Ile-de-France, 319 avenue Georges Clemenceau, BP 505, 77015 MELUN Cedex, France

1. INTRODUCTION

The glass used in cement-based materials can lead to two types of behaviors having antagonistic effects: alkali-silica reaction, which causes damage in concretes, and pozzolanic reaction, which is beneficial for concrete properties. The alkali-silica reaction (ASR) is usually associated with coarse particles containing amorphous silica. The destruction of the silica network releases silica that combines with alkali (and calcium) to form N,K-(C)-S-H gels causing expansion of the concrete. Different studies have shown the effect of glass particle size on the expansion of mortars and concretes [SHA 00, SHA 06] but the results are quite dispersed and difficult to generalize. The pozzolanic activity is usually related to fine particles also composed of amorphous silica. As for ASR, the silica network is attacked by hydroxide ions but the silica released combines with calcium from Portlandite (and a certain amount of alkalis that might be present in the pore solution) to form C-(N,K)-S-H which improve concrete properties. A few papers have reported that most alkali-reactive aggregates can show pozzolanic activity when they are ground to a few tenths of a micrometer or smaller, supporting the idea that the pozzolanic reaction only concerns fine materials [CAR 08, CYR 09]. Results of the literature showed that the pozzolanic activity of the glass depended on several parameters and that each type of glass should be studied to evaluate its activity [SHA 00, BY 04, SHA 06].

This paper deals with the use of mixed glass cullet of different colors in replacement of cement which represents an alternative to existing recycling ways. The main objective is to evaluate the pozzolanic activity of a large range of glass particle sizes, from less than 40 µm (540 m²/kg) up to 2.5 mm (2.2 m²/kg). Since studies in the literature are usu-

ally limited to small particles, coarser particles are used to determine the size up to which it is possible to detect a pozzolanic activity. Five different classes are assessed separately, in terms of compressive strength tests on mortars, consumption of lime, morphology and composition of hydrates.

2. EXPERIMENTAL PROCEDURES

2.1. Materials

The glass (G) used in this study was bottle soda-lime silica glass of mixed colours. It was composed of 40, 33, 20 and 1% of colourless, brown, green and blue glasses, respectively. The material also contained around 6% of impurities. Different sizes of glass particles noted Gx (X denotes the specific surface of the glass) were obtained after grading, washing, drying, crushing and sieving the raw material. **Table 1** give the chemical composition and the fineness of the classes used in this study. It can be seen that the chemical compositions of all classes are similar, confirming the homogeneity of the material. The mean density was 2.5 g/cm^3. The cement used was a Portland cement CEM I 52.5R according to EN 197-1 [AFN 01] (**Table 1).** The sand used for the pozzolanic study was a non-reactive quartz sand in accordance with standard EN 196-1 [AFN 06].

2.2. Sample preparation and test methods

The pozzolanic activity of the different size classes of glass was tested through compressive strength measurements on standardized mortars. Four types of mortars were prepared according to standard EN 196-1 [12]. After demoulding, the prismatic samples (4x4x16 cm) were cured in water at 20°C until the age of test (1, 7, 28, 90 and 210 days).
Lime consumption was determined by thermogravimetric analysis (TG) on pastes stored at 20°C and composed of 65% of glass (coarse G_2 or fines G_{540}) and 35% of $Ca(OH)_2$ by weight. The analysis of new-formed hydrates according to glass particle sizes was performed on suspensions containing $Ca(OH)_2$ or C_3S, glass (coarse G_2 or fines G_{540}) and a solution of 1 mol/l KOH (**Table 2**). These suspensions were prepared in small stainless steel reactors and kept in a thermostatic bath maintained at 60°C until the analysis. Precipitates were separated by filtration from the solution and then dried at 20°C in a vacuum freeze dryer. The morphology of hydrates was determined by scanning electron microscopy (SEM – JEOL JSM 6380 LV). Their

Chemical composition (% by mass)						
	Cement	Glass				
		G_2	G_4	G_{18}	G_{200}	G_{540}
SiO_2	19.8	69.4	69.3	69.4	69.4	68.9
Al_2O_3	5.6	2.0	2.1	2.1	2.1	2.1
Fe_2O_3	2.5	0.2	0.2	0.3	0.4	0.3
CaO	63.6	12.5	12.6	12.4	12.5	12.3
MgO	1.8	1.1	1.1	1.1	1.1	1.0
SO_3	3.1	0.2	0.2	0.2	0.2	0.2
Na_2O	0.1	13.7	13.6	13.7	13.2	13.6
K_2O	0.7	0.6	0.6	0.6	0.6	0.6
Loss on ignition	1.7	0.3	0.3	0.3	0.6	1.0
Physical characteristics						
Specific surface ** (m^2/kg)	440	2.2	4.5	18	200	540
Particle size ranges (μm)	-	1250-2500	630-1250	160-315	<80	<41
Mean diameters (μm)	-	1875	940	237	23	8
Specific gravity (g/cm^3)	3.15	2.40	2.41	2.41	2.43	2.48

* Gx: x is the specific surface of the glass
** Blaine for cement, G_{200} and G_{540}; calculated from the particle size distribution for G_2, G_4 and G_{18}

Table 1: Chemical and physical characteristics of cement and glass cullet

	Suspension $Ca(OH)_2$-Glass		Suspension C_3S-Glass	
Binder	$Ca(OH)_2$	6.0 g	C_3S	5.0 g
Glass	G_2 or G_{540}	3.0 g	G_2 or G_{540}	2.7 g
Solution	KOH 1 mol/l	50.0 g	KOH 1 mol/l	50.0 g

Table 2: Mixture proportions for the analysis of new-formed hydrates in diluted systems ($Ca(OH)_2$ and C_3S) containing glass

elementary compositions were measured using energy dispersive X-ray spectroscopy (EDX, 15 kV and 10 nA) and X-ray fluorescence (XRF).

3. RESULTS

Figure 1 presents the compressive strength of mortars containing the different size classes of glass (all numerical values are grouped into Annex 1). As can be seen, the strengths depend on the fineness and glass content. The highest strengths are obtained for the smallest particles (G_{540}), with values sometimes exceeding those of the reference without glass, regardless of the replacement rate used (up to 40%). Nevertheless, except for glass G_{540} the general trend is that the replacement of the cement by glass leads to a decrease of the compressive strength, principally due to a cement dilution effect.

The calculation of the dilution curves was made with Bolomey's law (**equation 1**), by considering only the effective quantity of cement used in the mortars (for instance 10% of glass implies that only 90% of cement contributed to the development of strength).

$$\sigma = K_b\left(\frac{C}{W+V} - 0{,}5\right) \qquad \text{(Equation 1)}$$

where σ is the compressive strength of mortar, C and W are respectively the masses of cement (without taking glass into account) and water, respectively, V is the volume of air void (taken here as 10% of the water content), and K_b is a coefficient that takes the characteristics of cement and aggregate into account. This coefficient was calculated at each hydration time by using the compressive strength of the reference without glass.

Figures 2 show the relative strengths (strength ratio of mortar with and without glass particles) of all glass-mortars up to 210d, versus the specific surface area of glass. The inert straight lines were calculated using Bolomey's law (**equation 1**).

It can be seen from **Figures 2**, at least for up to 30% of glass, that the relative strengths were higher than the inert curves (except for 1d), meaning that there was a non-negligible activity of glass particles of all sizes, including the coarser ones. For glass content of 10% and hydration times longer than 1d, there was a limited effect of fineness, since almost all sizes led to relative strength similar to the dilu-

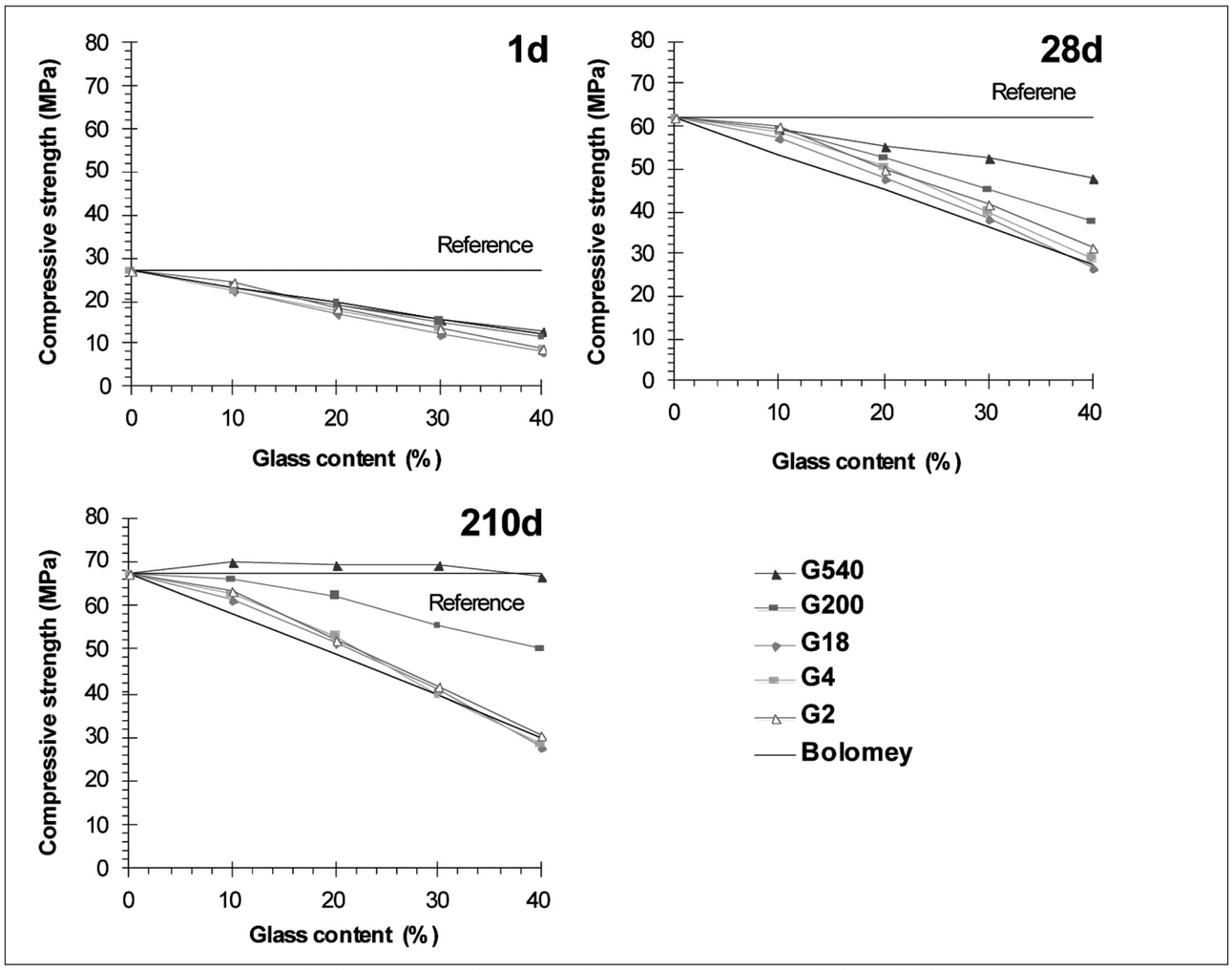

Figure 1: Compressive strength of mortars cured at 20°C and containing up to 40% of glass of different finenesses. Comparison with the dilution curves given by Bolomey's law

tion curve. Only the finer class began to detach from other curves at later ages (90 and 210d). This means that the cement can be replaced by glass of any size without affecting the activity and the relative strength too much, which stays over 0.9 in all cases. At 20, 30 and 40% of glass, a gradual change of behavior was observed, related to the size effect, which became more significant with the increase of glass content.

1. The relative strength of mortars with coarse particles (G_2, G_4 and G_{18}) moved toward the inert curve as the glass content increased: 20% glass was still better than inert but 40% glass behaved at best like an inert material. This means that, for a glass content of 40%, the strengths of classes G_2, G_4 and G_{18} were only due to the cement, without any perceptible effect of glass activity.
2. A significant pozzolanic activity seemed to develop over time for the two finer classes (G_{200} and G_{540}), highlighted by the increase in relative strength with hydration time. At 210 days, the relative strength remained around 1 for G_{540}-mortars containing up to 40% of glass. These results are in agreement with those presented by Shao et al. [SHA 00] and Shi et al. [SHI 05].

4. DISCUSSION

Results of expansion measurements on mortar prisms made with 20% of glass of different classes can be found in a complementary study [IDI 09]. These results show that a critical threshold of grain size under which no expansion occurred. Only coarse particle size classes (class G_2 > 1.25mm) led to significant expansion of mortar prisms. However, in that case, the absence of expansion was not sufficient to prove the non-existence of ASR, since it did not mean that there was no trace of ASR-gels in the mortars. Indeed, signs of ASR were detected in macroscopic

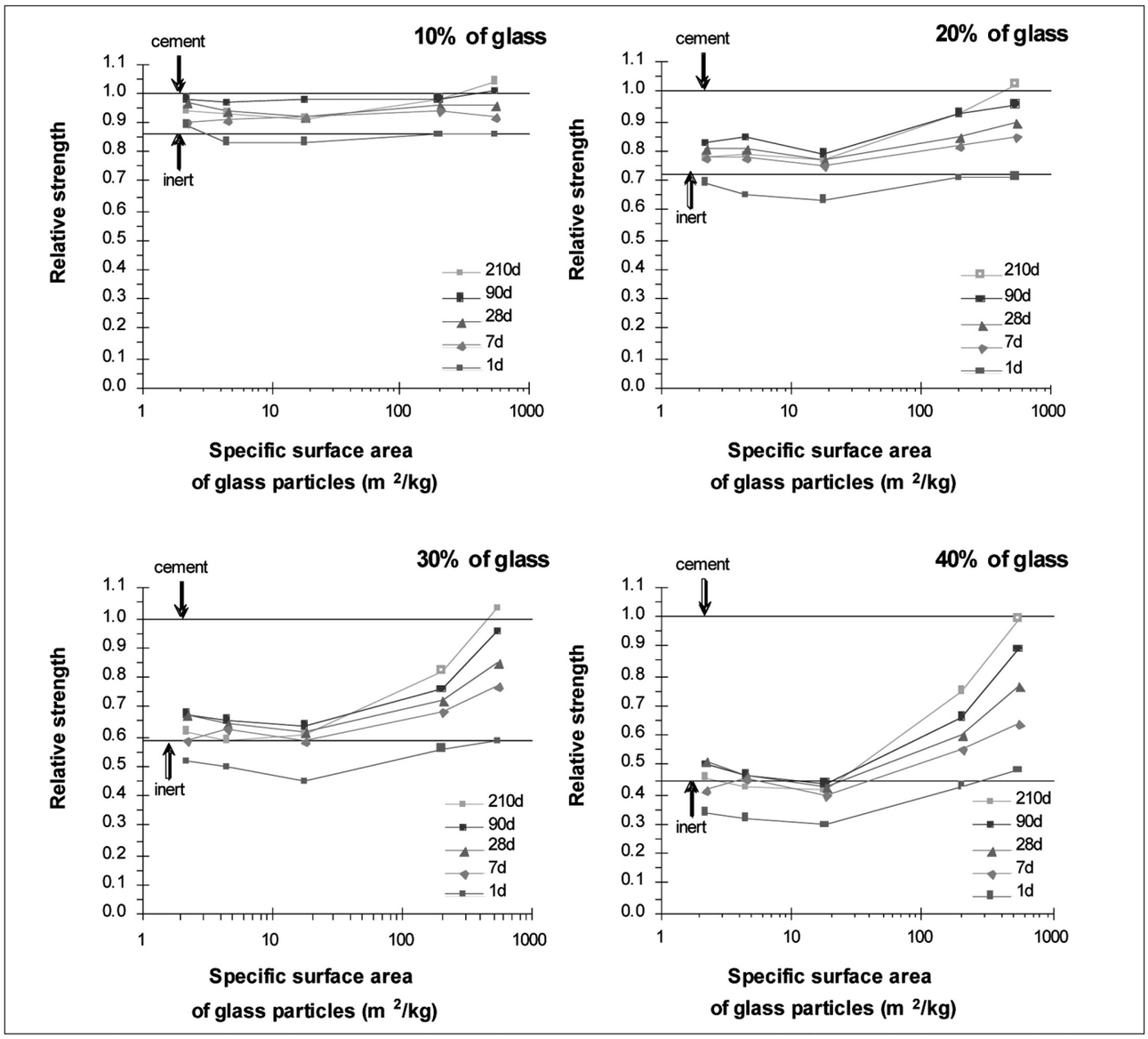

Figure 2: Relative strength (%) of mortars according to glass fineness. Comparison with the theoretical relative strength of mortars containing an inert admixture

and microscopic observations of the samples containing glass of particle sizes down to 315 µm.

So ASR cannot be excluded for finer glass particles but pozzolanic hydrates probably have a greater importance. The existence of two concomitant reactions cannot be excluded, but the effects of the pozzolanic reaction exceed those of ASR in the case of fine glass particles.

On one hand, it seemed evident from the compressive strength results that finer classes (G_{200}, G_{540}) had a chemical activity leading to significant increases of strength with time. On the other hand, small increases in strength were also measured for coarser classes (**Figure 2**). In the latter case, the increase in strength could not be due to a physical effect such as heterogeneous germination, since the particles were too large (SSB < 50 to 100 m^2/kg) [LAW 03]. Thus it can be supposed that a chemical activity (e.g. pozzolanic reaction) of coarse particles cannot be neglected.

This assumption was verified by studying new-formed hydrates according to the glass particle sizes. Thermal analysis, X-ray fluorescence and electronic microscopy (SEM) coupled with EDX were used. Measures in time of consumption of $Ca(OH)_2$ by TG show that glass G_{540} has a higher lime consumption than glass G_2, which seems reasonable considering the significant differences of fineness of the two classes. After 290 days, all $Ca(OH)_2$ has reacted with G_{540}, confirming the significant pozzolanic activity of this class. However, the reactivity of class G_2 cannot be neglected, since 15% of lime has been consumed at that time. Elementary analyses were made using EDX and XRF on new-formed hydrates from mixtures of $Ca(OH)_2$ or C_3S and glass (G_2 and G_{540}), cured for several weeks in a 1mol/l KOH solution. All these analyses are given in **Figure 3**, as (N+K)/S ratio versus C/S of hydrates.

Different new-formed products could be observed depending on the grain sizes. Thus, it appears that finer particles (G_{540}) led to the formation of only one type of hydrate, similar to pozzolanic C-S-H, both morphologically and in their composition (**Figure 3**). Coarse particles (G_2) were partially attacked and gave two types of hydrates:

– Hydrates detached from glass grains (precipitate), presenting compositions of C-S-H close to finer particles, although with slightly different composition (Figure 4) but usually with higher C/S ratio and lower alkali content (XRF analysis).
– Hydrates forming a reaction ring around the grains, which can be regarded as alkali-silica gels containing small amounts of calcium. Their composition (**Figure 3**) and morphology (**Figure 4**) were similar to ASR gels (EDS analysis).
– These analyses support the hypothesis given earlier that coarse particles of glass G_2 (1.25-2.5 mm) are able to produce C-S-H hydrates. Considering the high content of calcium in the solution, it is probable that a precipitation of C-S-H-like hydrates occurred after the superficial dissolution of coarse particles.

This process was probably slowed down by the formation of gel rings around the particles, like those generally observed around alkali-reactive aggregates. The attack of the silica network by hydroxyl ions and alkalis led to the production of (N,K)-S-H gels containing small amounts of calcium, since this element was slowed down by the diffusion process from pore solution to sound grains. Thus the composition of new-formed products depends on the kinetics of the reaction and on the availability of elements at a given place and a given time. The deficit of alkalis compared to calcium could lead to low (N+K)/S hydrates (high C/S) having compositions near C-S-H, while the inverse case could favor high (N+K)/S ratios, typical of ASR gels. This mechanism presents similarities with the reaction sequence proposed by HOU et al. [HOU 04] for the formation of ASR products:

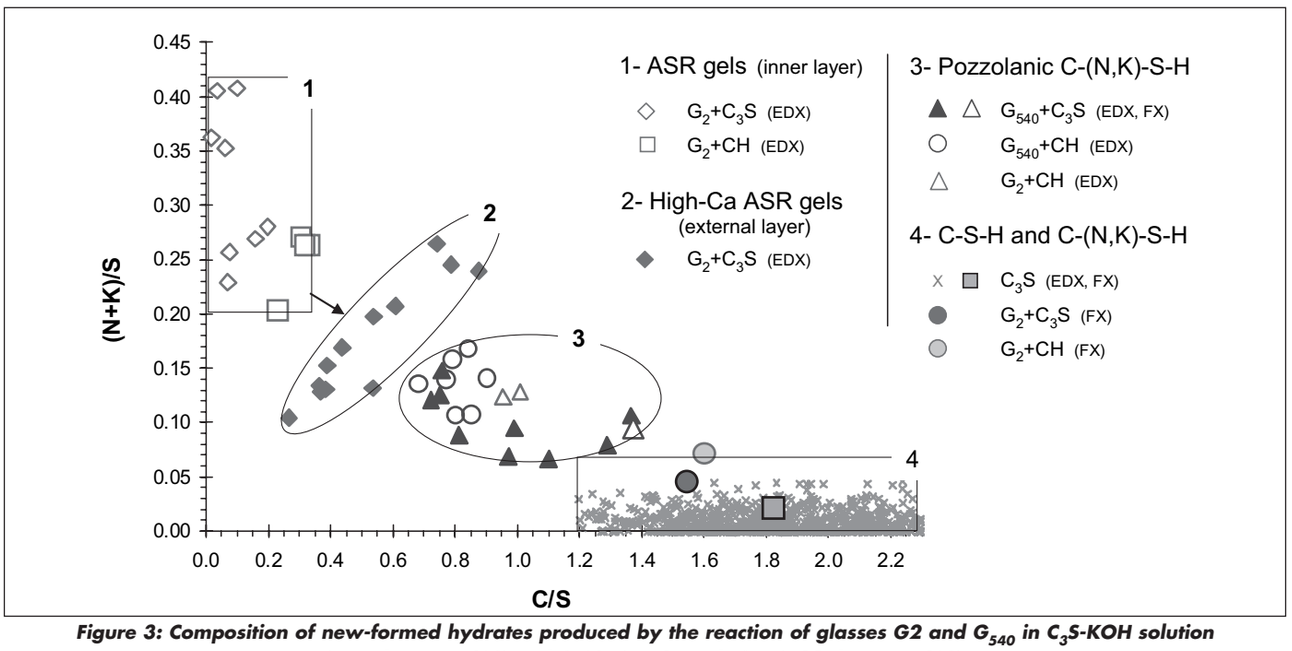

Figure 3: Composition of new-formed hydrates produced by the reaction of glasses G2 and G_{540} in C_3S-KOH solution (154 days at 60°C) and $Ca(OH)_2$-KOH solution (129 days at 60°C).

– attack of reactive aggregate by OH^-;
– consumption of the released silica due to reaction with portlandite and thus leading to the formation of C-S-H (until local depletion of portlandite);
– reaction of silica with primary C-S-H and formation of polymerized Si-rich C-S-H;
– increase of silica concentration in pore solution and gelation to (N,K)-S-H gel.

Up to the last step, this sequence is similar to the pozzolanic reaction.

This double process probably does not take place for finer particles, G_{540}, because of the small size of the glass particles. Thus only one type of hydrates is produced (**Figure 3**) following a sequence similar to the pozzolanic reaction.

5. CONCLUSION

This study aimed to evaluate the pozzolanic activity of glass cullet particles as a function of the glass content (10 to 40% of cement replacement) and fineness (from less than 40 µm-540 m^2/kg up to 2.5 mm-2.2 m^2/kg). The following conclusions can be drawn:

– Color-mixed glass cullet presents a pozzolanic activity which increases with the fineness of its particles.
– Compared to the reference without glass, equivalent or superior compressive strength can be obtained when using up to 40% of glass of fineness 540 m^2/kg.
– Strength activity indexes higher than 90% can be obtained:
  • after 7 days of curing for 10% of glass, whatever the fineness of the glass;
  • after 90 days of curing for 20% of glass, only when the specific surface is higher than 200m^2/kg.
– A transition fineness around 30 m^2/kg (140 µm) is highlighted, for which the pozzolanic activity becomes substantial.
– A slight but significant pozzolanic activity is detected for coarse particles (>140 µm), confirmed by the consumption of $Ca(OH)_2$, the formation of C-S-H-like hydrates and an increase of 10% (5 MPa) in the compressive strength compared to an inert admixture.
– However, the possible alkali-silica reactivity of these particles should be taken into account, since ASR is detected for specific surfaces lower than 4.5 m^2/kg.
– The composition of new-formed hydrates depends on the kinetics of the reaction and on the availability of calcium and alkalis at a given place and a given age. The deficit of alkalis compared to calcium could lead to low (N+K)/S hydrates (high C/S) having compositions near C-S-H, while the inverse case could favor high (N+K)/S ratios, typical of ASR gels.

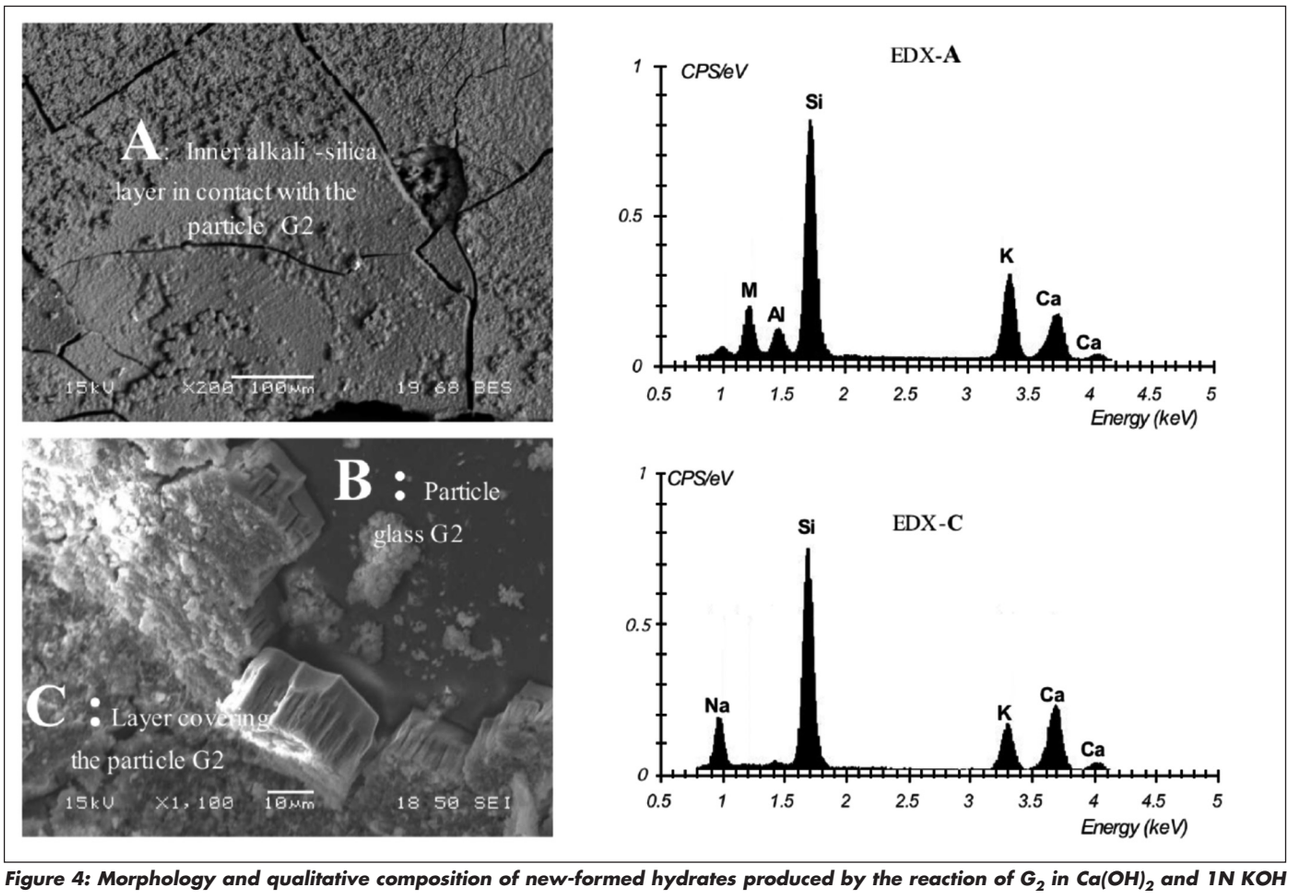

Figure 4: Morphology and qualitative composition of new-formed hydrates produced by the reaction of G_2 in $Ca(OH)_2$ and 1N KOH solution (129 days at 60°C).

Classe of glass	Age (days)	Substitution rate of cement				
		0%	10%	20%	30%	40%
G_2	1	26.9 ±0.3	24.1 ±0.3	18.7 ±0.3	13.9 ±0.2	9.1 ±0.2
	7	53.1 ±0.1	48.1 ±1.3	41.3 ±0.6	31.2 ±0.4	22.0 ±0.3
	28	61.9 ±2.3	59.8 ±0.7	50.2 ±0.9	41.8 ±0.2	31.8 ±0.4
	90	63.5 ±1.6	62.5 ±1.0	52.6 ±1.0	43.0 ±0.7	31.8 ±0.6
	210	67.1 ±1.0	63.4 ±1.1	52.3 ±1.0	41.6 ±0.5	30.7 ±0.5
G_4	1	26.9 ±0.3	22.5 ±0.3	17.5 ±0.2	13.3 ±0.3	8.7 ±0.1
	7	53.1 ±0.1	48.3 ±0.0	41.3 ±0.1	33.3 ±0.6	24 ±0.2
	28	61.9 ±2.3	58.5 ±1.4	50.3 ±0.7	39.8 ±0.8	29.0 ±0.6
	90	63.5 ±1.6	61.4 ±1.1	53.8 ±0.7	41.9 ±0.7	29.8 ±0.2
	210	67.1 ±1.0	62.5 ±1.3	53.0 ±1.1	39.0 ±0.5	28.3 ±0.5
G_{18}	1	26.9 ±0.3	22.5 ±0.2	17.1 ±0.2	12.1 ±0.2	8.0 ±0.2
	7	53.1 ±0.1	48.7 ±2.2	40.1 ±0.6	31.1 ±1.1	21.1 ±1.1
	28	61.9 ±2.3	57.2 ±0.9	47.7 ±0.8	38.3 ±0.6	26.4 ±0.7
	90	63.5 ±1.6	62.3 ±1.4	50.4 ±0.9	40.6 ±1.3	27.4 ±0.8
	210	67.1 ±1.0	61.2 ±2.0	51.9 ±1 .1	40.7 ±0.7	27.8 ±0.2
G_{200}	1	26.9 ±0.3	23.2 ±0.2	19.1 ±0.2	15.0 ±0.2	11.5 ±0.2
	7	53.1±0.1	48.7 ±1.5	40.1 ±0.7	31.1 ±2.0	21.2 ±0.7
	28	61.9 ±2.3	57.2 ±1.6	47.7 ±1.3	38.3 ±0.7	26.4 ±1.0
	90	63.5 ±1.6	62.3 ±1.1	50.4 ±0.7	40.6 ±1.2	27.7 ±0.8
	210	67.1 ±1.0	65.7 ±1.4	62.3 ±0.6	55.3 ±1.7	50.2 ±0.5
G_{540}	1	26.9 ±0.3	23.1 ±0.4	19.2 ±0.3	15.7 ±0.2	13.0 ±0.2
	7	53.1 ±0.1	48.7 ±1.1	45.1 ±1.3	40.9 ±0.1	33.9 ±0.3
	28	61.9 ±2.3	59.2 ±1.0	55.3 ±0.6	52.8 ±0.9	47.6 ±0.6
	90	63.5 ±1.6	63.9 ±1.8	61.0 ±1.7	60.7 ±0.8	56.7 ±0.9
	210	67.1 ±1.0	70.0 ±1.4	69.0 ±1.4	69.2 ±1.7	66.8 ±1.3

Annex 1 : Table summarizing the influence of percentage replacement of cement with different classes of glass on the hardening of mortars stored at 20° C

6. REFERENCES

[AFN 01] AFNOR EN 197-1 Cement – Part 1: Composition, specifications and conformity criteria for common cements, February 2001

[AFN 06] AFNOR NF EN 196-1 Methods of testing cement – Part 1: Determination of strength; April 2006

[CAR 08] Carles Gibergues A, Cyr M, Moisson M, Ringot E., "A simple way to mitigate alkali-silica reaction", Materials and Structures 2008, vol. 40, n° 1, p. 73-83

[CYR 09] Cyr M, Rivard P, Labrecque F. , "Reduction of ASR-expansion using powders ground from various sources of reactive aggregates", Cement and Concrete Composites, vol. 31,n° 7, p. 438-446

[HOU 04] Hou X, Struble LJ. Kirkpatrick RJ., "Formation of ASR gel and the role of C-S-H and Portlandite", Cement Concrete Research 2004, vol. 34, n° 9, p. 1683-1696

[IDI 09] Idir R, Cyr M, Tagnit-Hamou A. Use of fine glass as ASR inhibitor in glass aggregate mortars, Construction and Building Materials, vol.24, n°7, july 2010, p.1309–1312

[LAW 03] Lawrence P, Cyr M, Ringot E., "Mineral admixtures in mortars - effect of inert materials on short-term hydration", Cement Concrete Research 2003, vol. 33, n° 12, p. 1939-1947

[PAR 04] Park SB, Lee BC, Kim JH., "Studies on mechanical properties of concrete containing waste glass aggregate", Cement Concrete Research 2004, vol. 34, n° 12, p. 2181-2189

[SHA 00] Shao Y, Lefort T, Moras S, Rodriguez D. Studies on concrete containing ground waste glass, Cement and Concrete Research 2000 vol. 30, n °1, p. 91-100

[SHA 06] Shayan A, Xu A., "Performance of glass powder as a pozzolanic material a field trial on concrete slabs" , Cement Concrete Research 2006, vol. 36,n° 2, p. 457-468

[SHI 05] Shi C, Wu Y, Rieflerb C, Wang H., "Characteristics and pozzolanic reactivity of glass powders", Cement Concrete Research 2005, vol. 35, n° 5, p. 987- 993

BASIC OXYGEN FURNACE SLAG (BOF SLAG): CHARACTERIZATION AND EVOLUTIVITY

Essia BELHADJ[1], Cécile DILIBERTO[1], André LECOMTE[1]

[1]Institut Jean Lamour, UMR 7198, Nancy Université - UPVM - CNRS, CP2S-207, Matériaux pour le Génie Civil, IUT de Nancy-Brabois, CS 90137, F54601 Villers-lès-Nancy Cedex, France

essia.belhadj@lcsm.uhp-nancy.fr

1. INTRODUCTION

BOF slag is a by-product of the conversion of pig iron to steel in a basic oxygen furnace (BOF). Depending on the raw material, 100-200Kg are generated per ton of steel [MAH, 08]. In 2005, 170 million tons were produced in the world (1.2 million tons in France). The principle of converting cast iron into steel is to blow oxygen to decrease carbon content. Lime is added in the converter in order to fix undesirable elements contained in pig iron and to protect the fire brick. At the end of conversion BOF slag is separated from steel by gravimetric separation.

BOF slag are still undervalued. A small amount is used by agriculture in amendment to neutralize soil acidity. Road engineering used to consume an important quantity as aggregate since these materials have good mechanical properties and a low cost [MOT, 01]. Unfortunately this use is restricted because of free lime content of BOF slag which causes uncontrolled volume expansions [CAI, 00]. Several studies concerning aggregates degradation, volumetric instability and BOF slag swelling, are underway to optimize their use [LEC, 11 1-2-3].

With a chemical composition similar to Portland cement one, the exploitation of BOF slag in some hydraulic binders can also be considered. They nevertheless have poor hydraulic properties, mainly because of their high content of iron oxide and the weak content of tricalcium silicate [MUR, 97]. Indeed, the wüstite ($Fe_{1-x}O$), which is one of the major phases of BOF slag does not react with water. Furthermore, when materials are finely ground, calcium oxide they contain reacts with air moisture to form hydrated lime $Ca(OH)_2$. This last mineral reacts itself with the ambient CO_2 to form calcite $CaCO_3$. Thus the CaO content decreases over time. These phenomena may change or decrease the reactivity of the unstable materials.

BOF slag valorisation requires previously a through physical and chemical characterization to have a good awareness of their properties. Most of the literature on this subject only relates to the qualitative characterization of BOF slag and the quantification of free lime content, due to the problem of expansion.

Investigations presented in this study are more complete because they relate to the identification and quantification of all mineral phases present in BOF slag (C_2S, C_2F, etc.). They were performed on a variety of products with different origins and ages (fresh and weathered productions).

2. EXPERIMENTS

2.1. Materials

The BOF slag studied are coming from different industrial plants and melts. After cooling and treatment they are reclaimed as 0/100 mm granulates with a minimum fine fraction.
BS1samples are a mixture of several melts from the same origin but with different ages:
– BS1F: Fresh production
– BS1W: Weathered production
BS2 samples are fresh products, from a second industrial plant and separated melts which differ by the free lime content. This parameter depends on the grade of steel produced:
– BS2H: High lime content
– BS2L: Low lime content
Representative sampling of large granulates were performed for analysis. They were crushed, ground and sieved to 0-125 m size.

2.2. Characterization procedures

The specific surface area was determined by the Blaine test according to the EN standard 196-6. The absolute density was measured by a hydrostatic weighing in a non-reactive liquid.
The X Ray Fluorescence technique is an emission of secondary X Rays characteristic of the atomic elements in the sample. It was used to determine the chemical composition of powders, expressed as a percentage of oxides.
The crystalline phases were identified using a X-pert pro X-ray Diffractometer equipped with a monochromator using a copper anticathode. The diffractogram obtained has been exploited by the diffraction software Plus - EVA®.
The crystallinity of samples was verified by a transmission electron microscope coupled to a microdiffraction and a chemical microanalysis.
The plan view of different phases in the grain slag was given by an electron probe microanalyzer and EDS analyses were performed to identify the minerals' chemical composition and impurities that may present.
The free lime content is found by acid-base titration. This method must be complemented by TGA-DTA (Thermo-Gravimetric Analysis coupled with Differential Thermal Analysis), in order to find out the hydroxide and oxide calcium content separately. This last method allowed us also to determine the carbonate ($CaCO_3$) content. Indeed, this technique allows to follow up and to quantify mass changes due to dehydration and decarbonation of samples as a function of temperature.
The main characteristic of steel slag is the high iron oxide content, which exists in both the di- and trivalent states. This content is found by redox titrations; FeII is titrated by a potassium dichromate solution $K_2Cr_2O_7$ in the presence of sodium diphenylamine sulphonate indicator.

$$6Fe^{2} + Cr_2O_7^{2-} + 14H^{+} \rightarrow 6Fe^{3+} + 2Cr^{3}+ + 7H_2O \quad [1]$$

The FeIII is reduced to FeII by stannous chloride $SnCl_2$ in order to titrate both di and trivalent states contents.
The calcium silicate content is found by selective extraction. Calcium phases are dissolved by salicylic acid and the C_2S is calculated by difference with the already known lime content.

3. RESULTS AND DISCUSSIONS

3.1. Physical properties

The absolute density measured on these BOF slag equals 3700 kg/m^3 on average. This value is relatively high, due to the high iron content. Note here that, due the presence of iron oxide, a longer grinding time is needed comparing to the clinker one. The density is measured on a freshly ground powder; samples aging causes hydration and carbonation of free lime and, consequently, a decrease of density. This parameter may reach an average of 3300 kg/m^3 after 6 months aging.
The specific surface area of 0-0.125 mm fresh powder equals to almost 3800 cm^2/g.

3.2. Mineralogical characterization

The BOF Slag oxide composition, obtained by X Ray Fluorescence and compared to the clinker one, is shown in table 1.
These materials contain more than 80% of CaO, SiO_2 and Fe_2O_3. Despite the iron content, BOF Slag composition is close to the clinker one. The higher content of Fe_2O_3 is a major disadvantage for both physical and hydraulic properties since iron phases are inert with water contact. The chemical compositions of the four BOF slags studied are similar despite their diverse origins. The main difference is the Loss Of Ignition (LOI) value which is the mass loss at 1000°C. A high LOI value indicates the presence of hydrated and/or carbonated phases.
Figures 1 and 2 show respectively XRD patterns of BS1 and BS2 samples. The minerals phases are mainly, C_2S, C_2F, $Ca(OH)_2$, CaO, $Fe_{(1-x)}O$. Minor phases as $CaCO_3$, MgO and SiO_2 are identified in some cases.
X-ray diffraction (XRD) indicates that the major mineral in BOF slag is -C_2S. Unlike others slags, BOF slags contain in most cases the form [SHI, 02]. Usually, -C_2S changes to -silicate below 675°C, but this disintegration is not found in the presence of high "FeO" content.
The main difference between the two BS1 samples appears in calcic phases (figure 1):
– The calcite content is higher for BS1W slag due to the hydroxide calcium carbonation during weathering. This result is in agreement with the high LOI (Loss Of Ignition) value obtained by XRF (table.1)
– The hydroxide calcium content is higher for the BS1W. It is produced by the hydration of calcium oxide and calcium silicate.
The X-ray pattern of BS2 confirms that BS2H contains more lime phases (figure 2). The amount of calcite is relatively low since these slags are considered fresh ones.

Wt %	LOI	MgO	Al2O3	SiO2	P2O5	CaO	MnO	Fe2O3
BS1F	1.1	4.5	1.9	10.8	1.4	45.0	2.6	32.0
BS1W	8.3	5.5	1.9	8.6	1.4	40.1	2.0	30.8
BS2L	0.0	6.0	1.7	13.1	2.4	41.7	4.1	29.3
BS2H	0.0	7.5	2.1	11.3	2.0	42.9	3.7	28.3
K	0.2	4.3	4.7	20.8	0.2	63.6	0.1	3

Table 1 Chemical composition of BOF slag by XRF technique

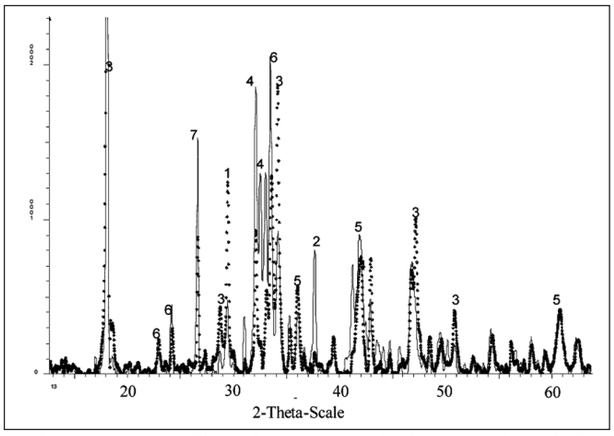

Figure 1: X-ray diffraction pattern of BS1; solid line BS1F, dotted line BS1W
1-$CaCO_3$, 2-CaO, 3-$Ca(OH)_2$, 4-C_2S, 5-FeO, 6-C_2F, 7-SiO_2

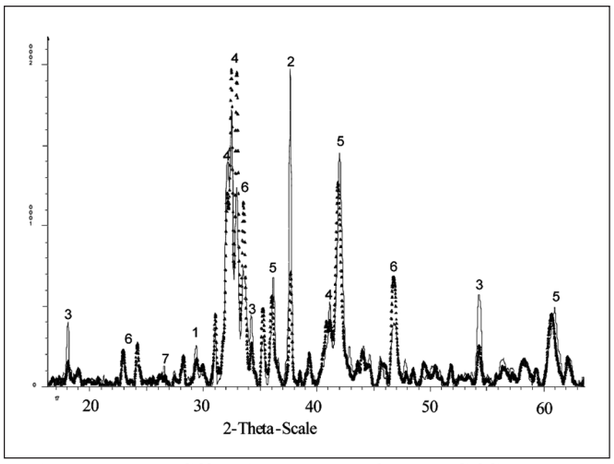

Figure 2 X-ray diffraction pattern of BS2; solid line BS2H, dotted line BS2L
1-$CaCO_3$, 2-CaO, 3-$Ca(OH)_2$, 4-C_2S, 5-FeO, 6-C_2F, 7-SiO_2

Most authors mention the presence of C_3S and C_4AF [MUR 97, MAH 08]. These two phases are hardly distinguishable in the XRD pattern because of peaks overlapping. However C_3S phase can stand out from C_2S by a peak at 1.76 Å which is not visible in the X ray pattern probably due to the low content of this phase. C_3S is especially present in BOF slag with a Ca/Si basic ratio higher than 2.7 [CAI, 00].

We note that no amorphous phase was detected by this technique. The transmission electron microscopy analysis showed that all samples are mainly crystallized. Only the C_2S phase containing phosphorus has a diffuse diffraction pattern which shows a low crystallinity.

The cooling rate may influence slag composition or the mineral phases present and, consequently, alter the mechanical properties of these materials [SRI, 06]. An amorphous phase can be formed with a 10°C/min cooling rate for the $CaO\text{-}SiO_2\text{-}Al_2O_3$ system, while its formation requires a more rapid cooling for the $CaO\text{-}SiO_2$-FeO one [DUR, 08]. BOF slag samples were then kept at 1250°C during 24h in an inert atmosphere and then cooled at 5°C/min. This cooling rate will allow a slow and complete crystallization of the samples phases, including that of a possible amorphous phase. Results highlighted the presence of a new crystalline phase with a chemical formula $Ca_5(PO_4)_2(SiO_4)_6$. No other crystalline phase appeared. The absence of any amorphous halo on the X-ray patterns shows that this phase, even if it exists, would be present only at a very low content which can not reasonably influence the hydraulic behavior of these materials.

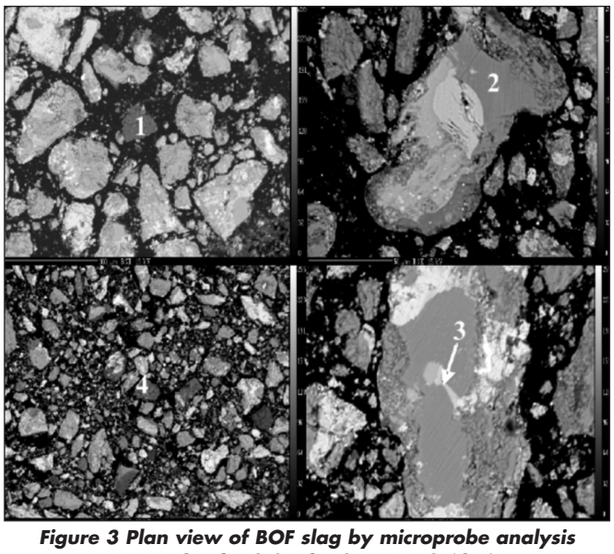

Figure 3 Plan view of BOF slag by microprobe analysis
1 : MgO – 2 : C_2S – 3 : C_2F – 4 : $Ca(OH)_2$

To evaluate the specific chemical compositions of phases identified above, the samples were characterized by the micro probe technique. A plan view, given in figure 3, shows the structural heterogeneity of BOF slag.
Generally, phases are intermixed in a grain. It is rare to observe independent phase as the grains of MgO and $Ca(OH)_2$ (grains 1 and 4 respectively in figure 3). Calcium silicates seem to be homogeneous phases with the Ca/Si ratio varying from 1.8 to 3.5 (grain 2). The average of Ca/Si ratio is 2.4; this means that the major phase is C_2S. The presence of C_3S is possible because of the relatively high Ca/Si ratio in some grains, but the content of this phase is too low to be detected with XRD. The average composition of silicate phases is given in table 2.

Wt % C_2S	Si	P	Ca	O	Ca/Si
	9-14	0.5-2	27-32	55-57	1.8-3.5

Table 2: Average atomic composition of C_2S phases

The only impurity detected in this phases is phosphorus. Geiseler shows that the C_2S can be present in solid solution with C_3P [GEI, 96].
Calcium ferrite (grain 3) is also a homogeneous phase with more or less high content in aluminum. The ratio of Fe/Ca is, in some points, close to the C_4AF phase one. This phase can be present in BOF slag [MAH, 08], but can not be identified in X ray diffraction due to the overlapping peaks with C_2F ones. The average composition of ferrite phases is given in table 3.

Wt % C_2F (Al)	Al	Ca	Ti	Fe	O	Fe/Al
	4-5	23-24	1-2.4	13-16	52-53	2.5-3.7

Table 3: Average atomic composition of C_2F phases

Most grains present solid solutions (Fe, Mg, Mn and Ca)O with variable contents, a common mineral in BOF slag [TSA, 07]. Tossavainen has identified by XRD two types of wustite solid solutions (Fe, Mn, Mg)O and a solid solution dominated by CaO [TOS, 07].

3.3. Chemical characterization

The residual lime content ($CaO + Ca(OH)_2$) expressed in equivalent CaO was measured by a glucose extraction and filtrate's titration by hydrochloric acid. This chemical titration includes also the free MgO content but this last one is neglected in our study since XRF results show a weak value and the micro probe technique confirm that it is mostly present in solid solution. This chemical titration is completed by a TGA technique in order to differentiate CaO and $Ca(OH)_2$. Two reactions can be distinguished in the temperature interval 20-800°C.
◊ 450°C: $Ca(OH)_2$ dehydration $Ca(HO)_2 \rightarrow CaO + H_2O$ [2]
◊ 750-800°C: $CaCO_3$ decarbonation $CaCO_3 \rightarrow CaO + CO_2$ [3]
According to the reactions (2) and (3) the content of $Ca(OH)_2$ and $CaCO_3$ can be calculated with mass balance. The results are given in table 4.

Wt %	Free lime	$Ca(OH)_2$	CaO	$CaCO_3$
BS1F	6,8	6,3	2,0	2,9
BS1W	7,8	7,3	2,3	4,0
BS2L	5,5	1,1	4,6	1,9
BS2H	10,3	2,9	8,1	2,6

Table 4: Calcareous phases content

From chemical titrations of FeII and FeIII and based on the fact that FeII is only present in $Fe_{(1-x)}O$ and FeIII in C_2F, these two phases contents are calculated and given in Table 5.

	"FeO" (%)	C_2F (%)
BS1F	11,9	30,3
BS1W	12,9	24,5
BS2L	11,5	20,2
BS2H	13,1	22,5

Table 5: Iron phases content

The last phase to quantify is calcium silicate. The method adopted is extraction of calcic phases with salicylic acid. Powder extracted was analyzed with XRD. C_2S, $Ca(OH)_2$ and CaO were dissolved by the acid and C_2F, $Fe_{1-x}O$, $CaCO_3$ and SiO_2 remain in the powder. C_2S and SiO_2 contents can be calculated with balance mass. The results are given in table 6. Metal iron is not considered in this calculation. It may be associated to SiO_2 content. This may explain the variability of this parameter.

3.4. Phases assessment

The compositions of studied samples are given in table 4. It should be noted that the chemical compositions of BOF slag are close despite their different origins and ages. It should be noted that some phases were neglected in this calculation such free MgO and iron metal whose contents are weak comparing to others minerals.

	C_2S	C_2F	FeO	$Ca(OH)_2$	CaO	$CaCO_3$	SiO_2
BS1F	41.8	30.3	11.9	6.3	2.0	2.9	4.7
BS1W	38.1	24.5	12.9	7.3	2.3	4.0	10.9
BS2L	52.0	20.2	11.5	1.1	4.7	1.9	8.5
BS2H	51.1	22.5	13.1	2.9	8.1	2.7	0

Table 6: Minerals contents in BOF slag

3.5. BOF slag evolutivity

The characterization of various BOF slag samples has shown that these materials have quite similar compositions, irrespective of their origins. But their chemical composition can evolve by hydration and/or carbonation of free lime and calcium silicate. Calcium oxide contained in the finely ground BOF slag reacts with moisture in the air to give hydrated lime Ca $(OH)_2$ which, itself, reacts with the ambient CO_2 to form calcite $CaCO_3$. Thus the CaO content decreases over time, this may alter the physical properties of these materials.

To investigate samples evolutivity, the $Ca(OH)_2$ and $CaCO_3$ contents were identified over time by thermogravimetric analysis. BOF slag powder, with 0/125 m particle size, was kept in an oven at 40°C and in air at ambient laboratory temperature. The results are shown in figure 4.

At 20°C, calcite $CaCO_3$ develops due to calcium hydroxide $Ca(OH)_2$ carbonation. However, the amount of $Ca(OH)_2$ phase remains almost constant. Its carbonation is simultaneously done with its formation by CaO hydration.

At 40°C the contents of the various phases do not evolve. An increase in carbonate content is rather expected since temperature accelerates the carbonation process. This must be due to a low humidity in the oven; this parameter affects the kinetics of carbonation. Indeed, a study has shown that the carbonation of the lime is 9-20 times faster in the presence of water vapor [NIK, 07]. This phenomenon requires a process of dissolution of $Ca(OH)_2$, and CO_2 is then more easily adsorbed on the grain surface by the OH^- ions.

4 CONCLUSIONS

The different complementary techniques used in this study were an original approach to quantify and qualify BOF slag's mineral phases. Four samples of two different origins were investigated. They have a similar chemical composition. The most significant difference between the two origins is the C_2S content, which is present in at least 38%. Dicalcium silicate was detected in the form of β-C_2S which is the active polymorph present in hydraulic binder. C_3S was also identified in same grains by micro-probe analysis but its content is so weak to be detected by XRD. The second mineral, mainly present, is C_2F. It always contains Al and can cover up C_4AF in XRD analysis.

Due to the presence of those minerals, BOF slags can be considered as suitable material in field of construction. However wustite, which is present in at least 11%, has no hydraulic properties. It also has the ability to take up to 27% calcium oxide. This last phase is trapped into solid solution and can not react.

Composition of BOF slag evolves once reduced to a fine powder. The carbonation of free lime is preferred in humid atmosphere where two reactions occur simultaneously:

– calcium oxide hydration $CaO + H_2O \rightarrow Ca(OH)_2$

– calcium hydroxide carbonation $Ca(OH)_2 + CO_2 \rightarrow CaCO_3$

This results in a significant decrease in the density of these materials and, probably, their mechanical properties.

The interpretation and comparison of results obtained for different slag revealed interesting points for their eventual reactivity. The complete methodology proposed in this work is an essential preliminary step to find the best way of their valorization in construction.

REFERENCES

[MAH 08] Mahieux P-Y., Aubert J-E., Escadeillas G., "Utilization of weathered basic oxygen furnace slag in the production of hydraulic road binders", *Construction and Building Materials*, Vol.23, 2008, p.742–747.

[MOT 01] Motz H., Geisler J., "Products of steel slags an opportunity to save natural resources", *Waste Management*, vol.21, 2001, p.285–293.

[CAI 00] Caijun S., Jueshi Q., "High performance cementing materials from industrial slags – a review", *Resources, conversation and recycling*, vol.29, 2000, p.195–207.

[LEC, 11 -1] Lecomte A., Dao L.P., Diliberto C., Sommier M., Basso P., "Valorisation des LAC dans les mélanges granulaires. Partie 1 : un modèle de dégradation", *EJECE*, in press

[LEC, 11 -2] Lecomte A., Dao L.P., Diliberto C., Sommier M., Basso P., "Valorisation des LAC dans les mélanges granulaires. Partie 2 : modélisation de la courbe d'expansion à la vapeur", *EJECE*, in press

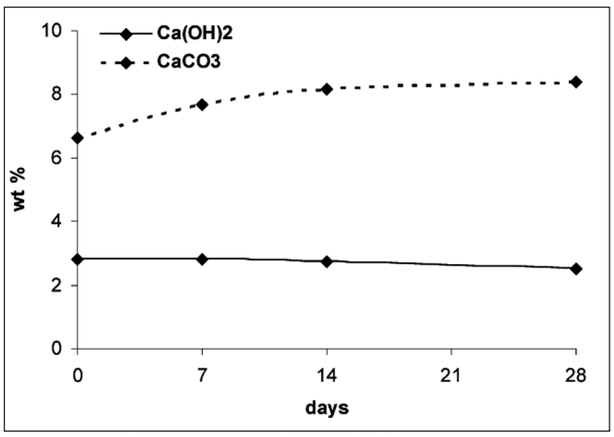

Figure 4a: BOF slag evolutivity at 20°C

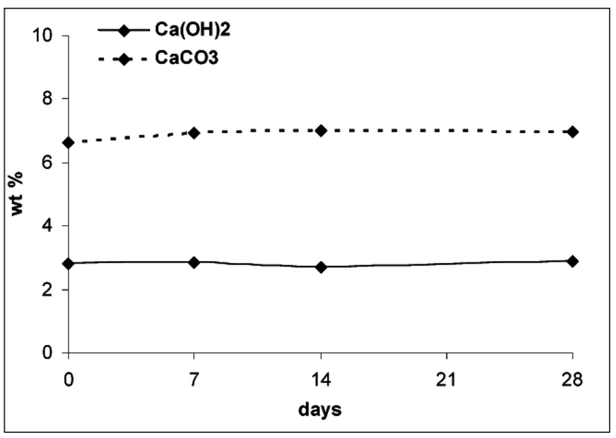

Figure 4b: BOF slag evolutivity at 40°C

[LEC, 11 -3] Lecomte A., Dao L.P., Diliberto C., Sommier M., Basso P., "Valorisation des LAC dans les mélanges granulaires. Partie 2 : modélisation de l'expansion d'un mélange quelconque", *EJECE*, in press

[MUR 97] Murphy J.N., Meadowcroft T.R., Barr P.V., "Enhancement of the cementitious properties of steelmaking slag", *Canadian Metallurgical Quarterly*, vol.36, n°5, 1997, p 315–331.

[SHI, 02] Shi C., "Characteristics and cementitious properties of ladle slag fines from steel production", *Cement and Concrete Research*, vol 32, pp 459-462, 2002

[SRI, 06] Srinivasa Reddy A., Pradhan R.K., Sanjay C., "Utilization of Basic Oxygen Furnace (BOF) slag in the production of a hydraulic cement binder", *Int. J. Miner. Process*, vol 79, pp 98-105, 2006

[DUR, 08] Durinck D., Engstrom F., Arnout S., Heulens J., Jones P.T., Bjorkman B., Blanpain B., Wollants P., "Hot stage processing of metallurgical slags", *resources conservations and recycling*, vol 52, pp 1121-1131, 2008

[GEI 96] Geiseler J., "Use of steelworks slag in Europe", *Waste Management*, vol.16, 1996, pp.59–63.

[TSA 07] Tsakirdis P.E., Papadimitriou G.D., Tsivilis S., Koroneos C., "Utilization of steel slag for Portland cement clinker production", *Journal of Hazardous Material,* vol.152, 2007, p.805–811.

[TOS 07] Tossavainen M., Engstrom F., Yang Q., Menad N., Lidstrom Larsson M., Bjorkman B., "Characteristics of steel slag under different cooling conditions", *Waste Management,* vol.27, 2007, pp.1335–1344.

[NIK, 07] Nikulshina V., G´alvez M.E., Steinfeld A., "Kinetic analysis of the carbonation reactions for the capture of CO_2 from air via the $Ca(OH)_2$-$CaCO_3$-CaO solar thermochemical cycle", *Chemical Engineering Journal*, vol 129, pp 75-83, 2007

USE OF SHAPE MEMORY ALLOY WIRES FOR THE CREATION OF PRESTRESS STATES IN CONCRETE BEAMS

Hanh TRAN[1], Aleksandra DEBSKA[1,2], Xavier BALANDRAUD[1], Jean-François DESTREBECQ[1]
[1]Clermont Université, Blaise Pascal University & French Institut for Advanced Mechanics (IFMA), EA 3867, Laboratoire de Mécanique et Ingénieries, BP 10448, F-63000 Clermont-Ferrand, France, hanh.tran@ifma.fr, xavier.balandraud@ifma.fr, j-francois.destrebecq@univ-bpclermont.fr
[2]Cracow University of Technology, Institute of Materials and Constructions, ul. Warszawska 24, 31-155 Cracow, Poland, aleksandra.debska@wp.pl

1. INTRODUCTION

Shape memory alloys (SMAs) are active materials that exhibit special properties such as pseudoelasticity and memory effect [1-2]. These properties are resulting from austenite vs. martensite reversible transformations governed by temperature and mechanical stress states. The austenite (parent phase) and the martensite (product phase) are present respectively at high and low temperature. A SMA has only one shape in an austenitic state, but it has the ability to retain the shape given to it in a martensitic state. A return to the original shape is obtained by returning the SMA to austenite by raising the temperature (memory effect). Because of their unique properties, SMAs have found applications in mechanical engineering, aerospace or for medical uses.

The use of SMAs in civil engineering is still very limited, partly because of their cost, but also because of a lack of knowledge of the mechanisms involved in their association with other materials such as concrete [3]. A few preliminary studies have provided insight into the benefits of exploiting the unique properties of these alloys by combining them with concrete in the form of internal or external reinforcements [4-6]. Other studies attempted to use the properties of these alloys, for example to create active structures able of adjusting their behaviour to the loading conditions [7]. Confinement effects were also obtained in concrete cylinders by means of SMA wires used as external reinforcements [8-9]. Also, damping effects related to the pseudoelasticity have been used to control dynamic effects [10-11] or for the seismic protection of bridges and historic buildings [12-15]. These studies have shown that the combination of concrete with SMA can provide significant gains in terms of strength and ductility or to delay cracking.

In the present study, nickel-titanium wires are used as external reinforcement to create prestress states in small-scale concrete beams. The aim of the study is to

investigate the relation between the mechanical properties of the SMA wires and the prestress states obtained. To this end, the austenite vs. martensite transformation temperatures were chosen so as to facilitate obtaining stresses at room temperature. At first, the wires were characterized in terms of their thermomechanical behaviour. In a second time, they were given a prestrain in a martensitic state before being firmly fixed on small scale concrete beams. The number of wires and the prestrain range were the parameters of the study. Thermal activation of the memory effect in the SMA wires caused their tensioning, which resulted in reaction in the creation of stresses in the tested beams. Progressive developments of the stresses in the concrete were assessed by measuring the strains induced in each tested beam.

From the experimental results, the influence of the magnitude of the initial stretching of the martensitic wires and the influence of the martensite vs. austenite transformation temperatures are finally discussed in view of the use of SMAs for the creation of prestress states in concrete components. In particular, it is shown that the magnitude of the prestressing force can be bounded in some cases by a production of martensite in the SMA wires upon return to ambient temperature.

2. CREATION OF FORCES USING SHAPE MEMORY ALLOY WIRES

2.1. Thermomechanical properties of SMAs

Depending on its temperature, a given SMA may exhibit very different mechanical properties. This section briefly reviews the physical phenomena involved in this study to create prestress effects in concrete components.

The macroscopic properties of SMAs originate from a phenomenon of solid-solid phase transformation governed by mechanical stress and temperature [1-2]. The parent phase is called austenite (marked *A* in the following). It has a body-centred-cubic crystal structure in all known SMAs. The product phase is called martensite (marked *M* in the following). Its crystal symmetry depends primarily on the composition of the alloy. Due to the loss of symmetry during the $A \rightarrow M$ transformation, martensite is in the form of several variants which correspond to the same crystal, but oriented differently in space relatively to the crystal of austenite. The displacement of atoms during the $A \rightarrow M$ transformation results in a transformation strain. When different variants exist in equal proportion, the macroscopic equivalent strain is almost zero. This is known as self-accommodating martensite [16].

Figure 1 presents the phase diagrams showing the status of the material as a function of stress and temperature. The material can be either purely austenitic (*A*), or purely martensitic (*M*) with different proportions of martensite variants, or a mixture of the two phases (*A*+*M*):

– Figure 1-a: starting from austenite, martensite can be obtained either by decreasing the temperature or by applying a mechanical stress. The two tilted lines correspond to the beginning and the end of the $A \rightarrow M$ transformation. Upon cooling down at zero stress, the transformation begins at temperature M_s (martensite start) and it ends at temperature M_f (martensite finish). Note that the martensite obtained is entirely self-accommodating, so there is no macroscopic strain. Martensite can also be obtained by mechanical loading at a given temperature. In this case, it is not self-accommodating: the orientation of the martensite variants caused by the mechanical stress results in a significant transformation strain (stretching of the martensite).

– Figure 1-b shows the phase diagram when one starts from the martensitic state. Stretching of the martensite at constant temperature results in a change in the proportions of martensite variants, while keeping the total percentage to 100%. The martensite is said to "orient" and the resulting deformation is preserved upon unloading. One can thus obtain different macroscopic forms after unloading. A return to the austenitic state is obtained by a temperature rise. At zero stress, the $M \rightarrow A$ transformation starts at temperatures A_s (austenite start) and ends at temperature A_f (austenite finish). The transition to the austenitic state is accompanied by a return of the material to its original shape. This unique property, called "memory effect" is thus obtained by simple thermal activation.

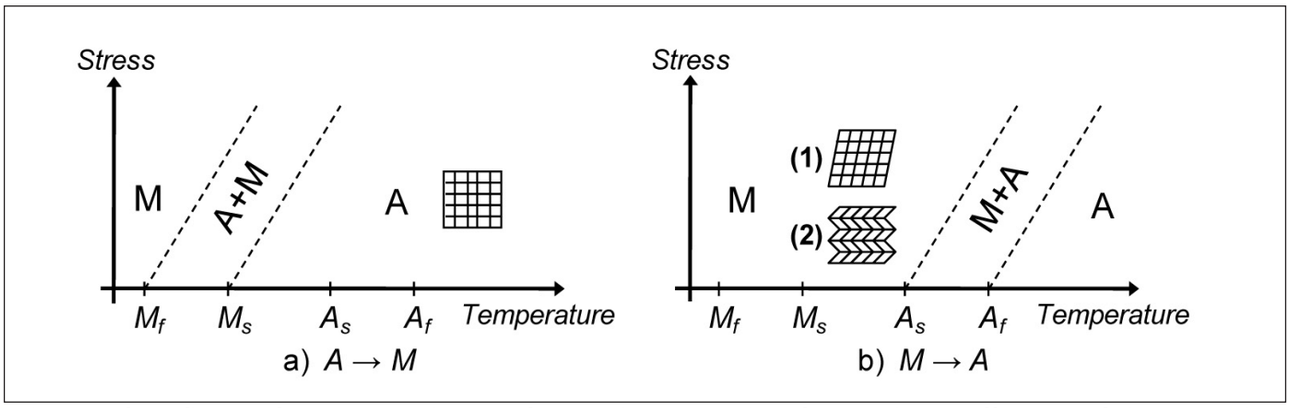

Figure 1. Phase diagrams between austenite (A) and martensite (M): (1) oriented martensite, (2) self-accommodating martensite.

2.2. Creation of forces by memory effect

In the present study, the creation of permanent forces at room temperature ($T_A \approx 20°C$) was made possible by choosing a nickel-titanium SMA wire for which $M_s < T_A < A_s$. A key issue concerned the thermomechanical loading to apply in order to create a force in a SMA wire. Figure 2 describes the seven steps procedure defined to this purpose [17]:

– Steps (1) to (3): heating ($T > A_f$) to put the wire in an austenite state, then cooling down ($T < M_f$) to put the wire in a self-accommodating martensite state, finally returning to room temperature T_A.
– Steps (4) and (5): stretching of the wire aiming at causing a deformation by orientation of the martensite. The residual strain after unloading is denoted ε_{mart} (prestrain).
– Step (6): heating of the wire ($T > A_f$) while keeping its length constant. Since the wire cannot recover its initial length, the memory effect induced by the return to the austenitic state causes the creation of a tensile force in the wire. The magnitude of the obtained force depends on the amplitude of the prestrain ε_{mart}.
– Step (7): return to room temperature T_A while keeping the wire length constant. Figure 2-b shows that two cases can possibly occur. In case 1, the stress reached after heating is preserved upon cooling down. In case 2, a partial production of martensite at the end of the cooling period causes a drop in the stress in the wire. Therefore, the final level of the force strongly depends on the test conditions.

NB: Steps (1) to (5) correspond to the preparation of the wires before setting up on the beams; Steps (6) and (7) simulate the response of the wires connected to the beams during activation of the memory effect.

3. THERMOMECHANICAL CHARACTERIZATION OF THE SMA WIRES USED

Nickel-titanium wires were used in the present study, with the following features: diameter 1 mm, composition $Ni_{50.8}$-$Ti_{49.2}$ (% at.), transformation temperatures A_s = 23°C, A_f = 28°C, M_s = -10°C, M_f = -25°C. Characterization tests were performed on 150 mm long wire coupons by means of a MTS testing machine ±15kN. The ambient temperature T_A was 19°C ± 1.5°C. The objective was to determine the relationship between the prestrain ε_{mart} at the end of step 5 and the force obtained in the wire during the thermal cycle. More precisely, two particular values were derived from the experimental measurements:

– the maximum value of the force obtained upon heating of the wire after return to the austenitic state (end of step 6). This value is denoted F_{aust} in the following.
– the ultimate value of the force obtained upon cooling down after return to room temperature (end of step 7). This value is denoted F_{res} in the following.

Figure 3 shows the values obtained for F_{aust} and F_{res} in terms of ε_{mart}. It is observed that F_{aust} increases with ε_{mart}. This force is preserved upon cooling down ($F_{res} = F_{aust}$) for low ε_{mart} *values*. A loss is observed ($F_{res} < F_{aust}$) after cooling down (end of step 7) when ε_{mart} exceeds a given value. This effect was expected in view of Figure 2-b (case 2), but the fact that F_{res} is constant whatever ε_{mart} over the limit

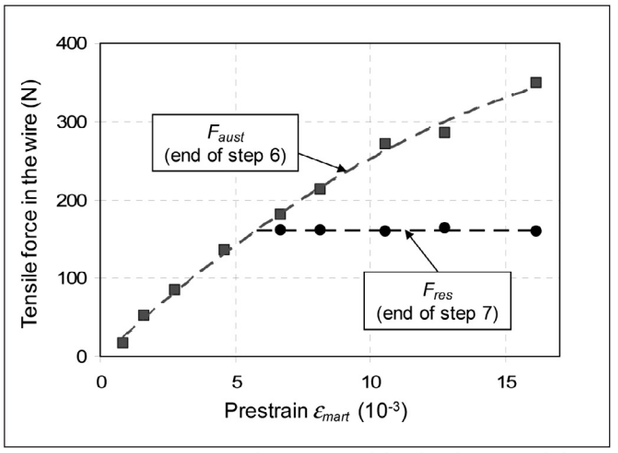

Figure 3. Maximum value F_{aust} and final value F_{res} of the tensile force obtained after thermal activation of the memory effect, in terms of the prestrain ε_{mart} given to the wire in the martensitic state.

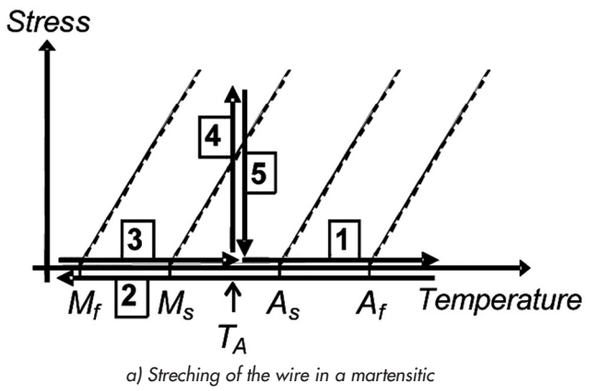

a) Streching of the wire in a martensitic state at room temperature

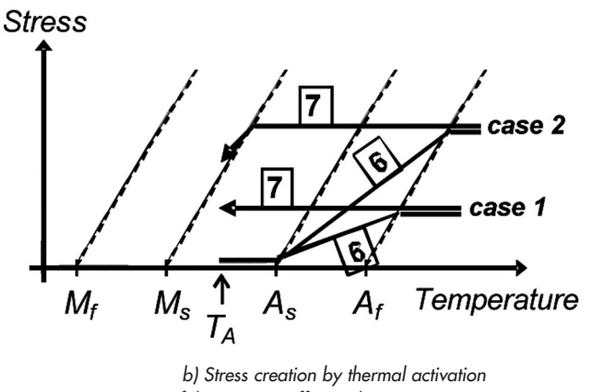

b) Stress creation by thermal activation of the memory effect with a constant strain

Figure 2: Seven steps procedure for the creation of a tensile force in a SMA wire by thermal activation of the memory effect.

value was not obvious a priori. An additional tensile test provided the Young's modulus of the wire in the austenitic state (62.9 GPa).

4. CREATION OF PRESTRESS STATES IN THE CONCRETE BEAMS

4.1. Preparation of the beams

Three plain concrete beams 48x60x520 mm in size were prepared for the tests. Given the size of the beams, the aggregate maximum size was limited to 8 mm. The beams were stored in plastic foils to prevent moisture loss during 28 days. Then they were kept in the ambient atmosphere of the laboratory until the tests performed between 6 and 10 weeks after casting day. Each beam was equipped with two strain gauges 30 mm in length bonded at mid-span on its upper and lower faces along the longitudinal axis. The modulus of elasticity of concrete was determined at the time of testing from strain measurements on the beams tested in three points bending (19.9 ± 1.7 GPa).

Anchor devices consisting of screws and steel plates were glued to the concrete at both ends of each beam (Figure 4). They were designed to securely attach the AMF wires onto the beam during the tests. Each anchor device was designed to accommodate 4, 8 or 12 wires. The wires were prepared according to the following procedure before being attached to the beams:

– Let the wires in a self-accommodating martensitic state – in this aim, the wires were heated to a temperature of +50°C (above A_f) and then cooled down to a temperature of -30°C (below M_f): see Figure 2-a, steps 1-3.
– Stretch the wires at room temperature (below A_s) to obtain a residual prestrain ε_{mart} in a oriented martensitic state after unloading: see Figure 2-a, steps 4-5.

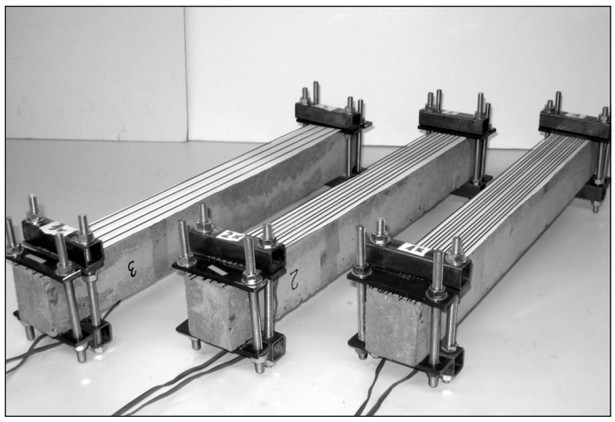

Figure 4: View of the three concrete beams equipped with AMF wires.

Six series of tests, each comprising three beams were conducted (Figure 4). Each series corresponds to a fixed value of the prestrain ε_{mart} in the oriented martensitic state. The selected values are given in Table 1 for each of the six series.

series:	1	2	3	4	5	6
$\varepsilon_{mart}(10^{-3})$:	1.6	2.6	4.0	6.0	8.2	10.2

Table 1: Prestrain of the AMF wires in an oriented martensitic state for the six test series.

4.2. Realisation of the tests

Each test series began with the preparation of the AMF wires according to the procedure explained above. Then, the wires in the prestrain martensitic state were attached to each of the three beams (4, 8 or 12 wires). The beams were placed in a controlled thermal chamber. The temperature was raised to 60°C at a rate of 1.6°C / min., then cooled down to room temperature at a rate of 0.8°C / min. The temperature rise beyond A_f caused the wires to return to an austenitic state. Since the wires were not free to recover their original length, the $M \rightarrow A$ transformation yielded the emergence of a tensile force in the wires which acted as a prestressing force and caused the deformation of the beam.

The strains measured during the tests are presented in Figure 5 for the three beams of Series 4 ($\varepsilon_{mart} = 6.0\ 10^{-3}$). For each beam, the solid line represents the longitudinal strain measured at mid-span on the side equipped with the AMF wires, while the dotted line represents the strain on the opposite side. Starting from a zero initial deformation, one observes that the strains increase in absolute value from about 27°C and then stabilize beyond 58°C. These strains result from the progressive tensioning of the wires due to the thermal activation of the memory effect (gradual return from an oriented martensitic state to an austenitic state). The slope observed upon cooling down results from the thermal contraction of the wires in the austenitic state.

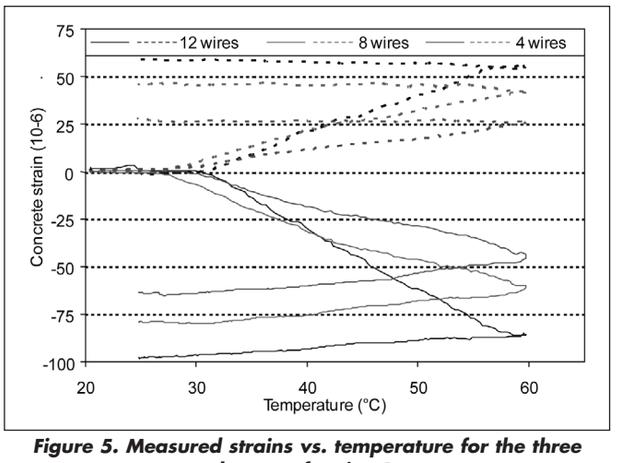

Figure 5. Measured strains vs. temperature for the three beams of series 4.

4.3. Interpretation of the test results

Basing on the classic equations of the beam theory, it is easy to deduce the evolution of the tensile force in the SMA wires from the strains measured during the tests. As

an example, the values vs. time are plotted in Figure 6 for the three beams of series 4. Each of the curves presented can be analyzed in three phases. The initial phase where the force remains equal to zero corresponds to the time required to reach the temperature corresponding to the beginning of the austenite to martensite transformation. The rising phase that follows it (up to 1800 s.) corresponds to the thermal activation of the memory effect. During this phase, the gradual return to the austenitic state is accompanied by a cancellation of the prestrain given to the SMA wires in the oriented martensitic state. Since this transformation occurs in blocked strain condition, it induces a gradual development of a tensile force in the wires. The third phase (beyond 1800 s) corresponds to the cooling phase of the wires in an austenitic state. The slightly ascending plateau observed during this phase is due to the gain of additional force resulting from the thermal contraction of the austenitic wires during this cooling phase. The final value of the force is the total prestressing force exerted on each beam by the AMF wires after return to room temperature in the austenitic state.

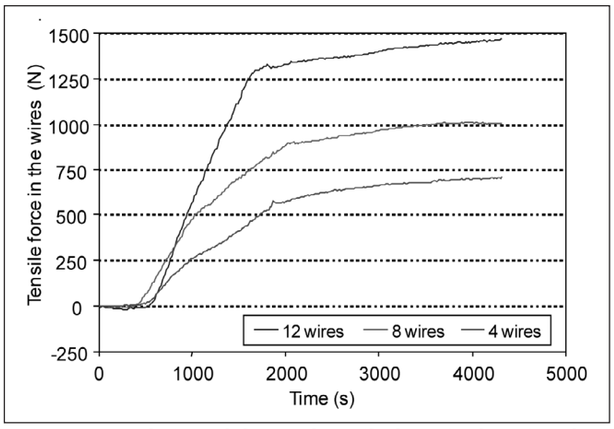

Figure 6. Evolution of the total tensile force in the wires for the three beams of series 4.

Figure 7 compares the evolutions of the tensile forces for the six beams equipped with 12 wires (series 1-6). It is observed that for the beams of series 1-4, which correspond to values of the prestrain ε_{mart} between 1.6 10^{-3} and 6.0 10^{-3}, the ultimate tensile force increases with the value of the prestrain ε_{mart} given to the wires in the martensitic state. For beams of series 5 and 6, corresponding to prestrains ε_{mart} equal to 8.2 10^{-3} and 10.2 10^{-3}, the tensile forces decrease during the cooling phases to a final value of approximately 1400 N close to that achieved for the series 4 beam. This result can be compared with the relationship shown in Figure 3 for the SMA wire behaviour. One observes in this figure that beyond a prestrain equal to about 6.0 10^{-3}, the F_{aust} force induced in the wire by thermal activation of the memory effect decreases to reach the value F_{res} after return to room temperature. As shown for case 2 in Figure 2-b, this phenomenon results from a stress induced production of martensite when the $A \rightarrow M$ threshold is reached upon cooling down. Since the $A \rightarrow M$ transformation temperature increases with the stress in the SMA, this phenomenon occurs only when the force in the wire exceeds its limit value at room temperature.

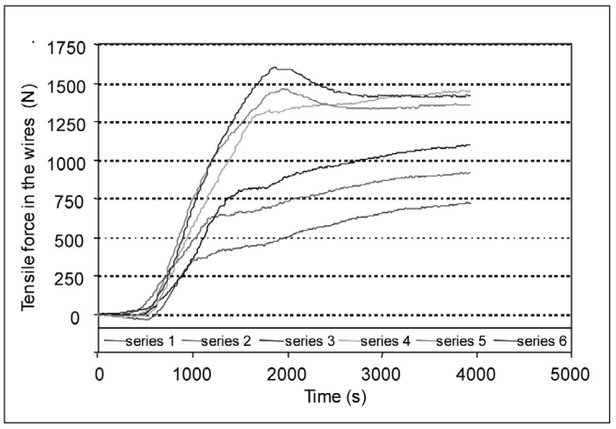

Figure 7: Evolution of the total tensile force for the 12 wires beams.

The prestressing effect created during the activation of the memory effect in the AMF wires can be estimated from the curvature of the beams derived from the longitudinal strains measured on the upper and lower faces of each tested beam. The final values obtained for the curvature after return to room temperature are shown in Figure 8 for the eighteen tested beams. One observes that the effect of prestressing increases quasi-linearly with the prestrain ε_{mart} as far as it does not exceed 6.0 10^{-3}. Beyond this value, increasing the prestrain has no more influence on the final curvature, which is limited for each of the beams due to the limitation of the prestressing force due to a production of martensite in the wires upon cooling down.

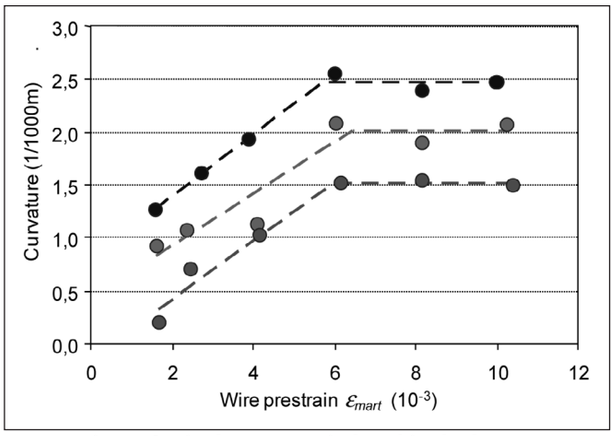

Figure 8: Final curvature induced in the beams by the prestressing effect.

This result emphasizes the influence of the transformation temperatures on the final effective prestressing force. An inappropriate choice can lead to an instant loss by partial production of martensite upon cooling down. Long term losses of a similar nature can also occur if the component is exposed to an excessive fall in temperature during its existence (outdoor works especially). Thus, one sees that

the choice of the transformation temperatures is critical to minimize the losses and ensure the permanence of the prestress states created in concrete components by memory effect.

5. CONCLUSION

The present study demonstrates the possibility to induce prestress states in concrete beams using nickel-titanium SMA wires. The procedure is to stretch the wires in a martensitic state before securely fasten them on the concrete beams. The memory effect is activated by raising the temperature above the transformation temperature A_f in order to cause the return of the wires to an austenitic state. This transformation causes the emergence of a tensile force in the wires which acts as a prestressing force towards the concrete component. This force has been estimated from the deformations measured in every tested beam. The tests enable to describe the process of developing the prestressing force during the thermal activation of the memory effect. The intensity of the force obtained depends on the number of wires and the prestrain given to the wires in the martensitic state. In the present case, it is highlighted that the final value of the prestressing force after return to room temperature is bounded by the value obtained for a prestrain equal to $6\ 10^{-3}$. This effect results from a partial production of martensite which limits the prestressing force in the wires upon cooling down. An inspection of the relationship obtained between the prestrain and the curvature induced after return to room temperature shows that this effect results from the thermomechanical properties of the alloy constituting the wires, but it is not affected by the number of wires fixed to the beams. These results show that the choice of the transformation temperatures is a key point to ensure the permanence of the prestressing and to prevent losses in case of temperature fall.

Although the cost of nickel-titanium alloys can be an obstacle to their use for the creation of prestress states in concrete components, activation of the memory effect by simply raising the temperature is a significant advantage over other conventional methods of prestressing. There exists also iron-based SMA with lower performances than nickel-titanium SMA, but with lower costs more suited to industrial applications. A possible field of application could be the use of SMA as an alternative method for behaviour improvement or strengthening of existing structures.

6. REFERENCES

[1] OTSUKA K., WAYMAN C.M., *Shape Memory Materials*, Cambridge University Press, 2002.

[2] GUENIN G., *Alliages à mémoire de forme*, Techniques de l'Ingénieur, Matériaux métalliques, 1996, Doc. M530, 1-15.

[3] MOTAVALLI M., CZADERSKI C., BERGAMINI A., JANKE L., *Shape memory alloys for civil engineering structures – on the way from vision to reality*, AMCM'2008, Lodz, Poland, 2008, June 9-11, 91-108.

[4] JANKE J., CZADERSKI C., MOTAVALLI M., RUTH J., *Applications of shape memory alloys in civil engineering structures: overviews, limits and new ideas*, Mater. Struct. 2005, 38(5), 578-592.

[5] DENG Z, LI Q, SUN H., *Behavior of concrete beam with embedded shape memory alloy wires*, Eng. Struct. 2006, 28(12), 1691-1697.

[6] LI H, LIU Z, OU J. *Behavior of a simple concrete beam driven by shape memory alloy wires*, Smart Mater. Struct. 2006, 15(4), 1039-1046.

[7] CZADERSKI C., HAHNEBACH B., MOTAVALLI M., *RC beam with variable stiffness and strength*, Constr. Build. Mat. 2006, 20(9), 824-833.

[8] CHOI E., CHUNG Y.S., CHO B.S., NAM T.H., *Confining concrete cylinders using shape memory alloy wires*, Eur. Phys. Journal, 2008, 158(1), 255-259.

[9] DESTREBECQ J.F., BALANDRAUD X., *Interaction between concrete cylinders and shape-memory wires in the achievement of active confinement*, in Materials with Complex Behaviour, Advanced Structured Materials, Springer 2010, 19-34.

[10] BARTERA F., GIACCHETTI R., *Steel dissipating braces for upgrading existing building frames*, J. Constr. Steel Res. 2004, 60(3-5), 751-769.

[11] LIU H., LI H., SONG G., OU J., *Investigation of vibration mitigation of stay cables incorporated with superelastic shape memory alloy dampers*, Smart Mat. Struct. 2007, 16(6), 2202-2313.

[12] DESROCHES R., DELEMONT M., *Seismic retrofit of simply supported bridges using shape memory alloys*, Engng. Struct. 2002, 24(3), 325-332.

[13] SHARABASH A.M., ANDRAWES B.O., *Application of shape memory alloy dampers in the seismic control of cable-stayed bridges*, Engng. Struct. 2009, 31(2), 607-616.

[14] MAZZOLANI F.M., MANDARA A., *Modern trends in the use of special metals for the improvement of historical and monumental structures*, Engng. Struct. 2002, 24(7), 843-856.

[15] PARET T.F., FREEMAN S.A., SEARER G.R., HACHEM M., GILMARTIN U.M., *Using traditional and innovative approaches in the seismic evaluation and strengthening of a historic unreinforced masonry synagogue*, Engng. Struct. 2008, 30(8), 2114-2126.

[16] BHATTACHARYA K., *Microstructure of martensite: why it forms and how it gives rise to the shape-memory effect*. Oxford University Press, 2003.

[17] TRAN H., BALANDRAUD X., DESTREBECQ J.F., *Recovery stresses in SMA wires for civil engineering applications: experimental analysis and thermomechanical modelling*, Mat. Sc. Engng. Techn. (Wiley), 2011.

RÉNOVATION DES BÉTONS. EFFICACITÉ DES IMPRÉGNATIONS HYDROFUGES À HAUT POUVOIR DE PÉNÉTRATION. RÉSULTATS SUR SITE

Préparé par Michel DONADIO
Responsable Technique Marché Rénovation
Sika Services AG

1. INTRODUCTION

Pour les structures de génie civil ainsi que pour les bâtiments, l'eau doit être maintenue à l'écart. En effet, en plus des problèmes d'humidité, l'eau peut être le vecteur pour ramener dans le béton des agents solubles agressifs tels que les chlorures et les sulfates.
Un problème commun à de nombreux pays pour les structures de génie civil est la récurrence de l'Alcali Rréaction (AR) qui a besoin d'humidité pour se déclencher.
Les ouvrages massifs de génie civil sont construits pour une très longue durée de service (*le pont Sitra[1]* est prévu pour durer 120 ans).
Cette longue durée de vie ne peut être atteinte que par la combinaison d'une conception appropriée de la structure (qualité du béton, des armatures, etc.) et d'une stratégie de maintenance.
Dans le cadre de cette stratégie de maintenance, les imprégnations hydrophobes à fort pouvoir de pénétration peuvent aider les concepteurs, architectes et ingénieurs, à augmenter cette durée de vie en maintenant éloignés les agents solubles agressifs et en réduisant éventuellement les effets dus à l'Alcali Réaction.

2. ESSAIS EN LABORATOIRE (RÉSUMÉ)

2.1. Une barrière efficace contre les chlorures

T-J. Zhao et al[2] ont étudié l'utilisation d'imprégnation hydrophobe en tant que barrière contre les chlorures. Ils ont montré que pour être efficaces, les imprégnations

hydrophobes devaient être appliquées en quantité suffisante. Appliqués en trop faible quantité, la protection n'est pas totalement efficace.

2.2. Influence des fissures

F. H. Wittmann et al[3] et *J. Dai et al[4]* ont étudié les performances des imprégnations hydrophobes à fort pouvoir de pénétration dans un béton fissuré.
Ces études ont montré que la meilleure protection était apportée quand le traitement avait lieu avant que les fissures n'apparaissent.
Toutefois, en utilisant des hydrofuges de surface qui pénètrent profondément le béton, un certain niveau de protection était malgré tout apporté même si les fissures se développaient après le traitement.
L'étude de *J. Dai et al[4]* montre aussi qu'en utilisant un produit à faible concentration, le béton n'était pas suffisamment protégé dans le temps.

2.3. Alcali Réaction

K.Kosun et al[5] ont étudié en laboratoire l'utilisation d'imprégnation hydrophobe à base de Silane pour réduire les effets de l'Alcali Réaction. Ils ont pu montrer que l'efficacité de ce traitement était d'autant plus importante que le béton était plus âgé.

3. EXPÉRIMENTATION SUR SITE

3.1. Tunnel en Suède

3.1.1. Procédures

A. Johansson et al[6] ont conduit une étude sur le long terme pour évaluer les effets d'un traitement hydrophobe sur un béton soumis aux sels de déverglaçage dans les zones d'éclaboussures. Un tunnel à fort trafic routier dans la ville de Stockholm a été sélectionné pour cette étude. Chaque année, la route est exposée aux traitements de sel de déverglaçage pendant au moins quatre mois.
Des cubes de béton avec un rapport eau / ciment (E/C = 0,45) ont été traités avec un Silane liquide (> 98% de matière active) conforme aux spécifications du guide du « *Swedish Road Administration »[7].*
Après le traitement, les échantillons de béton (traités et témoin de contrôle) ont été placés à 50 m à l'intérieur du

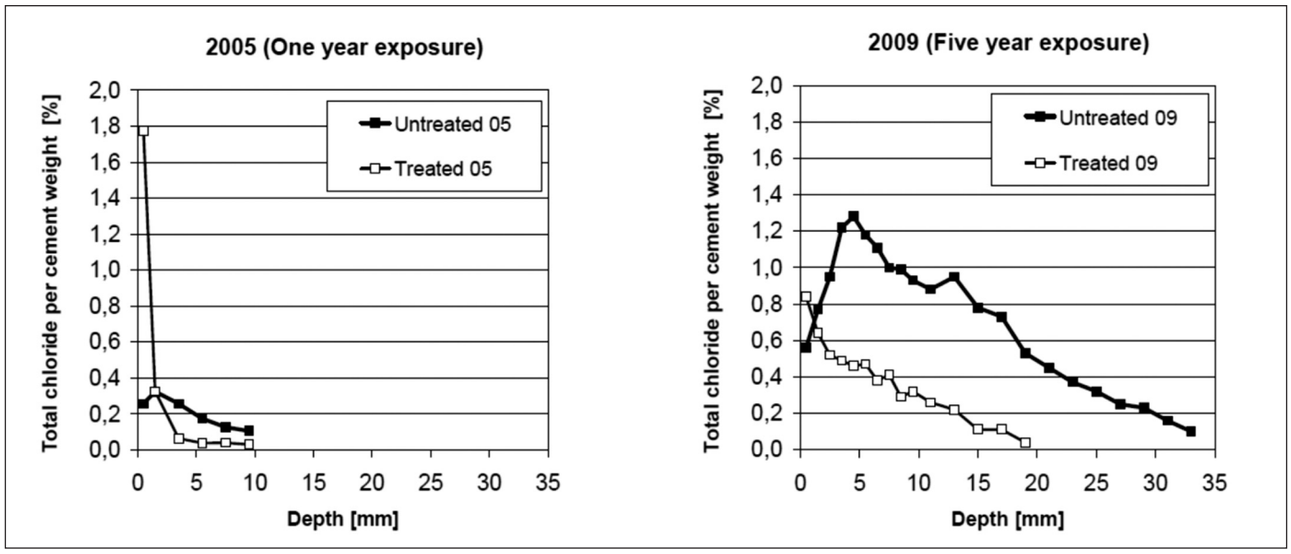

Figure 1 : Profil des chlorures

tunnel dans la zone d'éclaboussures. Chaque année, un échantillon traité et un échantillon non-traité sont prélevés pour être analysés. Les mesures des ions chlorures sont réalisées avec la technique des ions sélectifs.

3.1.2. Discussion/Résultats

En utilisant une imprégnation hydrophobe correspondant aux critères du guide Suédois, *A. Johansson [6]* a montré que le traitement reste efficace contre la pénétration des chlorures après 5 ans d'exposition dans les conditions climatiques sévères de la Suède.
L'étude montre que les chlorures ont commencé à pénétrer profondément dans les échantillons non traités; à l'inverse les surfaces traitées présentent une pénétration de ces chlorures très réduite.
Cette étude s'inscrit sur le moyen terme. Les résultats après une plus longue exposition seront communiqués dès que possible.

3.2. Port en Belgique

3.2.1. Procédures

L. Schueremans et al[8] ont conduit une investigation en 1993 sur une structure portuaire traitée avec une imprégnation hydrophobe (produit liquide, > 98% de matière active). La structure est un terminal de containers situé dans le port de Zeebrugge en Belgique.
Pour analyser l'efficacité du traitement, trois études consécutives ont été conduites en 1996, 1998 et 2005. Différentes zones du quai en béton ont été traitées : la zone de marnage, la zone d'éclaboussures et la partie horizontale supérieure du quai. Une portion similaire de béton pour chaque zone était laissée non traitée.
Pour mesurer les performances du traitement, les essais suivants ont été réalisés :
• Pénétration de l'imprégnation hydrophobe
• Profondeur de carbonatation
• Profil de chlorures dans le béton

3.2.2. Discussion/Résultats

En janvier 2005 (~12 ans d'exposition), la 3e étude était conduite par *L. Schueremans [8].*
Il a pu montrer que le traitement avec l'imprégnation hydrophobe restait efficace dans toutes les zones traitées.
La profondeur de pénétration de l'imprégnation variait entre 1 et 6 mm avec une valeur moyenne de 3,5 mm. – les pénétrations les plus faibles étant obtenues dans la partie supérieure du quai.
Le front de carbonatation (voir tableau 1) du béton témoin non traité est proche de zéro sur les 3 localisations. Ceci indique que le béton non traité est saturé en eau et de ce fait empêche la migration du gaz dioxyde de carbone. D'un autre coté, les résultats des zones traitées montrent une profondeur de carbonatation plus importante - ce qui est l'indication d'un assèchement du béton. Il est noté que ce front de carbonatation est encore très éloigné des armatures internes en acier.

Localisation	Profondeur de Carbonatation (mm)		
	2005	1998	1996
A : Zone Témoin			
Zones d'éclaboussure	0	0 – 0,05	0
Zones de marnage	0	0	1
Zones B & C : Traité			
Zones d'éclaboussure	8 - 12	6 - 12	4
Zones de marnage	4 - 6	5 - 10	5
Partie horizontale du quai	12 - 16	5 - 10	5

Tableau 1 : Front de carbonatation

Les chlorures solubles et insolubles ont été analysés selon la norme Belge NBN B 15-250. Seuls les chlorures solubles des résultats dans la zone de marnage sont présentés dans cet article (figures 2 & 3). Les autres résultats présentent les mêmes tendances.

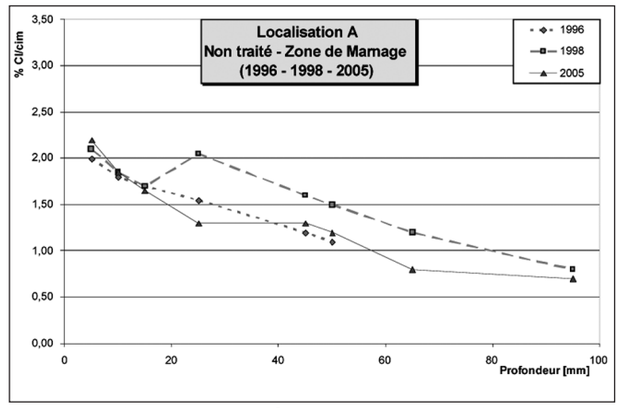

Figure 2 : Zone de marnage – non traitée

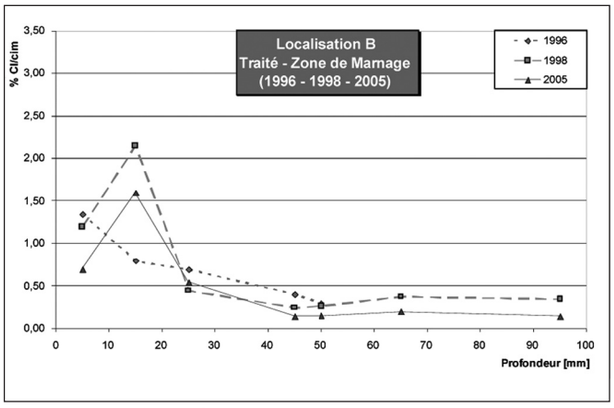

Figure 3 : Zone de marnage - traitée

Après 12 ans, le taux de chlorures dans les zones traitées reste significativement plus faible comparativement aux mêmes zones non traitées. A la profondeur de 50 mm, dans l'échantillon prélevé dans la zone de marnage non traitée, le taux de chlorures excède 1% du poids du ciment – un niveau suffisant pour augmenter les risques de corrosion des aciers; alors qu'à la même profondeur, le taux de chlorures dans la zone traitée reste inférieur à 0,50%.

Note : les variations de taux de chlorures entre les différentes études sont dues aux variations inhérentes à cette analyse (différence dans la qualité du béton, hétérogénéité, épaisseur de l'échantillon, tailles des agrégats au droit du prélèvement, variation de l'analyse, etc.).

Les auteurs ont réalisés une prédiction de durée de vie résiduelle sur la base du coefficient de diffusion des chlorures en faisant varier les niveaux de probabilité. (tableau 2). En utilisant le niveau moyen de probabilité, nous pouvons donc estimer le temps de démarrage du processus de corrosion dans les différentes zones de la structure (voir figure 4).

Coefficient de diffusion D - paramètre de distribution normale et prédiction de la durée de vie après 5 et 12 ans d'exposition					
Localisation	μ(D) [cm²/s]x10^{-8}	σ(D) [cm²/s]x10^{-8}	Durée de vie [y] C_T = 0,7% Cl⁻/ciment		
			$P_{f,T}$=0,5 β_T=0,0	$P_{f,T}$=0,15 β_T=1,0	$P_{f,T}$=0,07 β_T=1,5
A (non traité)	9,58	10,55	16,5	7	5
B (traité)	1,61	2,49	107	35	22
C (traité en surface du quai)	2,13	3,46	91	29	18

Tableau 2 : Coefficient de diffusion des chlorures et prédiction de la durée de vie

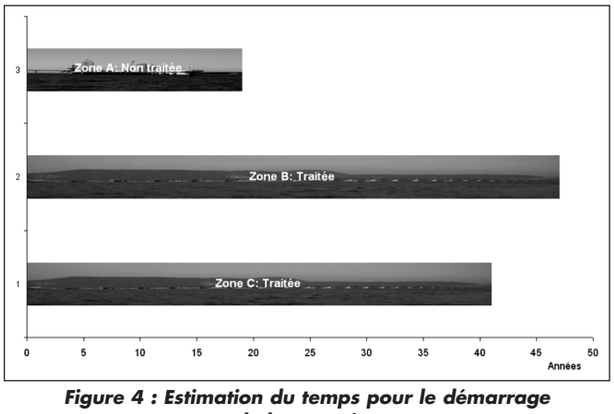

Figure 4 : Estimation du temps pour le démarrage de la corrosion

La figure illustre clairement la différence entre les zones traitées et non traitées.

Avec le béton non protégé, 20 ans après la construction de la structure, nous pouvons estimer que le processus de corrosion a commencé alors que dans les zones traitées il est très réduit ; l'initiation de la corrosion devant avoir lieu dans les 40-50 ans à venir.

3.3. Ponts en Suède

3.3.1.Procédures

Les imprégnations hydrophobes telles que celles à base de Silane sont utilisées en Suède depuis plus de 20 ans et la plupart du temps, le traitement fonctionne correctement. Toutefois, le niveau de performance de ce type de traitement sur une plus longue période n'est pas très documenté. *A. Johansson[8]* présente une étude montrant les absorptions d'eau de structures traitées par des Silane/siloxane ; certaines étant âgées de plus de 15 ans.

Des carottes de béton ont été prélevées sur 27 ponts pour vérifier les effets du temps comparativement à une étude précédente conduite en 2000 par *Nyman and Leon[9]* sur ces mêmes structures. Puisque le béton de référence non traité n'était pas disponible, les essais d'absorption capillaire ont été réalisés sur les 2 cotés des carottes (voir figure 5) après un régime de séchage approprié.

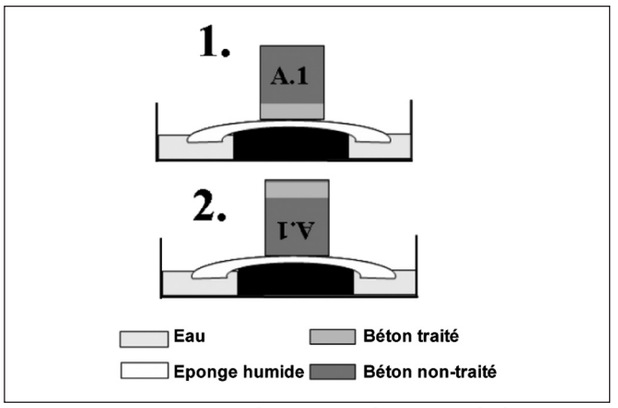

Figure 5 : Description schématique des essais d'absorption capillaire

3.3.2. Discussion/Résultats

Les essais d'absorption capillaire effectués en 2000 et 2005 montrent, dans la plupart des cas, une réduction significative de l'absorption d'eau entre les parties traitées et non traitées.

Les auteurs n'ont pu conclure à l'effet du vieillissement ; par contre ils ont pu montrer que *« la durée de vie d'un traitement efficace avec une imprégnation hydrophobe pouvait atteindre au moins 15 ans ».*

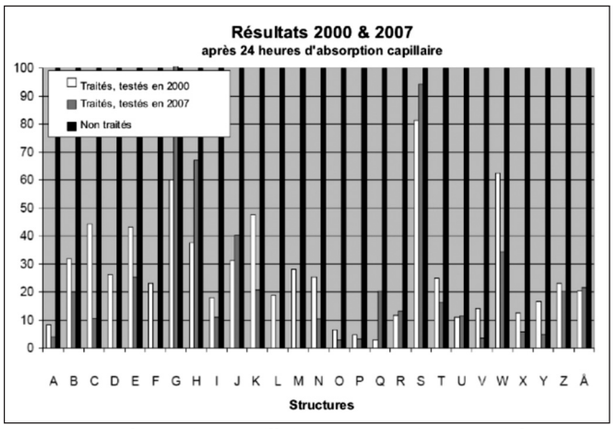

Figure 6 : Absorption capillaire comparativement à la partie non traitée (base 100)

3.4. Mitigation de l'Alcali Réaction en Australie

3.4.1. Procédures

En Australie, *F. Salome[10]* a étudié la alcali réaction dans des traverses ferroviaires en béton. Ces traverses présentaient des fissures peu de temps après leur fabrication. Des études ont montrées que le processus de dégradation était progressif et qu'il était du à la présence d'agrégats réactifs - à l'origine de l'Alcali Réaction.

Figure 7 : Traverses en béton

Deux sections de lignes (~100 traverses par section) ont été sélectionnées pour des essais d'hydrofugation dans le temps. Une étude systématique et détaillée de chaque traverse a permis de développer une classification numérique des défauts permettant de décrire les états initiaux et leur évolution éventuelle. Une valeur numérique arbitraire a été assignée à chaque type de défauts remarqué. Ces valeurs individuelles ont été additionnées pour chaque zone (traitée et non-traitée).
Une traverse sur deux était traitée avec un Silane monomérique pur et l'application réalisée sans préparation de surface préalable, a été faite sur les parties exposées des traverses (la partie donnant sur le sol n'étant pas traitée). Les consommations étaient d'environ 0,8 à 1,0 litre par traverse (0,4 à 0,5 l/m²).
L'investigation a été conduite sur 3 ans.

3.4.2. Discussion/Résultats

Initialement les valeurs numériques moyennes pour les 2 séries (traitées et non traitées) de chaque zone étaient proches l'une de l'autre (Sur la ligne Northam 119, la valeur moyenne initiale pour les traverses non traitées est de 10,20 et de 9,20 pour celles traitées).
Dans le temps, l'étude conduite par l'auteur montre que les traverses non traitées se détériorent à une vitesse plus rapide que celles ayant été traitées.

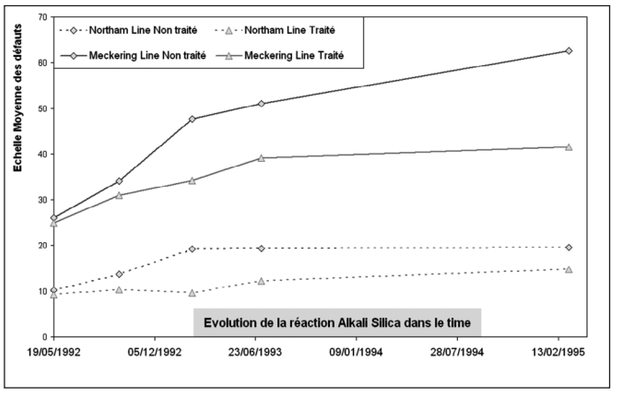

Figure 8 : Effet d'un traitement avec un Silane sur des traverses de béton sujettes à l'Alcali Réaction

Pour les 2 lignes étudiées, la vitesse de détérioration des traverses traitées par imprégnation hydrophobe a été divisée par 6.
Dans sa conclusion, l'auteur note que la rapidité de détérioration due à l'Alcali Réaction peut être réduite d'une manière significative en réduisant la pénétration de l'eau dans le béton en utilisant des imprégnations hydrophobes de type Silane.

4. NORMES

En Europe, la norme EN 1504-2 précise les spécifications de performance des imprégnations hydrophobes utilisées pour la protection des bétons de génie civil et de bâtiment. Ces imprégnations hydrophobes correspondent à une des méthodes recommandées pour les principes 1 (protection contre toute pénétration), principe 2 (contrôle de l'humidité) et principe 8 (augmentation de la résistivité) – se référer à la norme EN 1504-9.

Performance	Critère
Absorption d'eau initiale	<7,5% en ratio du témoin non traité
Absorption d'eau après immersion en alkalis	<10% en ratio du témoin non traité
Vitesse de séchage	Classe I: >30% Classe II: >10%
Profondeur de pénétration (E/C = 0,70)	Class I: <10mm Class II: =10mm
gel/dégel avec sel de déverglaçage (E/C = 0,70)	La perte de matière doit intervenir au moins 20 cycles plus tard que le témoin non traité.

Tableau 3 : EN 1504-2 Spécifications des imprégnations hydrophobes

Pour les 3 principes, le produit doit être conforme à tous les critères pour toutes les utilisations, excepté pour la spécification des cycles de gel dégel avec sels de déverglaçage qui concerne uniquement les zones sujettes à un hiver rigoureux. La sélection du type de produit dépend du type de projet, des conditions climatiques et des ambiances agressives éventuelles (ex. milieu marin).
Sur la base des diverses investigations présentées dans cet article, il est important pour la pérennité du traitement (et de fait pour la durabilité de la structure) de préconiser des imprégnations hydrophobes ayant les caractéristiques appropriées. Par exemple, pour infrastructure de génie civil :

- Classe II pour la profondeur de pénétration (> 10mm)
- Classe I pour le temps de séchage afin de minimiser les effets sur les transferts de vapeur d'eau (permettant au béton de s'assécher)
- et finalement en fonction des conditions climatiques de spécifier la résistance aux cycles gel dégel.

5. CONCLUSIONS

Cet article a exploré quelques études significatives et a présenté des résultats sur l'utilisation des imprégnations hydrophobes appliquées sur des structures en béton. Il peut être résumé comme suit :

– Pour être efficace, l'imprégnation hydrophobe doit pénétrer profondément le béton.
Si le produit reste en surface, il ne pourra pas fournir la protection nécessaire sur le long terme. La durabilité ne sera pas assurée.
– Seuls les produits ayant un taux de matière active important peuvent apporter cette protection sur le long terme.
– Les imprégnations hydrophobes en crème ou gel sont les plus performantes car elles pénètrent plus facilement le béton (sans être sujettes à l'évaporation ou la dispersion par l'effet du vent).

– Le traitement de protection reste efficace même en présence de fissures (la meilleure protection est apportée si le produit est appliqué après apparition des fissures).
– L'efficacité est prouvée sur site après plus de 15 ans d'exposition climatique drastique.
– Le traitement est efficace pour réduire les effets de l'Alcali Réaction.
– Seuls des produits conformes aux diverses spécifications normalisées doivent être utilisés. Le marquage CE de ces produits utilisés pour la protection de surface du béton est obligatoire depuis le 1er janvier 2009.

6. RÉFÉRENCES

[1] *Mostafa A. Hassanain*. The New Sitra Bridges, Specifying and executing concrete for durability in the Middle East; September 2010, Concrete International

[2] *T-j. Zhao, F.H. Wittmann and H-y. Zhan*. Water repellent surface treatment in order to establish an effective chloride barrier. Hydrophobe IV 2005 Stockholm

[3] *F.H Wittmann, P. Guo and T. Zhao.* Influence of cracks on the efficiency of surface impregnation of concrete. Hydrophobe V 2008 Brussels

[4] *J. Dai, Y. Akira, E. Kato and H. Yokota*. Investigation of chloride ingress in cracked concrete treated with water repellent agents. Hydrophobe V 2008 Brussels

[5] *K. Tosun, B. Felekoglu and B. Baradan*. Effectiveness of Alkyl Alkoxy Silane Treatment in Mitigating Alkali Silica Reaction, ACI Materials Journal 105-M03, January/February 2008

[6] *A. Johansson, M. Janz, J. Trägårdh and J. Silfwerbrand*. Long-term measurements on chloride ingress in water repellent treated concrete in a road tunnel environment. Concec10, 2010, Mexico

[7] Test report Ref F507580 B rev dated 2005-05-09 – compliance with the instruction in "BRO 2002" of the Swedish National Road Administration

[8] *L. Schueremans, D. Van Gemert, M. Friedel and S. Giessler-Blank*. Durability of water repellents in a marine structure. Hydrophobe V 2008 Brussels

[9] *A. Johansson, M. Janz, J. Silfwerbrand and J. Trägårdh*. Swedish Cement and Concrete Research Institute; Long Term Performance of Water Repellent Treatment – Water Absorption Tests on Field Objects in Stockholm. Restoration of Buildings and Monuments Vol. 14, No. 1, 39–48 (2008)

[10] *A. León and B. Nyman. The Effectiveness of Water Repellent Treatments.* The Journal Bygg & teknik, No. 7, pp. 34-36. 2001

[11] *F. Salome*. Field Evaluation of the Mitigation Effect of Silane Treatment on AAR in Concrete Railways Sleepers.

MINERAL FOAMS WITH IMPROVED PERFORMANCES

C. BAUX[1], C. LANOS[2], A. PHELIPOT-MARDELÉ[2]
[1]Société K&Co, 84300 Cavaillon.
[2]UEB - LGCGM, Equipe Matériaux Thermo-Rhéologie, INSA-IUT, Rennes.
christophe.lanos@univ-rennes1.fr

1. INTRODUCTION

In a context of sustainable development and energy saving, there is a need for thermally efficient load-bearing materials in the field of restoration and construction.
Moreover, new standards enforce to reduce the use of fibrous compounds (e.g. rock wool and fiberglass) and of VOC-bearing polymers (e.g. PE and PU).
Hence, new types of building materials exhibiting the best compromise between insulating performances and mechanical properties must be developed. Hollow clay bricks for load-bearing walls are an interesting solution towards mechanical and thermal properties. Such cellular products can be optimized by:
– reducing the size of cells,
– increasing their number,
– and reducing their thickness.
This optimization step must remain compatible with the dedicated shaping techniques (e.g. extrusion, molding…). Cellular concrete is thus another quite good compromise. Its structure resembles the one of mineral foam whom cells' size is ranging from 0.2 to 2mm and whom wall thickness is around 0.1mm.
Some others solutions relying on environment friendly materials are being studied [ALL, 05]. Those environment friendly materials are hemp, reed, linen or wood-based composites. These materials are made of:
– vegetal hollow aggregates,
– mineral binders (e.g. lime, cement, gypsum…).
Most of these solutions are based on coupling of air filled cavities at different scales. They lead to products with quite low densities and thermal conductivities. In the same objectives, the development of mineral foams is an alternative solution that must be rediscovered.
After reminding the conditions that are needed to obtain foams in wet conditions, various foam production systems will be reviewed. Afterwards, some significant results obtained with gypsum-based binder will be presented. The influence of the formulation and of the forming conditions on the thermal and mechanical properties will be presented and discussed.

2. PRODUCTION OF FOAMS

2.1. Foam physics

An occlusion of gas bubble into a mineral binder is based on equilibrium between:
– The fluidity of the mix during shaping,
– The surface tension,
– The density,
– The pressure.
Foam shaping is based on physical principles [BRU 04] and [LAB 04], as expressed in the Laplace and Young relation see Eq. 1:

$$\Delta p = \gamma.(\frac{1}{R_1} + \frac{1}{R_2}) \quad \text{(Eq.1)}$$

Where:
– Δp is the pressure difference between the gas inside cells and the matrix binder

– and γ is the surface tension at the interface between the gas and the fluid.

R_1 and R_2 are the algebraic expression of the main radii of interface curvature (for spherical interface, $R_1 = R_2$).

For more precise explanation about these principles, see [BRU 04] and [LAB 04].

Foams can be obtained from different ways:

– Outgassing
– Modification of the solid/gas interface equilibrium, as example changing the surface tension by mean of wetting agent or changing air content…

2.2. Syntactic foam

Syntactic foam is a cellular composite material. Cavities are obtained with hollow-core aggregates, such as microspheres embedded in organic binders (e.g. epoxy, polyester, polyurethane, and polypropylene) (see. Fig. 1 left).

In some case of mineral binders (calcium silicate or gypsum-based binders), glass made hollow-core aggregates are used (see Fig. 1 right).

The foams that are made in such a way suffer weak mechanical performances induced by the hollow spheres. In the case of organic matrices, the foams are obtained by injection. In the case of mineral foams, an extra mixing step dramatically damages the spheres.

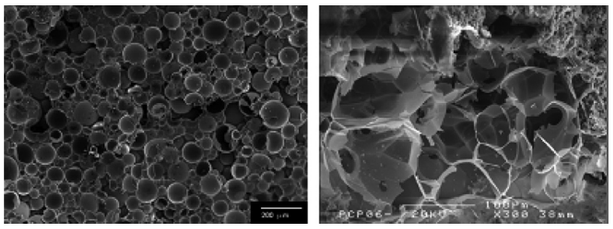

Figure 1: left: Syntactic foam made of hollow spheres embedded in an organic resin. (data obtained from wikipedia). Right: multi-celled glass hollow spheres embedded in a mineral matrix (Thermax CL product).

2.3. Foams obtained by in-situ outgassing

Releasing a gas in fluid suspension can promote foaming phenomena. This outgassing can be induced by different chemical reactions (see below). The carefully tailored synergy between outgassing and setting time is a key point for the good shaping of the considered foam.

The gas release can be induced, for example, by acid-base chemical:

– Addition of calcite to K-struvite cement [WAG 04] with release of CO_2
– Addition of perborates or percarbonates to strong bases (alkali-silicates for example releasing O_2 or CO_2).

In 1889, Hoffman was already reacting calcite in sulfuric acid to promote the release of carbon dioxide in lime-based mortars.

Other ways can be used, such as redox reactions, and foamed clays have already been obtained by mixing MnO_2, ovalbumine and H_2O_2 to clay pastes.

The most representative and known example of such materials is cellular concrete. This type of concrete is obtained by wet autoclave curing of lime/sand/ blends as demonstrated by W. Michaelis in 1880. Water resistant C-S-Hs are thus obtained (see Figure 2 left). In this case, foaming occurs when H_2 bubbles form concomitantly with the setting of the mineral matrix (Hoffmann 1889). The bubbling is due to the reaction of metal silicon, aluminum or zinc powders (J.W. Aylswoth and F.A. Dyer 1914) with the alkaline media, namely cement or calcic lime. When aluminum powder is added to calcic lime pastes, C_3AH_6 are formed while H_2 releases. Those hydrated phases are responsible for the setting of the mineral matrix. Further autoclave curing leads to the formation of tobermorite ($C_5S_6H_5$).

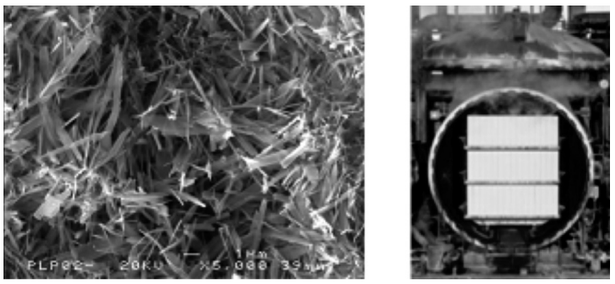

Figure 2: left: Structure of a calcium silicate matrix (Skamol product). Right: Post remolding autoclave curing (T = 180°C P = 10 atm.) - Febecel.

2.4. Effect of wetting agents

Adding wetting agents to the blend can improve the foaming ability of the paste. The surfactants:

– help to stabilize the gas-fluid interface,
– increase the pressure gradient between the liquid phase and the gaseous phase,
– affect the size of the bubbles.

Several chemical moieties can be used and are derived from the detergents and soaps chemistry (e.g. sodium lauryl sulfate, sodium laureth sulfate, cetyl trimethylammonium bromide, fluorosurfatants…).

Regarding the case of mineral foams, the surfactant must be carefully chosen: some of them can exhibit adverse effects towards the chemistry of mineral foams and binders (setting delay, lower mechanical strengths…).

The best compromise between the quantity of bubbles and the quantity of water will make this technique performs well or not. Indeed, water is required to create bubbles but excess water will dramatically affect the mechanical strengths of the hardened mineral foams. The main adverse effects that can be observed because of excess water are the too high dilution of the mineral phase and the coalescence of bubbles. This being written, one solution can consists in use of yielded fluid. In other words, stabilizing mineral foams is nothing less than entraining the highest quantity of air in a yielded concentrated suspension. A quite common solution is the use of a blender. Another solution consists in using a foam gun (see Fig. 3)

in synergy with water and specific surfactants. The obtained foam is then added to the mineral paste (see Fig. 4 left). This dissociated method performs quite well but its main disadvantage is the high amount water that is required.

Figure 3: Example of an industrial foam gun (stator and rotor details).

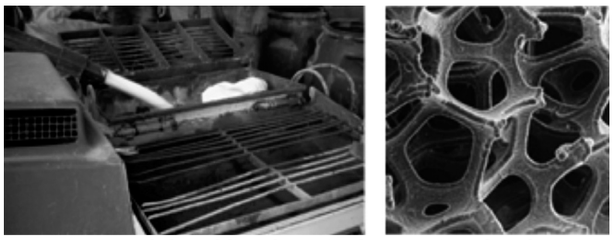

Figure 4: left: Adding foam in the gauging chamber of a mixer. Right: Foam deposit on a metal substrate (www.recemat.nl).

2.5. Effect of dispersive agents

Adding a dispersive agent to a mineral suspension can lead to the formation of stable foam. This can also occur when a plasticizer is added to the aqueous suspension. The molecules are adsorbed on the fine particles surfaces and help to break the flocks that form when water is added to charged particles. A strong steric hindrance effect occurs on the grains surfaces and the particles repel each other. If the particles size is fine enough, the surface tension will be modified at the air/fluid interface (see Fig. 5) and a stable bubble will form. In this case, the wall of the bubble is obtained without any extra-surfactant or increase of water as far as the dispersive agent behaves like a plasticizer. The so-called third generation superplasticizers, such as poly-carboxylate ethers, are of particular interest for hydrophobization of grains. Mineral foams can thus quite easily be obtained.

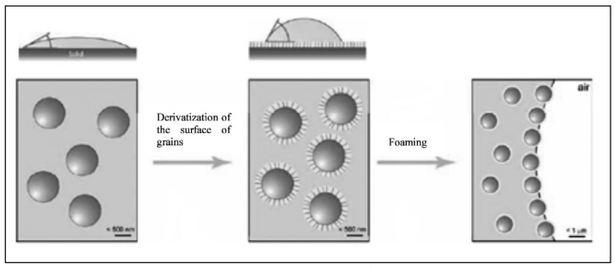

Figure 5: Hydrophobisation of grains [STU, 07].

2.6. Other methods

Other way to obtain foam does exist. Lightweight foams can be obtained by the deposit method (see Fig. 4 right). The raw material is usually foam with open cells (e.g. polyurethane.). Metal is then sputtered on the foam. The resulting 3D network is extremely porous. To the best of our knowledge, this method has not been applied yet to the case of mineral foam.

3. CASE OF GYPSUM ($CASO_4.2H_2O$)

3.1. Foam obtained by outgassing

Gypsum-foam can be easily obtained by adding a few percents of aluminum sulphate to a gypsum-plaster ($CaSO_4.0,5H_2O$) slurry. A chemical reaction occurs and leads to the formation of gas. A slightly plasticizing effect is also observed and the setting time of gypsum-plaster is shortened (setting occur within the first two minutes of the reaction). Gypsum foam is thus obtained. The bubbles size is about 1 mm (see Fig. 6 left) and the connectivity between bubbles is low. Chemical analyses of the exhausted gas revealed SO_3, i.e; a toxic gas. Considering health issues, this method is thus not safe and is of lab interest only. The SEM pictures (see Fig. 6 right) of the grains surfaces reveal that the crystallization of the gypsum is affected by the presence of aluminum. White deposits (see Fig. 6) are observed on the grain surfaces and are due to the presence of sodium carbonate (sodium salts are added to control the reaction rate and act as setting regulators).

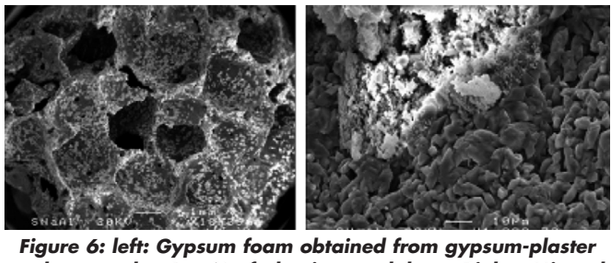

Figure 6: left: Gypsum foam obtained from gypsum-plaster and water plus 6 wt% of aluminum sulphate. Right : Mineral structure of the foam.

Those gypsum foams are hard to produce regarding the setting time that is not easily adjustable. Moreover, even if the voids are closed, they are too coarse to present satisfying properties.

3.2. Foams obtained with wetting agents and superplasticizers

Several foamed gypsum are formulated with different surfactants and superplasticizers. The binder is a mixture of 95 wt% of Kerysten® (anhydrous calcium sulphate produced by K&Co) and of 5 wt% of Portland cement (CEMI 52,5). Various surfactants are tested. Their contents are limited to the range advised by the suppliers. As mentioned by the

suppliers, a retarding effect of these admixtures is noticed and the setting of the gypsum foams is thus delayed. The selected superplasticizer is produced by K&Co: SemperActis™ SP20. This powder admixture containing polycarboxylate is well adapted to calcium sulphate. It is proportioned with less than 1%. Water proportioning is generally chosen between 30 and 35 % of the dry mass except when the foaming method is dissociated.

Various manufacturing processes of the foam are used: traditional mortar planetary mixer (Hobart Mixer), whisk mixer, foam generator (dissociated method of foaming). The mix method is adapted in order to obtain large density range of the gypsum foams. After mixing and foaming, the foam samples are abandoned in their mould until hardening. The form removal occurs within the first two hours after the setting. The specimens are cured at 20°C and 50 % HR.

Examples of foams obtained according to the considered foaming techniques are presented figure 7. The connectivity between the cells appears to be directly related to the thickness of the membrane between cells. If the membrane is too thin, the surface energy minimisation leads to the formation a "hollow disc" connection type. The thickness of the wall and the diameter of the hollow disc in the wall between two cells are directly related to the gradient of pressure between the two phases and the surface tension. Therefore the morphology of foam is only linked to the quantity of gas phase that is trapped in the liquid phase during the manufacture of foam. The optimization of the relation between the structure of the foam and the formulation thus remains difficult to control.

Considering the crystallization of the solid matrix, one can notice that the crystallites are more randomly oriented than in the case presented on the figure 6 right. The foams obtained starting from the same formulation present very similar mineral matrices. On the other hand the matrices of the foams obtained with the dissociated method are much looser.

3.3. Assessment of thermal and mechanical characteristics

Performances of various gypsum foams are compared. Tensile and compression strength tests are realized on different specimens (prismatic: 4x4x16 cm^3, cylindrical: ϕ = 11 cm). In addition, some thermal conductivity measurements are carried out using hot wire method.

Figure 8 presents a comparison of compression strengths obtained on gypsum foam for density ranging from 250 to 1600 kg/m^3. Results on other cellular materials (e.g. cellular concrete, more complex to produce) and environment friendly materials are indicated for comparison purpose. It is interesting to note that the considered foaming methods lead to gypsum foams with a weak water mixing rate and with a quite low density.

Some conclusions can be made from Figure 8:

– mechanical strength results of different gypsum foams fit well with a regular trend line,
– the more the binder is compact, the more the strength is high,

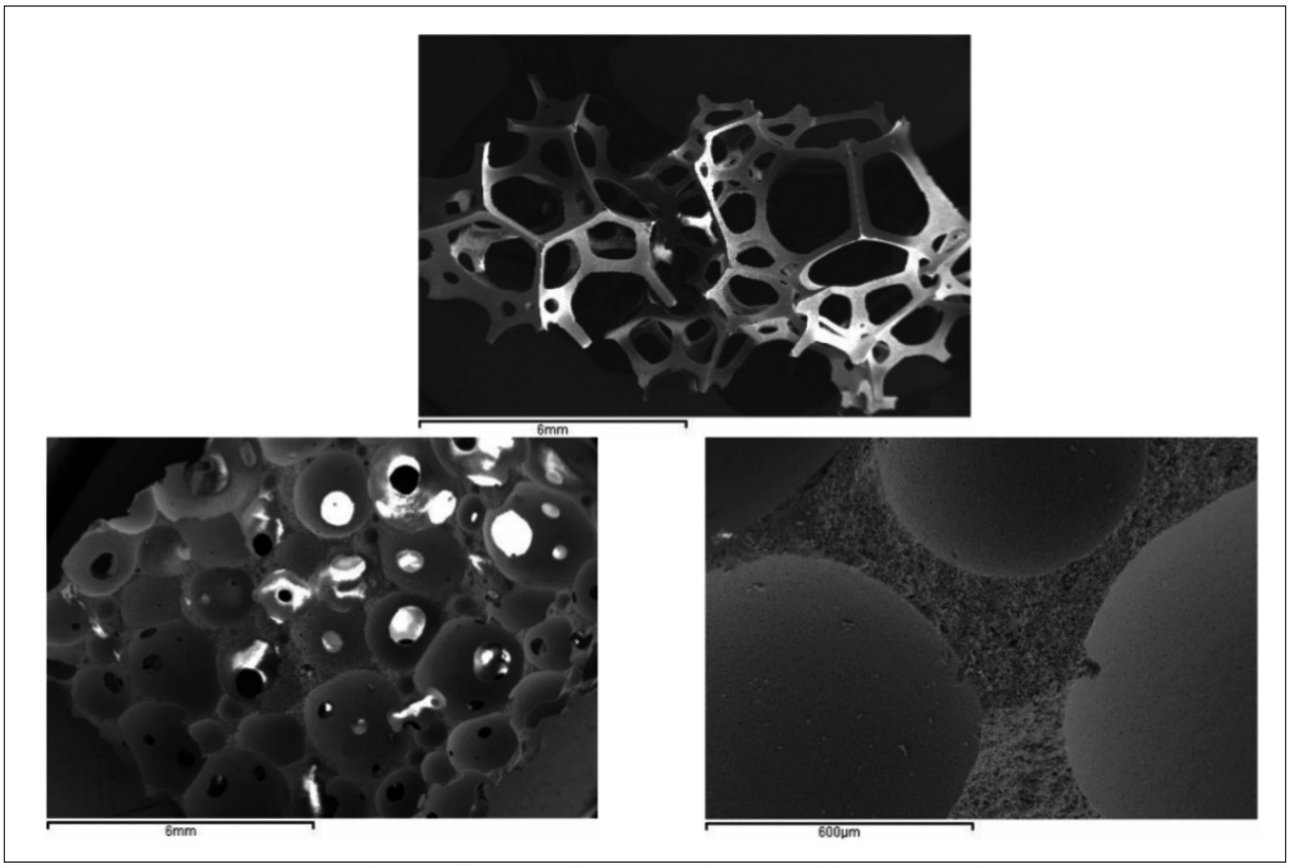

Figure 7. Various mineral foams obtained with various surfactants and different manufacturing processes.

– mechanical performances of gypsum foams and of cellular concrete are similar, and higher than hemp concrete ones.

Thermal conductivity results show a regular increase with density (figure 9). All the presented materials seems to have quite similar thermal performances. However, thermal conductivity values of tested gypsum foams appear lightly higher than the mean curve.

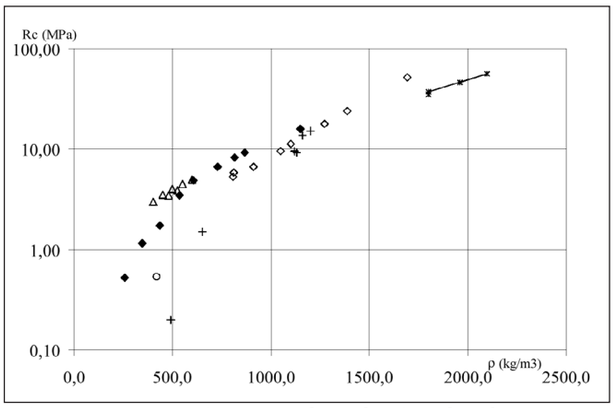

Figure 8: Compression strength vs density: rhomb : gypsum foams (dark mark : E/L = 0,30, white mark : E/L = 0,35), triangle : cellular concrete, circle : hemp concrete, cross : gypsum foam from dissociated method.

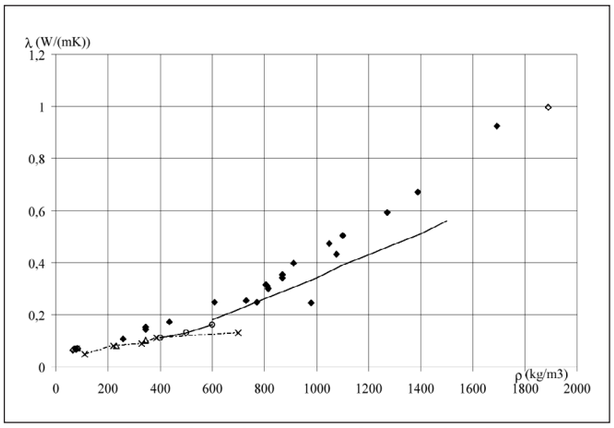

Figure 9: Thermal conductivity vs density: rhomb : gypsum foams, cross : hemp concrete and straw, circle : cellular concrete, triangle : polystyrene concrete, full curve : normalized conductivity values of plaster.

4. GENERALIZATIONS TO OTHER BINDERS AND CONCLUSIONS

The method of producing such paradoxical foams (lightweight foams based on dense mineral matrices) can be extended to other binders than gypsum. Figure 10 shows the structure of foams obtained with two distinct binders:

– the first one is full of insoluble micro-particles (Figure 10 left),
– the second one is made by coupling organic and mineral binders (Figure 10 right).

Bubble surface has got different characteristics without important structural modification.

The mineral foam optimization requires:

– an effective binder with a low gauging ratio, and at the same time, a rather good fluidity,
– an efficient technique to trap air into the matrix,
– a short setting time (or stiffening), so that foam structure remains stable.

Thermal and mechanical performances of these studied foams appear to be very relevant. So, applications of such mineral foams can evolve in the future by substituting some fibrous products.

5. REFERENCES

[BRU,04] BRUCHON J., Etude de la formation d'une structure de mousse par simulation directe de l'expansion de bulles dans une matrice liquide polymère, Thèse de doctorat, Ecole Nationale Supérieure des Mines de Paris, 2004.

[LAB, 04] LABIAUSSE V., Rhéologie non linéaire des mousses aqueuses, Thèse de doctorat,

[STU, 07] STUDART A.R., GONZENBACH U.T. , AKARTUNA I., TERVOORT E., GAUCKLER L.J., Materials from foams and emulsions stabilized by colloidal particles. *Journal of Materials Chemistry,* 17 [31] 3283-3289, 2007.

[WAG, 04] WAGH A.S., *Chemically bonded phosphate ceramics, 21st century materials with diverse applications*, Elsevier; 2004.

[ALL, 05] HALLIN S., *Building with hemp*, ed Seed Press, 2005.

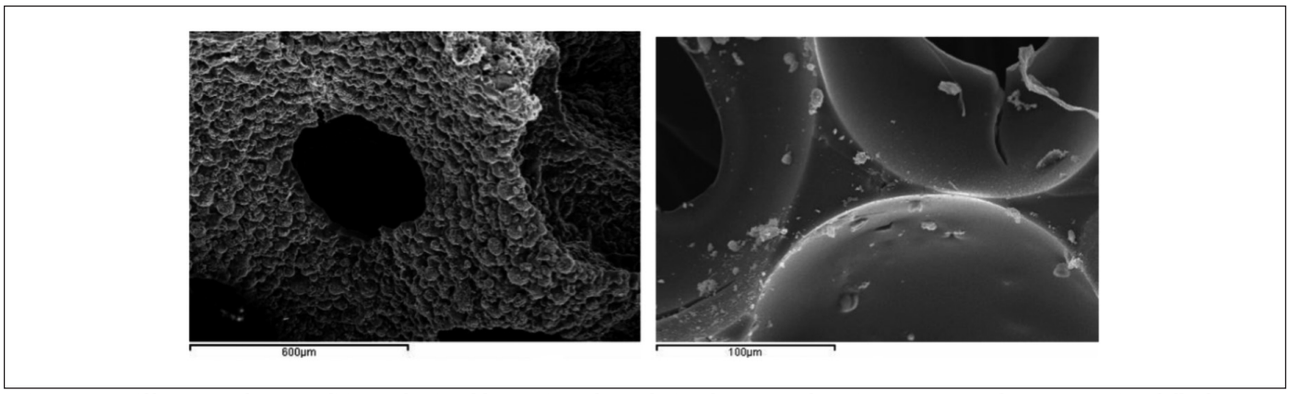

Figure 10: Different surface conditions obtained by various formulation but same foaming process: Left: a suspension full of micro-particles. right: a mix of organic and mineral binders.

BIOPOLYMERS: A NEW WAY FOR THE PROTECTION OF CONCRETE STEEL REINFORCEMENTS

Françoise FEUGEAS[1], Sébastien ROUX[2], Nicolas BUR[1], Bernard TRIBOLLET[3]
[1]IMFS, 2, rue Boussingault 67000 Strasbourg (UDS-CNRS-INSA de Strasbourg-ENGES), francoise.feugeas@insa-strasbourg.fr
[2]Nancy Université UMR 7198 IJL-CP2S-207, IUT de Nancy Brabois dpt GC, Le Montet – Rue du Doyen Urion, 54600 Villers les Nancy, sebastien.roux@iutnb.uhp-nancy.fr
[3]UPMC, LISE, UPR 15 du CNRS, case 133, 4 place Jussieu, 75252 Paris Cedex 05, bernard.tribollet@upmc.fr

1. INTRODUCTION

The aim of this study is to develop products made with biological components allowing to develop more eco-friendly concrete. It contributes to the effort in sustainable development that consists to limit the impact of buildings on environment and humans, with a guarantee of better quality concerning esthetical, durability and resistance criteria. In order to reduce CO_2 release associated with the clinker production, it appears of primary importance to develop the use of concrete containing products like Ground Granulated Blast-furnace Slag (GGBS). Concrete with GGBS containing biopolymers should be more durable and the biopolymers could allow the curing and preservation of more aged works. The goals concerning sustainable building are:

- To use recyclable material during the building in order to preserve natural resources,
- To control the aging of works

Among the many pathologies affecting the reinforced concrete works, the rebars corrosion in one of the most frequently found and can induce the failure of the structure [1]. Although initially protected by the alkalinity of the sound concrete, (pH about 13), the rebars environment may change because of the pH decrease due to the cement matrix carbonation [2-4] and/or to the penetration of aggressive chemicals compounds such as chloride ions through the porous network [5, 6]. The rebars corrosion leads to an increase of their volume up to 9 times the volume of the not corroded rebars [7] and can then induce the cracking of the embedding concrete. The classical solutions against rebars corrosion are: (i) increase of the embedding depth as specified by standards [8], (ii) cathodic protection of the rebars [9, 10] and (iii) impregnation of water repellent or corrosion inhibitor on concrete surface [11]. At the present time, about 20 patents describe corrosion inhibition products as additives in fresh concrete or to apply on hardened concrete. Those inhibitors are made of chemical substances listed in table 1 (table 1), few of them are not eco-friendly regarding the pictogram of their Sanitary and Environmental Data Cards (FDES).

Chemical Substances	Eco-friendly	Not eco-friendly
Alkaline metals		x
Hydroxylamines		x
Silane/Siloxane		x
Sodium gluconates	x	
Aluminium nitrates		x
Sodium Molybdates		x
Ammonium benzoates		x
Alkaline-earth nitrite metals		x
Alkaline-earth nitrate metals		x

Table 1: Chemical substances present in corrosion inhibitors for concrete rebars

Some bacterial species secrete biopolymers, called Extracellular Polymeric Substances (EPS), aiming to protect cells when their environment becomes aggressive and to increase their adhesion on surfaces by forming biofilms [12]. Among these biopolymers, the EPS 180 are exopolysaccharides secreted by the *Lactobacillus reuteri* bacteria. They have already showed corrosion inhibiting properties on steel in seawater [13, 14].
This study aims to develop a new eco-friendly way to protect rebars against corrosion by using biopolymers as admixtures in cement based materials. Furthermore, the associations of this admixture with cement containing GGBS will contribute to develop sustainable building. In a firth step, we have evaluated the influence of EPS 180 in admixture incorporated in cement pastes on the corrosion of low-carbon steel rebars. Open circuit potential (OPC) measurements and electrochemical impedance spectroscopy tests were carried out on C15 steel rebars in CEM I and CEM V/A cement pastes immersed in natural seawater.
In order to protect monuments, corrosion inhibitors are applied on the surface of concrete, it is why the EPS 180 were also incorporated in a solution applied on the cement surface. In this case, the protection against corrosion is more often due to the reduction of penetration towards the concrete of aggressive elements present in the water than to a direct inhibiting action on the rebars surfaces. The corrosion inhibitors are effectively able to clog the concrete porous network and then to decrease the capillary imbibition rate of concrete [15]. For this study, the capillary behaviours of samples sprayed or painted with a solution containing EPS 180 and of samples containing an admixture with EPS 180 were compared. Capillary imbibition tests were carried out on cement paste and mortars to characterize the influence of the biopolymer (EPS 180) on the porous network and the hydric transfers of cement pastes and mortar.

2. MATERIAL AND METHODS

EPS 180 are natural extracellular polymeric substances secreted by the gram-positives bacteria *Lactobacillus reuteri* from sucrose thanks to the glucansucrase GTF 180 enzyme [16]. These biopolymers are safe for Human people: the patent [17] describing it specifies that the *Lactobacillus reuteri* bacteria can be used in food industry. EPS 180 are furnished as dehydrated powder and are dissolved in distilled water at 1.3 g/l concentration. The proportion of the admixture water free for the cement grain hydration is estimated at 50% of the total EPS 180 admixture volume. This EPS 180 solution is considered as an admixture regarding the NF EN 934-2 French standard: the admixture content in the sample is limited to 5% of the cement mass.
The samples were manufactured using two cement bases: one ordinary Portland cement CEM I 42.5 R CE CPS (95,5% clinker, 4.5% GGBS, Blaine fineness: 3750 cm²/g) and one composed cement CEM V/A (S-V) 32.5N PM-ES CP1 (51 % clinker, 23% GGBS and 26% siliceous fly ashes, Blaine fineness: 4400 cm²/g).
The cement paste batch was composed of 180 grams water and 450 grams cement, i.e. the mass ratio water/cement is 0.4. The mortars samples were manufactured according to the procedure described by the European standard [18]. The mortar batch was composed of 225 grams water, 450 grams cement and 1350 grams standard sand, i.e. the mass ratio water/cement was 0.5. The EPS 180 admixture contents in the samples batches were 0%, 0.5%, 1% and 2.5% of the cement mass of the cement paste samples; 0%, 2.5% and 5% for the mortars. The electrochemical tests were carried out on cement pastes reinforced with C15 low-carbon steel rebars. Capillary imbibition tests were carried out on cement paste and mortar samples.
The electrodes modeling the reinforcing bars were C15 steel bars 8 mm in diameter, 22 mm length and their extremities are polished. A copper wire was hammered and tin brazed at upper side of the rebars and each end was covered with insulating varnish as shown by Figure 1. Samples were molded as 2 cm edge cubes and the rebars were placed in their vertical axis. After 28 days standard curing (20°C±2°C, RH>90%) these samples were immersed in the natural running seawater in Den Helder harbor (Netherlands).

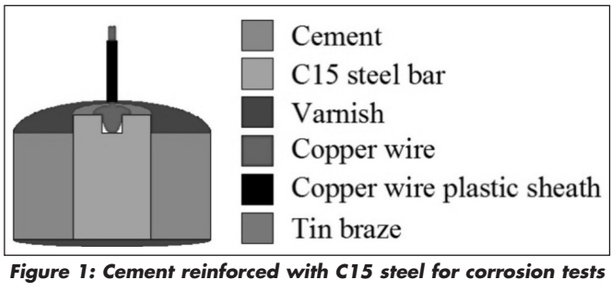

Figure 1: Cement reinforced with C15 steel for corrosion tests

Open circuit potential was measured according to the time with a Keithley 191 multimeter and a silver – silver chloride / potassium chloride reference electrode ($E_{Ag\text{-}AgCl/ESH}$ = 0.197V, $E_{Ag\text{-}AgCl/SCE}$ = -0.045V).

Electrochemical impedance spectroscopy (EIS) tests were carried out using:
– a measurement cell: platinum counter electrode, Ag/AgCl-KCl electrode and working electrode (sample)
– a Faraday cage for protection against external electromagnetic perturbation
– a potentiostat: Solartron SI 1286 electrochemical interface and Solartron SI 1255 frequency response analyzer.
The electrolyte was natural seawater and tests did not start before OCP stabilization. This potential was then imposed by the potentiostat. The results obtained were analyzed using Zview© software. The EIS parameters used were signal amplitude of ± 10 mV vs. OCP, a frequency range from 100 kHz down to 1 mHz and a measurements step of 5 points per decade.
For the capillary imbibition tests, samples were firstly molded as 5 cm edge cubes and the sawed in four 50x25x25 mm^3 parallelepiped samples. Four cement paste samples were studied: the reference samples without EPS 180, samples with EPS 108 solution used as admixture (5% of the cement mass), samples covered with EPS 180 solution by painting or spraying. Two types of mortars were used: the reference samples without EPS 180, samples with EPS 180 solution used as admixture (5% of the cement mass).
Before capillary imbibition tests, samples were vacuum dried (pressure lower than 50 µm mercury – 6.7 Pa) and then stocked in a dessicator until the test. The tests were carried out in an opaque plastic box to protect the set-up from the light and the temperature evolutions. The imbibition surface was the inferior molded surface of the samples and was put on a capillary geotextile supported by a PVC holder. The ends of the capillary geotextile were immersed in distilled water [19]. The samples mass was measured according to the time with a Sartorius BP211P1 precision scale.

3. RESULTS AND DISCUSSION

3.1. Influence of the biopolymer on samples porosity

Figure 2 presents the results of the capillary imbibition tests carried out with the CEM I and CEM V cement pastes with 3 modes of application:
• painted,
• sprayed,
• used as admixture.
Figure 3 presents the results of the capillary imbibition tests carried out with the CEM I and CEM V mortars with 0, 2.5 and 5% of EPS 180 admixture.

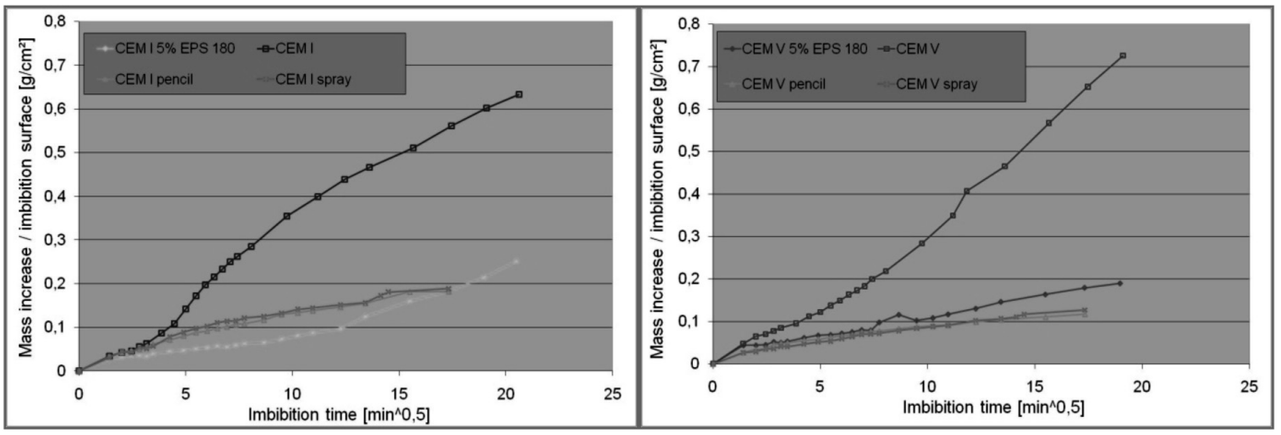

Figure 2: Capillary imbibition tests – mass increase of CEM I and CEM V cement pastes samples

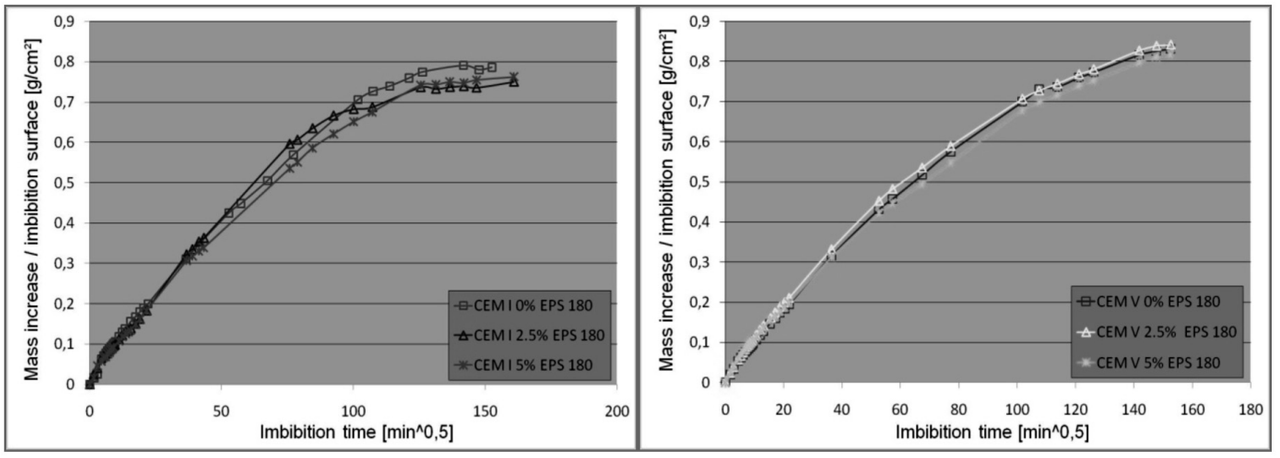

Figure 3: Capillary imbibition tests – mass increase of CEM I and CEM V mortars samples

The behaviour of the cement pastes with the three implementations modes of the EPS 180 solution (admixture, applied in surface by painting or spraying) and without EPS 180 is analyzed. For each cement base, the EPS 180 solution induces an important slow down of the capillary absorption whatever the implementation mode. Compared with reference samples, the EPS 180 solution causes a decrease of the imbibition rate of 68% for CEM I samples after 5 hours of testing and 72% for CEM V containing EPS 180 solution as admixture and finally 83% for the CEM V surface-treated samples. The sample masse increase is linear with the square root time: the absorption of water in the samples is comparable to the absorption of water in a tube and no other physical effect such as the reaction water-cement matrix (*self-sealing effect* [20]) is observed. The influence of cracks, main heterogeneity of the porous structure, was not observed during the capillary fringe rise. The addition of polymers in the cement based material batch is known to influence the hydric transfers inside the hardened material porous network. For example, the superabsorbent polymers [21] interrupt capillary pores, acrylic and styrene-butadiene [22] influence the cement paste porosity clogging the microcracks. In both case, the polymers additions slow down the transfers and transport properties. The EPS 180 solution seems to have the same effect on the transfer properties inside the cement paste porous network.

The results obtained with the mortars samples with EPS 180 admixture (Figure 4) highlight a similar behaviour of all the samples whatever the admixture content for each cement base: the EPS 180 solution has no influence on the water imbibitions kinetics of mortars. The porous structure of cement pastes and mortars are different due to the presence of sand in mortars that induces the formation of the Intergranular Transition Zone (ITZ) [23]. The ITZ correspond to a porosity family of which access diameters are between 0,1 µm and 4 µm [24] and are not found in the cement paste of which pore access diameters are lower than 1 µm and mainly lower than 0,1 µm [25]. The ITZ porosity of mortars is highly connected and offers many penetration ways into the porous network for liquid and aqueous phases [24]. The amount of biopolymer added in the mortars batch is quite low: 5% EPS 180 solution correspond to 66.7 mg of pure ESP 180 per kilogram of cement. This quantity is then high enough to influence the water absorption in cement paste but is too low to modify the imbibition kinetics in mortars.

The embedding depth of the C15 steel rebars is about 6 mm (Figure 1) and the water penetration after 3 hours imbibition test is at least 9 mm for all the cement paste whatever the EPS 180 admixture content. After one-week immersion, the seawater then reached the rebars embedded in cement paste. The EPS 180 are effectively able to clog the cement paste porous network and then to decrease its capillary imbibition rate, but, after one week, the clogging cannot forbid seawater to reach the rebars. The modification of the electrochemical behavior of the rebars embedded in cement paste containing EPS 180 is due to the modifications of the steel-cement paste interface.

3.2. Influence of biopolymer as admixture on corrosion resistance of steel rebars

Table 2 presents the OCP values for the C15 low-carbon steel rebars embedded in the CEM I and CEM V cement pastes with different proportions of admixture.

EPS 180 admixture content	0%	0,5%	1%	2,5%
CEM I - OCP [V/Electrode Ag-AgCl]	-0,148	-0,069	-0,178	-0,193
CEM V - OCP [V/Electrode Ag-AgCl	-0,554	-0,467	-0,456	-0,433

Table 2: C15 steel rebars OCP, CEM I and CEM V cement pastes

Figures 4 and 5 present the Nyquist plot of the EIS results for the C15 steel rebars embedded in CEM I and CEM V cement pastes with different proportions of admixture.

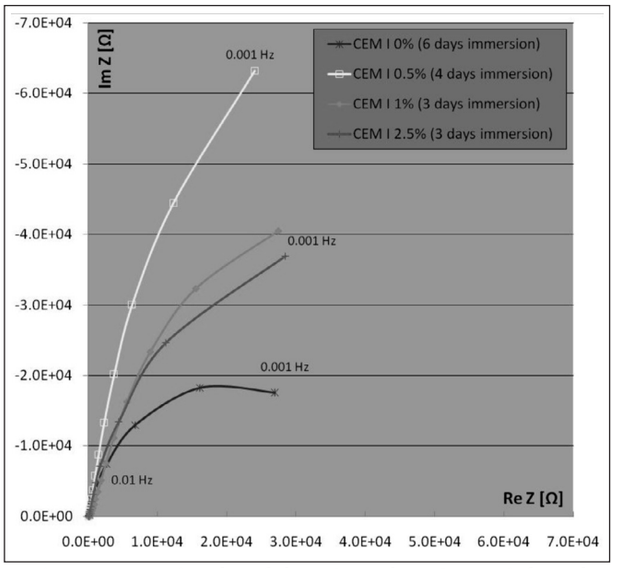

Figure 4: Nyquist plot of the EIS results – CEMI reinforced cement pastes samples

The impedance of the electrolyte and of the embedding cement paste is modeled by an electrolyte resistance Re. At corrosion potential (OCP), the current is equal to zero and the cathodic impedance is parallel to the anodic one. The anodic impedance corresponds to the rebars passive layer and can be modeled by a Constant Phase Element (CPE) defined by two parameters Q and α [26]. The parameter is linked to the passive layer heterogeneity at different level (surface roughness, etc.) and Q corresponds to the differential capacitance when α is equal to 1. The cathodic impedance corresponds to the oxygen reduction reaction and is modeled by a charge transfer resistance Rtc. Figure 6 presents the equivalent circuit and the table 3 presents the values of its components calculated thank to the fitting software Zview.

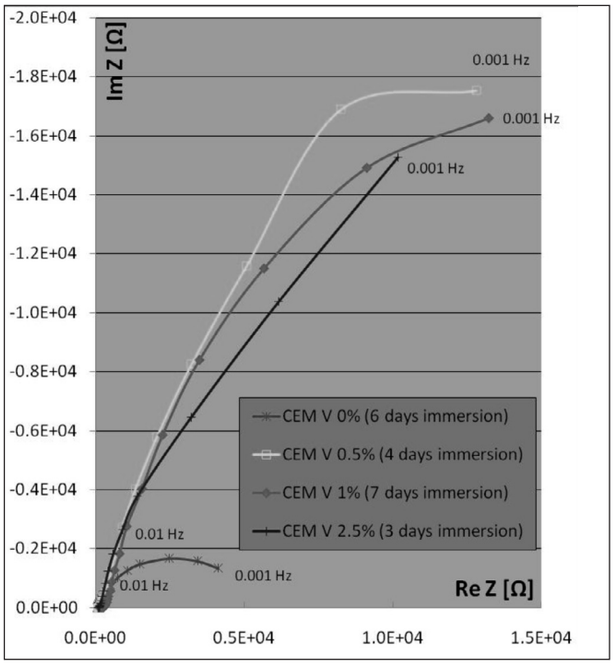

Figure 5: Nyquist plot of the EIS results – CEM V reinforced cement pastes samples

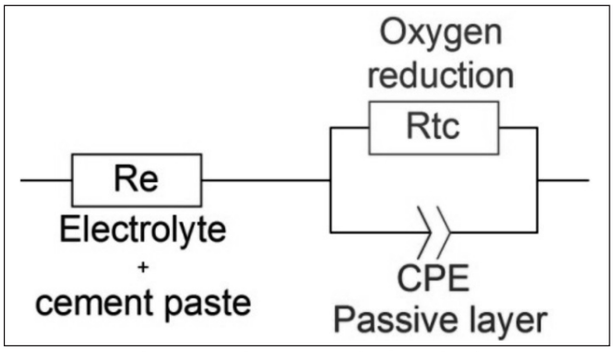

Figure 6: EIS tests - equivalent circuit

The stabilized corrosion potential of the C15 low-carbon steel immersed in the natural seawater is -0,630 V/ECS that is coherent with the -0.7V/ECS value for mild steel in seawater given in the literature [27]. The interstitial solution of sound cement based materials is resulting of the mixing water and the dissolution of cement grains. The composition of this solution depends on the cement composition (clinker, blast furnace slag, siliceous fly ashes) and mainly contains Ca^{2+}, Na^{+}, K^{+}, OH^{-} and SO_4^{2-} ions [28]. When carbon steel is embedded in such materials, the chemical composition and the pH about 13.5 of the interstitial solution leads to the formation of a passive layer at rebars surface. This passive layer is mainly composed by iron hydroxide ($Fe(OH)_2$) and calcium hydroxide ($Ca(OH)_2$) and influences the rebars OCP [29, 30]. It is then not surprising that the OCP of the rebars embedded in cement paste without EPS 180 admixture goes up: + 440 mV for the CEM I and + 40 mV for the CEM V. When EPS 180 admixture is added, there is no notable evolution of the rebars OCP: from – 50 mV up to + 80 mV for the CEM I and from + 90 mV up to + 110 mV for the CEM V.

The analysis of the EIS results highlights that the CPE parameters values (Q, α) for each cement base samples are quite close whatever the EPS 80 admixture content. However the CPE parameters values are different for the two cement bases. These results show that the cement chemistry influences the composition of the passive layer more than the EPS 180 admixture content.

The EPS 180 induces a significant increase of the Rtc values. Compared with the samples without EPS 180 admixture, Rtc values are multiplied by factors between 2.36 and 7.75 for samples CEM I with EPS 180 and between 8.5 and 12.31 for those of CEM V. The decrease of the cathodic reaction kinetics is observed for all EPS content including the lowest concentration of EPS 180 admixture (0.5%).

Samples	Re [Ω]	Rtc [kΩ]	Q [$s^{\alpha}.\Omega^{-1}.cm^{-2}$]	α
C15 rebars in CEM I 0%	1 050	553	0,000 14	0,86
C15 rebars in CEM I 0,5%	870	4 284	0,000 13	0,89
C15 rebars in CEM I 1%	2 200	2 476	0,000 11	0,79
C15 rebars in CEM I 2,5%	870	1 305	0,000 15	0,87
C15 rebars in CEM I 5%	1 240	13 300	0,000 11	0,85
C15 rebars in CEM V 0%	660	58,4	0,000 32	0,76
C15 rebars in CEM V 0,5%	1 690	719	0,000 23	0,815
C15 rebars in CEM V 1%	3 100	616	0,000 23	0,785
C15 rebars in CEM V 2,5%	1 270	497	0,000 25	0,83

Table 3: Equivalent circuit parameters

4. CONCLUSION

After the samples immersion in natural seawater, the EPS 180 biopolymer admixture added in reinforced CEM I and CEM V cement pastes induces the modification of the cathodic reaction of the C15 low-carbon steel rebars. This admixture also modifies the porous network of the cement paste that is highlighted by a slowdown of the capillary imbibition kinetics, this phenomenon is not observed for the mortars. The corrosion inhibition is then essentially influenced by the modification of the cement paste – steel interface rather than by the clogging of the porous network. This new admixture inhibits the corrosion of low carbon-steel rebars in CEM I and CEM V cement paste samples.
These first results confirm that the use of ecofriendly biopolymer admixtures could be an alternative to classical corrosion inhibiting treatment for the reinforced concrete in natural environment. The aim is to contribute to the effort in sustainable development thanks to the micro-organisms (*Lactobacillus reuteri* bacteria) allowing the production of more eco-friendly concrete.

5. ACKNOWLEDGEMENT

This study was carried out in the frame of the D33 COST Action (*Nanoscale Electrochemical and Bio-Processes at Solid-Aqueous Interfaces of Industrial Materials*) and supported by the Alsace Regional Council and the Holcim Company.

6. BIBLIOGRAPHY

[1] Ollivier, J.P. and A. Vichot, *La durabilité des bétons - Bases scientifiques pour la formulation de bétons durables dans leur environnement* 2008, Paris: Presses de l'école nationale des Ponts et Chaussées. 868.
[2] Chang, C.-F. and J.-W. Chen, *The experimental investigation of concrete carbonation depth.* Cement and Concrete Research, 2006. **36**(9): p. 1760-1767.
[3] Johannesson, B. and P. Utgenannt, *Microstructural changes caused by carbonation of cement mortar.* Cement and Concrete Research, 2001. **31**(6): p. 925-931.
[4] Wiktor, V., *Biodétérioration d'une matrice cimentaire par des champignons : Mise au point d'un test accéléré de laboratoire*, in *Génie des procédés*2008, Ecole Nationale Supérieure des Mines de Saint-Etienne: Saint-Etienne (France). p. 182.
[5] Ahmad, S., *Reinforcement corrosion in concrete structures, its monitoring and service life prediction—a review.* Cement and Concrete Composites, 2003. **25**(4-5): p. 459-471.
[6] Waanders, F.B. and S.W. Vorster, *Concrete Infrastructure Corrosion.* Hyperfine Interactions, 2003. **148-149**: p. 237-242,.
[7] Baroghel-Bouny, V., B. Capra, and S. Laurens, *La durabilité des armatures et du béton d'enrobage*, in *La durabilité des bétons*, J.-P. Ollivier and A. Vichot, Editors. 2008, Presses de l'école nationale des Ponts et Chaussées: Paris. p. 303-385.
[8] EN 1992 - Eurocode 2, *Calcul des structures en béton*, in *AFNOR*2005.
[9] Glass, G.K., A.M. Hassanein, and N.R. Buenfeld, *Monitoring the passivation of steel in concrete induced by cathodic protection.* Corrosion Science, 1997. **39**(8): p. 1451-1458.
[10] Hassanein, A.M., G.K. Glass, and N.R. Buenfeld, *Protection current distribution in reinforced concrete cathodic protection systems.* Cement and Concrete Composites, 2002. **24**(1): p. 159-167.
[11] Ormellese, M., et al., *A study of organic substances as inhibitors for chloride-induced corrosion in concrete.* Corrosion Science, 2009. **51**(12): p. 2959-2968.
[12] Block, J.C., *Espace intercellulaire des biofilms : structure et réactivité*, in *Biodétérioration des matériaux - Action des microorganismes de l'échelle nanométrique à l'échelle macroscopique*, A. Cornet, F. Feugeas, and B. Tribollet, Editors. 2008, Ellypse: Paris. p. 59-66.
[13] Ferrari, G. *EPS as corrosion inhibitors in coatings, protection of steel constructions*. in *Combined Meeting of Working Groups 1 and 3 of COST Action D33*. 2008. Preston, United Kingdom.
[14] Stadler, R. *Corrosion inhibition by extracellular polymeric substances*. in *COST D33 Workshop*. 2007. Den Helder, Netherlands.
[15] Roux, S., et al., *Influence of a biopolymer admixture on corrosion behaviour of steel rebars in concrete.* Materials and Corrosion, 2010. **61**(12): p. 1026-1033.
[16] Van Leeuwen, S.S., *Structural analysis of in vitro produced -D-glucans : Biopolymers synthesised from sucrose by using native and engineered Lactobacillus reuteri glucansucrase enzymes*, 2007, Utrecht University: Utrecht, The Netherlands. p. 192.
[17] Van Geel-Schutten, G.H., *Glucans and glucansucrases derived from lactic acid bacteria*, in *World Intellectual Property Organization*, Nederlandse Organisatie Voor Toegepast-Natuur-Wetenschappelijk Onderzoek Tno Editor 2003, Nederlandse Organisatie Voor Toegepast-Natuur-Wetenschappelijk Onderzoek Tno, : The Netherlands.
[18] Norme française EN 196-1, *Méthodes d'essais des ciments. Partie 1 : Détermination des résistances mécaniques*, in *AFNOR*1994. p. 1-25.
[19] Bur, N., et al., *Pore structure of mortar.* European Journal of Environmental and Civil Engineering, 2010. **to be published**.
[20] Rucker-Gramm, P. and R.E. Beddoe, *Effect of moisture content of concrete on water uptake.* Cement and Concrete Research, 2010. **40**(1): p. 102-108.
[21] Assmann, A. and H.-W. Reinhardt, *Some aspects of superabsorbent polymers (SAPs) in concrete technology* in *8th fib PhD Symposium* FIB, Editor 2010: Kgs. Lyngby, Denmark p. 1-6.
[22] Vincke, E., et al., *Influence of polymer addition on biogenic sulfuric acid attack of concrete* International Biodeterioration & Biodegradation, 2002. **49**(4): p. 283-292.

[23] Otis, N., *Influence de divers superplastifiants sur le ressuage et l'interface pâte/granulat dans les matériaux cimentaires*, in *Département de Chimie*2000, Université de Sherbrooke: Sherbrooke, Canada.

[24] Ollivier, J.-P. and J.-M. Torrenti, *La structure poreuse des bétons et les propriétés de transfert* in *La durabilité des bétons*, J.-P. Ollivier and A. Vichot, Editors. 2008, Presses de l'école nationnale des aPonts et Chaussées: Paris. p. 51-133.

[25] Roux, S., *Evaluation des risques de biodégradation des bétons en contact avec une eau douce naturelle*, in *Sciences pour l'Ingénieur* 2008, Université Louis Pasteur: Strasbourg, France. p. 199.

[26] Hirschorn, B., et al., *Determination of effective capacitance and film thickness from constant-phase-element parameters.* Electrochimica Acta, 2010. **55**(21): p. 6218-6227.

[27] Liu, W., et al., *Corrosion behavior of the steel used as a huge storage tank in seawater.* Journal of Solid State Electrochemistry, 2010. **14**(6): p. 965-973.

[28] Ghods, P., et al., *The effect of concrete pore solution composition on the quality of passive oxide films on black steel reinforcement.* Cement and Concrete Composites, 2009. **31**(1): p. 2-11.

[29] Baroghel-Bouny, V., *Nouvelle approche de la durabilité du béton. Indicateurs et méthodes.* Techniques de l'Ingénieur, 2005. **C 2 245**: p. 1-14.

[30] Huet, B., *Comportement à la corrosion des armatures dasn un béton carbonaté. Influence de la solution interstitielle et d'une barrière de transport*, in *Génie des matériaux : Microstructure, Comportement mécanique, Durabilité*2005, Institut National des Sciences Appliquées de Lyon: Lyon, France. p. 196.

RELIABILITY ANALYSIS OF STAINLESS STEEL COVER PLATE JOINTS

J. AVERSENG[1], A. BOUCHAÏR[2], A. CHATEAUNEUF[2]
[1]Université Montpellier 2, Laboratoire de Mécanique et Génie Civil, UMR 5508 – CC 048, Place Eugène Bataillon 34095 Montpellier Cedex 5. (julien.averseng@lmgc.univ-montp2.fr)
[2]Clermont Université, Université Blaise Pascal, LaMI, Polytech, BP 206, 63000 Clermont-Ferrand (bouchair, alaa.chateauneuf @polytech.univ-bpclermont.fr)

1. INTRODUCTION

Stainless steel practice in structural applications is in increasing development because of the many qualities of this material. Indeed, it has a highly ductile non-linear behavior and a substantial strain hardening capacity, which allows large energy dissipation under cyclic or accidental loading and significant force redistributions inside structures before failure. In addition, it is an esthetically attractive material, resistant to corrosion and high temperatures. Thus, it is perfectly suited for applications in steel construction and especially for structural joints where resistance and deformation capacity are required.

In the existing European design codes dedicated to steel structures, some of these qualities are taken into account but other provisions derived from those applicable to carbon steel components remain incomplete. In this paper, a reliability analysis of the behavior of a cover-plate joint, made using a numerical model, is presented. The results are used to assess and enrich the existing provisions while following the reliability objectives of the Eurocodes.

1.1. Stainless steel in structural joints

The behavior of stainless steels, contrary to that of carbon steel, is non-linear all along their deformation range and is

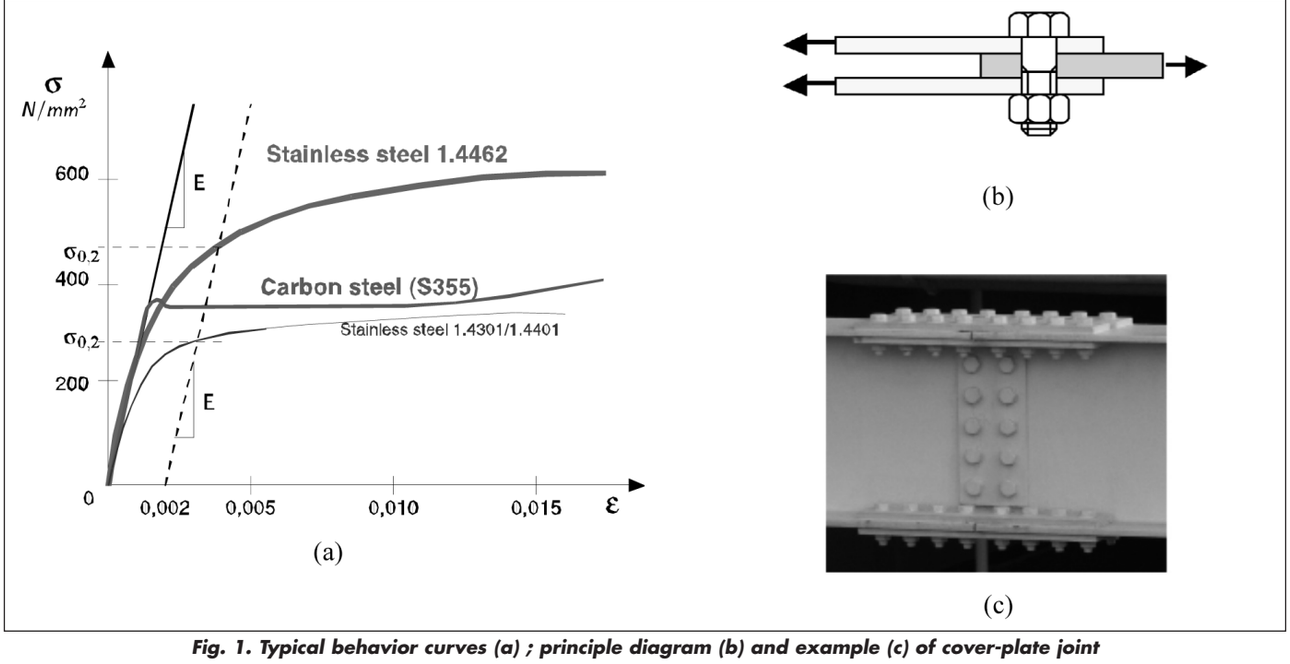

Fig. 1. Typical behavior curves (a) ; principle diagram (b) and example (c) of cover-plate joint

subject to anisotropy. In consequence, the elastic limit is conventionally defined at a plastic deformation of 0.2 % (figure 1.a). Besides, this material can exhibit an important creep in ambient temperature, which imposes to restrain long-term stresses [EUR 06].
Usual structural joints are composed of bolts working in traction, shear or a combination of both. Among the different types, cover plate joints are common because their mechanical principle is simple. Indeed, traction or compression forces are transmitted between two plates through one or several bolts in shear (figure 1.b). This kind of assembly exists also in more complex joints to realize beam continuity or beam to column assembly in which a bending moment is transmitted using cover-plate joints in the compression and traction zones (figure 1.c).

1.2. Eurocode provisions

In the European design codes, stainless steel structures are covered by the EN 1993-1-4 document [CEN 04] that compiles additions to the rules established for carbon steel to take into account the specifics of stainless steel. The main difference for structural joints is the justification of resistance in net section and in bearing. Thus, in the case of a hollowed plate in traction, the net section resistance is given by [1] :

$$N_{u,\,Rd} = k_r \cdot A_{net} \cdot f_u/\gamma_{M2} \qquad [1]$$

where $k_r = (1+3.r.(d_0/u - 0,3)) \leq 1$; r is the fraction of the number of bolts in the section over the total number of bolts in the joint ; $u = 2.e_2 \leq p_2$; A_{net} is the nette section area ; d_0 is the nominal diameter of the hole ; e_2 is the distance from the center of the hole to the adjacent end, and p_2 is the transverse spacing between centers of holes (figure 2).

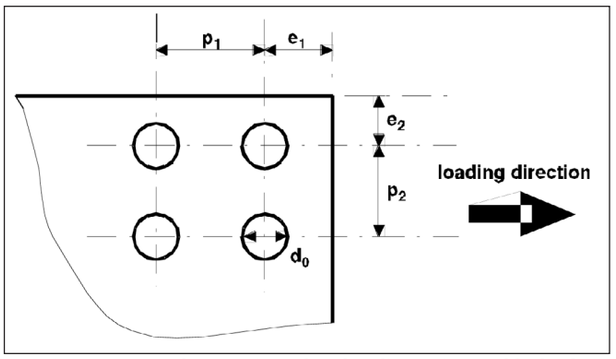

Fig. 2. Eurocode notations for the dimensions of bolted connections

The bearing resistance is given without modifications with the case of carbon steel in equ. [2] :

$$F_{b,\,Rd} = K_1 \cdot \alpha_b \cdot f_u \cdot d \cdot t / \gamma_{M2} \qquad [2]$$

in which $\alpha_b = \min \{ e_1/(3.d_0) ; p_1/(3.d_0)-1/4 ; f_{ub}/f_u ; 1.0 \}$, $k_1 = \min\{ 2,8.e_2/d_0-1,7 ; 2,5 \}$ and e_1 is the distance between the center of the hole and the adjacent end of the plate, in the loading direction. Though, in the case of stainless steel, the hole deformation under serviceability loading can be critical. In consequence, a reduced value of the ultimate resistance f_u, defined in [3] is introduced in order to avoid verification under service limit state, which involves a complex determination of the deformations in the joint.

$$f_{ur} = 0,5f_y + 0,6\, f_u \qquad [3]$$

1.3. Context of the study

Several studies have been conducted on stainless steel structural components [BUR 00][KOU 00][VAN 00] to assess the Eurocode 3 provisions. Among them, a particular investigation achieved at LaMI [RYA 00][BOU 02][SCI 00] was dedicated to the behavior of stainless steel cover plate joints (figure 3.a), and to the assessment of the design rules concerning the resistance, the relative joint capacity and the bearing deformation [BOU 05]. It has been demonstrated that verification under ultimate limit state loading is insufficient and can lead to unacceptable deformations in serviceability limit state. Indeed, this is hardly the case with carbon steel because of a low ratio between the ultimate and elastic limits, generally going form 1.1 to 1.5. With austenitic stainless steel, this ratio can be superior to 2 whereas the ratio between ultimate and serviceability loads is still in the range 1.35 – 1.5.
Recently, a multi-component analysis of cover-plate joints (figure 3.b) was proposed using a numerical model [BOU 08][AVE 09], taking into account material and geometric non-linearities as well as the local deformations in the contact zone between bolts and plates (figure 3.a). The results of this study were validated by comparison with experimental data on three different joints. This approach allowed to identify the influences of the sources of deformation (figure 3.a) and the main parameters involved in the global behavior of this kind of joint : the constitutive material law, the thickness of the plate, the distance of the hole to the end of the plate and its width.
Although this approach is able to reproduce accurately the global behavior of these joints, it does not consider the variability of the material characteristics and dimensions. We showed also that the analytical expressions of resistance provisioned by the design rules, which are established in the respect of a reliability target, are only partially adapted to the characteristics of stainless steel. This is why we propose a complementary study based on reliability methods using a meta-model of the limit state function built from a set of numerical results.

2. META-MODEL OF A COVER PLATE JOINT COMPONENT

In order to assess the reliability of a criterion that concerns the resistance or the rigidity of a structural joint, it is necessary to focus on the respective limit state function. However, this function involves many variables and its evaluation can be very complex so it can be convenient to make use of an alternative meta-model. This approximated model of same order can then provide quickly, through a

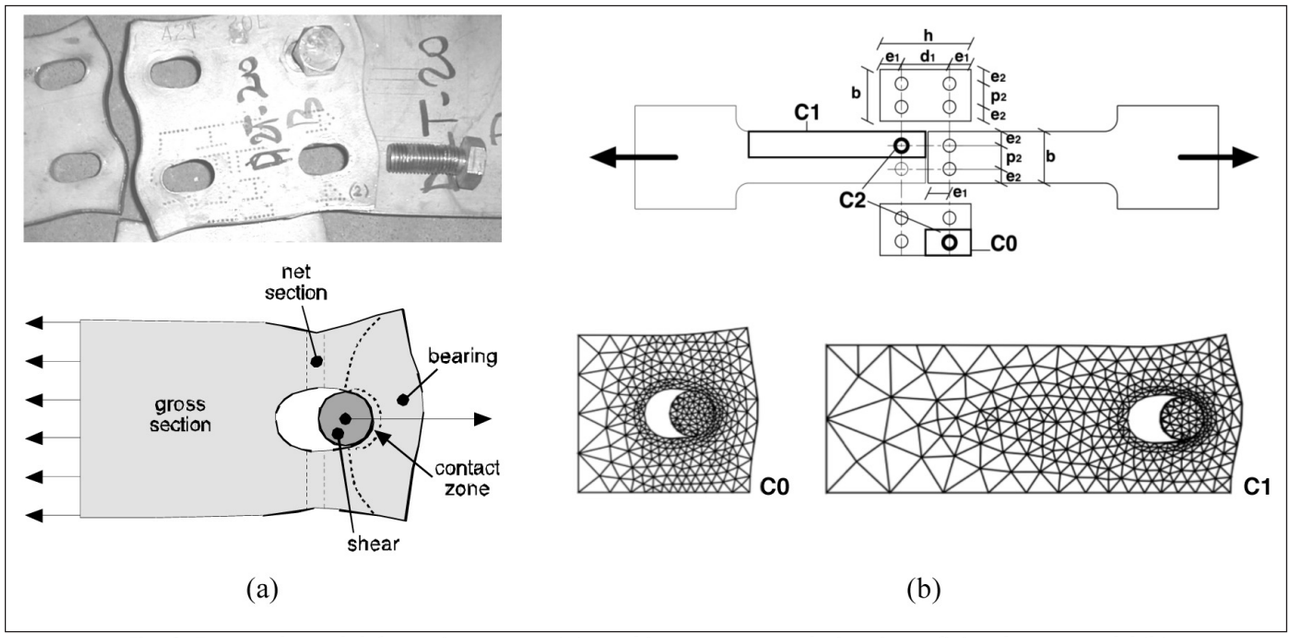

Fig. 3. Test results and deformation sources (a) ; multi-component analysis using a finite-element model (b)

unique entity, the main characteristics of the behaviors of a whole set of joints without having to achieve systematically a heavy numerical analysis. As other advantage, this model built from a fitting of several results attenuates the numerical uncertainties of each numerical non linear computation, which stabilizes the reliability calculation algorithm. Finally, it is a continuous model that allows performing extrapolations. The results from which this meta-model is built are coming from the reference model of a simple component representing an axis in contact with a hollowed plate (figure 4).

2.1. Finite element model

This model is part of an existing general joint model [AVE 09]. The axis is modeled here as a flat cylinder with a diameter d and a height twice that of the thickness t of the plate. The lower end face is restrained along z and the two ends along y and the direction x of the imposed displacement. The plate comprises a hole with a diameter d_0 situated on its longitudinal axis. Its lower and left edges are restrained transversally like the C1 component f the initial model (figure 3.b). Along z, the corners and 4 points of the lower face around the hole are fixed (figure 4).

Load is introduced as an imposed displacement on the axis of 10 mm along x, which allows going beyond the ultimate limits usually adopted [KIM 99]. The material law for the plate is derived from that of a carbon steel by a factor k. It is bilinear, with an elastic modulus E=210 GPa and such that f_u/f_y is equal to k at an arbitrary deformation level of 70 %. The constitutive material of the bolt, supplied from experimental tests [RYA 00], is a stainless steel with an ultimate limit f_{ub} = 800 MPa for an elongation of 25 %.

2.2. Experimental plan

The numerical model is used to generate the force-displacement behavior laws of a set of more than 400 joints defined by those variables (figure 4) : width b, end distance e, thickness t and the behavior law, through the k ratio. The length L of the plate and the diameters d and d_0 of the bolt and the hole are fixed. The variation range of each parameter is given in Table 1.

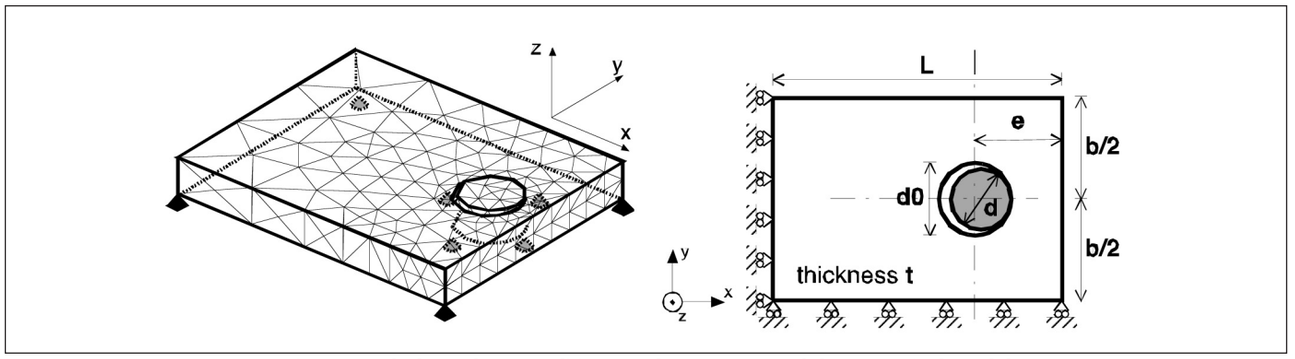

Fig. 4. Mesh, boundary conditions and parameters of the numerical model

variable parameter	value
b	30 à 80 mm
e	15 à 50 mm
t	8 à 12 mm
k	1 à 1,4
variable parameter	**value**
L	100 mm
d_0	22 mm
D	20 mm

Table 1. Parameters values for the numerical model

For each computed joint, several data are extracted from the behavior curve : the initial rigidity, the displacement and rigidity at the final state and the maximum force. In this study, secant values of the resistance for conventional displacements of 2 and 5 mm are identified, which allows qualifying the joint in terms of resistance and deformations capacity (figure 5).

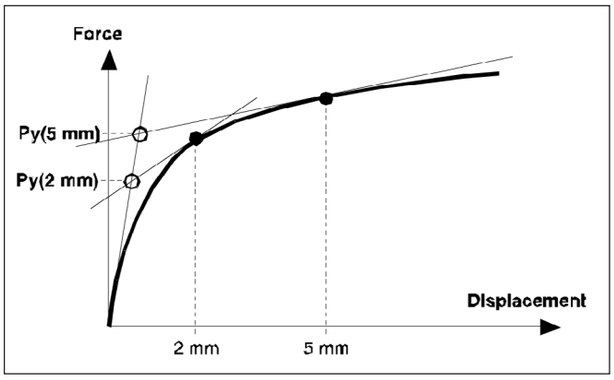

Fig. 5. Definition of the secant resistance P_y from the force-displacement response

2.3. Meta-model

The meta-model is a quadratic response surface obtained by least-square regression on the dataset provided by the results from the reference finite element model. The relative error with the raw data is less than 5 %, which ensures a good adequation in the variation range of the parameters (Table 1).

A comparison with the resistance expressions of the Eurocode 3 confirms that the kind of joint chosen for this study is mostly subject to failure in bearing, which is conform to the first experimental study [RYA 00].
Indeed, the F_{br} resistance is systematically the lowest among the studied criteria (figure 6.a). By comparison with the P_y values from the numerical model, we observe that is also a lot lower in the majority of cases (figure 6.b), which implies an underestimation of the real capacity. In this study, the partial security factor for the material is taken equal to 1 and the ultimate stress is reduced according to the ratio f_u/f_y (equ. [3]). The secant resistances identified in the model are defined as the point at the intersection between the initial tangent line and the tangent of the behavior's curve for a displacement of 2 mm and 5 mm.

3. STRUCTURAL RELIABILITY

3.1. Principle

Structural reliability consists in verifying the probability of verifying the limit state, taking into account the uncertainties due to the material and dimensional parameters, the applied loadings, the numerical models, and the conditions of construction and usage. Each limit state expresses the occurrence of a failure mode in function of parameters for which uncertainties and fluctuations can be modeled as random distributions. The purpose of the reliability analysis is to estimate the probability of occurrence of a particular failure mode. For each one, the limit state function $G(X_i,d_k)$ is defined from random variables X_i, the realizations of which are noted x_i, and from design variables d_k. By convention, this function defines the safety state using positive values. Then, the failure probability associated to the limit state is calculated by [LEM 05] :

$$P_f = Pr\left[G(x_i,d_k) \le 0\right] = \int_{G(x_i,d_k)\le 0} f_{X_i}(x_i)\, dx_1 \cdots dx_n \quad [4]$$

in which $f_{xi}(x_i)$ represents the probability density of variables X_i. However, the evaluation of the integral in [4] is complex, which led to the development of the FORM (First Order Reliability Method) method [DIT 96] that introduces a reliability indice β. This indice represents the minimal margin between the point representing the design functioning state and the point of most probable failure P* in the

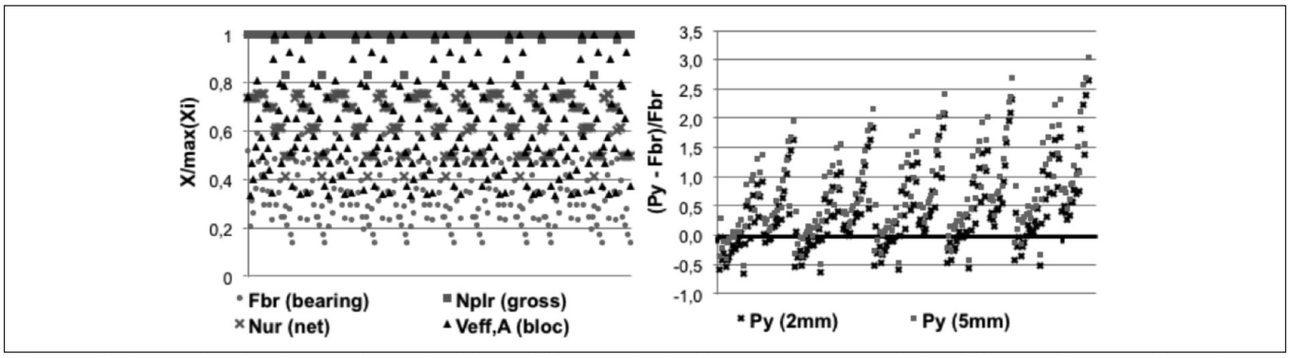

Fig. 6. Relative levels of resistance determined from different criteria of Eurocode 3 (a) ; Relative difference between the resistance at 2 mm and 5 mm from the model and the bearing resistance of EC3 (b) ; Results obtained for all specimen defined in Table 1.

space of normalized variables. This indice can be evaluated by solving the constraint optimization problem :

$$\beta = \min \sqrt{\sum_j u_j^2} \quad \text{under the condition : } G\left(x_i, d_k\right) \le 0 \qquad [5]$$

where u_j are the reduced normalized variables obtained by the probabilistic transformation T of the physical variables x_i.

$u_j = T_j(x_i, d_k)$ and $x_i = T_i^{-1}(u_j, d_k)$ [6]

Using the approximation of the FORM method, the failure probability is then evaluated using [DIT 96]:

$P_f = \phi(-\beta)$ [7]

where ϕ is the standard Gaussian distribution. The only difficulty when applying this method can then be found in the evaluation of the limit state function, which can be very complex.

3.2. Reliability of a cover-plate joint

The meta-model established in this study is used to avoid a direct calculation of the limit state function from a non-linear model, which could be costly in computing time. [CHA 02]. This reduced surface response model provides the limit load $P_y(b, e_1, t, k)$ in function of the parameters of the joint submitted to the design load P_A. As a result, the limit state function is defined as :

$G(x_i, d_k) = P_U(b, e_1, t, k) - P_A(P_G, P_Q)$ [8]

where P_G and P_Q are respectively the actions due to permanent and exploitation loads. For a given joint, the loading P_A is obtained from the existing Eurocode rules. Given that we search the variability of the resistance, the loading is defined in a determinist form by $P_A = 1.35P_{G,k} + 1.5P_{Q,k}$, where the partial safety factors ensure a low probability of occurrence for this loading during the lifetime of the structure. In consequence, the obtained probability is not that of a structural failure but that of a failure related to the design rule loading.

When evaluating the capacity corresponding to the value at the intersection of the initial stiffness and the tangent at 5 mm ($P_{y,5mm}$), the quadratic surface response is :

$$\begin{aligned} P_U\left(b, e_1, t, k\right) = & -217{,}77 + 36{,}01\ b - 22{,}26\ e_1 + 178{,}77\ t \\ & - 16{,}36\ k - 6{,}30\ b^2 - 6{,}36\ e_1^2 - 140{,}05\ t^2 \\ & - 21{,}06\ k^2 + 8{,}54\ b\ e_1 + 17{,}14\ b\ t \\ & + 11{,}21\ b\ k + 20{,}28\ e_1\ t + 15{,}08\ e_1\ k \\ & + 97{,}21\ t\ k \end{aligned} \qquad [9]$$

The considered random variables are given in Table 2. The FORM analysis leads to a reliability indice $\beta = 4{,}50$ corresponding to a failure probability of $P_f = 3{,}4 \times 10^{-6}$, which is very conservative by comparison with the objectives of the Eurocodes (10^{-2} for serviceability limit state and 10^{-4} for ultimate limit state). We observe that is is then possible to reduce the dimensions of this kind of joint, or to increase the admissible loading for the given dimensions. The figure 7 illustrates the importance of the random variables and reveals that the material ratio k and the thickness t take a great part in the failure criterion. This can be seen on the partial safety factors that must be 1.25 for k and 1.16 for t. Concerning the other parameters, nominal values are acceptable directly as partial safety factors are close to 1.

variables	distribution	mean	ecart-type
b	lognormal	60 mm	1.0 mm
e_1	lognormal	30 mm	1.0 mm
t	lognormal	10 mm	0.5 mm
k	lognormal	1.00	0.07

Table 2. Random variables for the reliability analysis

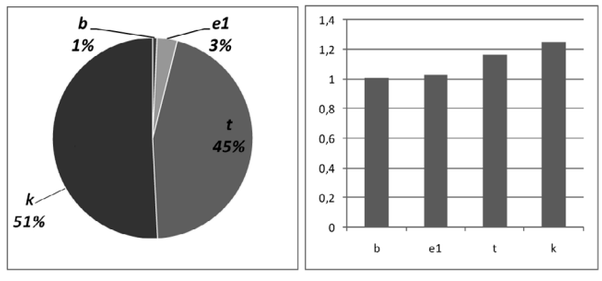

Fig. 7. Relative importance of random variables and partial safety factors

4. CONCLUSION

The presented study associates experimental, numerical and reliability analyses for the qualification of stainless steel bolted structural joints. Whereas the existing design rules applicable to carbon steel are derived for the design of stainless steel structures, the reliability analysis shows the available potential due to the great ductility and resistance of this material. The deformation capacity kept in reserve, revealed by the high reliability level and a low failure probability, demonstrates that it is possible to better exploit the qualities of stainless steel while respecting the reliability objectives of the Eurocodes. An improvement of these rules could then make of this material a more interesting alternative in structural applications. Studies are ongoing to extend this work to a broader range of geometric and material configurations of stainless steel cover plate joints.

5. REFERENCES

[AVE 09] AVERSENG J., BOUCHAIR A., "Modelling and analysis of bolted stainless steel cover plate joints". European Journal of Environmental and Civil Engineering, Vol. 13(4), 2009, pp. 443–455.

[BOU 02] BOUCHAÏR A., BAPTISTA A., "Strength and deformation of stainless steel bolted joints with reference to Eurocode 3", *3th Eurosteel Conference,* Coimbra, Portugal, septembre 2002, Vol. 2, pp. 879-888.

[BOU 05] BOUCHAÏR A., "Resistance and ductility of stainless steel bolted connections", *COST-C12, Improvement of Buildings Structural Quality by New Technologies, Final Conference*, Innsbruck (Austria), 20-22 janvier 2005, Edition Shaur et al., pp. 311-321.

[BOU 08] BOUCHAÏR A., AVERSENG J., ABIDELAH. A., "Analysis of the behaviour of stainless steel bolted connections", *Journal of Constructional Steel Research*, Vol. 64, 2008, pp. 1264-1274.

[BUR 00] BURGAN B.A., BADDOO N.R., GILSENAN K. A., "Structural design of stainless steel members - comparison between Eurocode 3, Part 1.4 and test results". *Journal of Constructional Steel Research*, Vol. 54, n°1, 2000, pp. 51-73.

[CEN 04] Comité Européen de Normalisation, *Eurocode 3 - prEN 1993 – Partie 1-4 : Règles générale – Règles supplémentaires pour les aciers inoxydables*, Bruxelles, 2005.

[CHA 02] CHATEAUNEUF A., PENDOLA M., HEINFLING G., DEFAUX G., *Etude des aéro-réfrigérants par couplage éléments finis et fiabilité*, Revue européenne des éléments finis, vol. 11, n°1, 2002, pp. 101-126.

[DIT 96] DITLEVSEN O., MADSEN HO., *Structural reliability methods*, John Wiley and Sons, 1996.

[EUR 06] *Design Manual for Structural Stainless Steel*, EuroInox, Third edition, 2006.

[GAY 04] GAYTON N., MOHAMED A., SORENSEN J.D., PENDOLA M., LEMAIRE M. "Calibration methods for reliability-based design codes", *Structural Safety*, 26 (1), 2008, pp. 91–121.

[KIM 99] KIM H.J., YURA J.A., "The effect of ultimate-to-yield ratio on the bearing strength of bolted connections", *Journal of Constructional Steel Research*, Vol. 49, 1999, pp. 255-269.

[KOU 00] KOUHI J, TALJA A, SALMI P, ALA-OUTINEN T. "Current R&D work on the use of stainless steel in construction in Finland". *Journal of Constructional Steel Research*, Vol 54, 2000, pp. 31-50.

[LEM 05] LEMAIRE M., en collaboration avec CHATEAUNEUF A. et MITTEAU JC., *Fiabilité des Structures - Couplage Mécano-Fiabiliste Statique*, Hermes Science Publication, 2005, ISBN 2-7462-1057-6.

[RYA 00] RYAN I., Bolted connections (WP4.2), ECSC Project - 7210-SA/327, Final Report for partner Ugine-CTICM, 2000.

[SCI 00] SCI, Development of the use of stainless steel in construction, Contract 7210-SA/842, 903, 904, 327, 134, 425, Final Report to ECSC, 2000.

[VAN 00] VAN DEN BERG G. J., "The effect of the non-linear stress-strain behaviour of stainless steels on member capacity", *Journal of Constructional Steel Research*, Vol. 54, n°1, 2000, pp. 135-160.

RESPONSABILITÉ & ENVIRONNEMENT

recherches débats actions

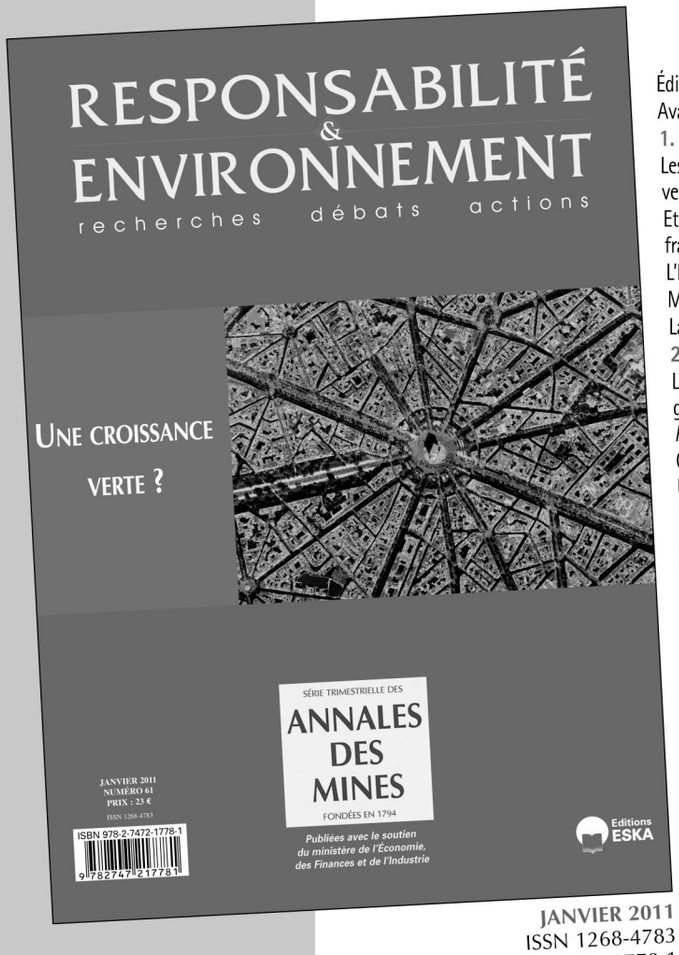

JANVIER 2011
ISSN 1268-4783
ISBN 978-2-7472-1778-1

SOMMAIRE

UNE CROISSANCE VERTE ?

Dossier coordonné par Hélène Serveille et Richard Lavergne

BULLETIN DE COMMANDE

A retourner aux Éditions ESKA, 12, rue du Quatre-Septembre, 75002 PARIS

Tél. : 01 42 86 55 65 - Fax : 01 42 60 45 35 - http://www.eska.fr

❑ Je désire recevoir ..... exemplaire(s) du numéro de **Responsabilité & Environnement janvier 2011 - numéro 61 (ISBN 978-2-7472-1778-1)** au prix unitaire de 23 € TTC.

Je joins ❑ un chèque bancaire à l'ordre des Éditions ESKA

❑ un virement postal aux Éditions ESKA CCP PARIS 1667-494-Z

Nom ..... Prénom .....

Adresse .....

Code postal ..... Ville .....

recommandations aux auteurs

CONTEXTE GÉNÉRAL

Les Annales du BTP sont avant tout une revue technique francophone s'adressant à un public d'ingénieurs et de décideurs œuvrant dans les multiples secteurs du BTP au sens le plus large du terme, à savoir la construction, le bâtiment, les travaux publics, l'ingénierie, les infrastructures urbaines et territoriales.

Les grands enjeux sous-tendus dans tout article pouvant paraître dans la revue sont à mettre en regard avec les problématiques d'aujourd'hui, progrès et innovation technologiques, développement économique dans le respect de l'environnement, valorisation des produits de la recherche dans le monde professionnel, défense du secteur de la construction dans l'économie mondiale…

Les auteurs sont invités à prendre en considération ces aspects dans toute leur diversité. Beaucoup d'articles en effet ne manqueront pas de se baser sur une présentation de travaux de recherche, qu'elle soit fondamentale ou appliquée. Néanmoins, à la différence d'une revue scientifique, les Annales attendent de ses contributeurs plus une description exhaustive de l'intérêt que leurs travaux pourraient présenter à la communauté professionnelle qu'une description précise de leur cheminement intellectuel.

Quand un article est le prolongement d'un colloque ou d'une rencontre scientifique, l'auteur devra donc veiller dans la réécriture à ne pas trop détailler sa démarche, mais à montrer l'intérêt de sa recherche pour le lectorat de la revue, en montrant en particulier dans l'introduction et la conclusion quels étaient ses grands objectifs. Il ne s'approfondira pas plus que nécessaire sur l'aspect scientifique, sachant que le lecteur ne sera pas forcément un spécialiste de sa discipline. En un mot l'auteur doit chercher à vulgariser son discours.

PRÉSENTATION DU MANUSCRIT

Le texte doit être soumis sous format électronique .doc ou .odt envoyé au rédacteur en chef François BUYLE-BODIN à l'adresse **annalesbtp@gmail.com**

En cas de refus de transmission pour cause de lourdeur des fichiers, l'auteur pourra envoyer un cédérom à **M. BUYLE-BODIN, rédacteur en chef de la revue Annales du BTP, Polytech'Lille – Université Lille 1, Cité Scientifique, 59655 Villeneuve-d'Ascq Cedex.**

Afin de faciliter la diffusion du savoir, l'éditeur n'exige pas des auteurs une mise en forme particulière de leur article. Aucune contrainte de longueur n'est posée, mais l'idéal est aux alentours de 15 pages en arial 10 interligne simple.

Les unités de mesures et les symboles doivent respecter les règles typographiques internationales.

Il est nécessaire de préciser :

- le titre en français et en anglais ;
- le ou les auteurs : nom, prénom, titres, coordonnées ;
- un résumé de 15 lignes maximum en français et en anglais ;
- les figures et photographies originales peuvent être fournies à part en .eps, .tif ou .jpg. Elles seront publiées en noir et blanc et doivent donc être d'un bon niveau de gris, au moins 400 dpi ;
- une illustration caractéristique de l'article pourra figurer en couleur sur la une de couverture et devra donc être d'une résolution maximale. Ne pas oublier de mentionner les crédits photographiques.

FONCTIONNEMENT DE LA RELECTURE

Le rédacteur en chef accuse réception du manuscrit et lance la phase d'approbation. Il s'appuie pour la relecture et la sélection finale des articles sur un comité comprenant des experts reconnus de la profession, ainsi que des membres des conseils scientifiques des principales associations du BTP partenaires des Annales.

Le rédacteur en chef de la revue fait part à l'auteur de la décision de publier ou non le texte, il précise éventuellement les corrections à apporter.

Le rédacteur en chef se charge de la transmission du manuscrit à l'éditeur.

AGPA Editions, 4, rue Camélinat, 42000 Saint-Etienne.

L'auteur recevra gratuitement 10 exemplaires du numéro de la revue dans lequel est publié son article.